Relation Between Surface Structural And Chemical Properties Of Platinum Nanoparticles And Their Catalytic Activity In The Decomposition Of Hydrogen Peroxide

Rui Filipe Serra Maia

Dissertation submitted to the faculty of the Virginia Polytechnic Institute and State University in partial fulfillment of the requirements for the degree of

Doctor of Philosophy
In
Geosciences

F. Marc Michel, Chair

J. Donald Rimstidt

Christopher Winkler

Mitsuhiro Murayama

August 6th, 2018

Blacksburg, Virginia

Keywords: Catalysis, Hydrogen Peroxide Decomposition, Metal Nanoparticles, Metal Nanocatalysts, Crystal Structure, Surface Chemistry, H_2O_2 decomposition Mechanism, H_2O_2 Decomposition Kinetics, Catalytic Activity of Platinum

Relation Between Surface Structural And Chemical Properties Of Platinum Nanoparticles And Their Catalytic Activity In The Decomposition Of Hydrogen Peroxide

Rui Filipe Serra Maia

ABSTRACT

The disproportionation of H_2O_2 to H_2O and molecular O_2 catalyzed by platinum nanocatalysts is technologically very important in several energy conversion technologies, such as steam propellant thrust applications and hydrogen fuel cells. However, the mechanism of H_2O_2 decomposition on platinum has been unresolved for more than 100 years and the kinetics of this reaction were poorly understood. Our goal was to quantify the effect of reaction conditions and catalyst properties on the decomposition of H_2O_2 by platinum nanocatalysts and determine the mechanism and rate-limiting step of the reaction. To this end, we have characterized two commercial platinum nanocatalysts, known as platinum black and platinum nanopowder, and studied the effect of different reaction conditions on their rates of H_2O_2 decomposition. These samples have different particle size and surface chemisorbed oxygen abundance, which were varied further by pretreating both samples at variable conditions. The rate of H_2O_2 decomposition was studied systematically as a function of H_2O_2 concentration, pH, temperature, particle size and surface chemisorbed oxygen abundance.

The mechanism of H_2O_2 decomposition on platinum proceeds *via* two cyclic oxidation-reduction steps. Step 1 is the rate limiting step of the reaction. Step 1: $Pt + H_2O_2 \rightarrow H_2O + Pt(O)$. Step 2: $Pt(O) + H_2O_2 \rightarrow Pt + O_2 + H_2O$. Overall: $2\,H_2O_2 \rightarrow O_2 + 2\,H_2O$. The decomposition of H_2O_2 on platinum follows 1st order kinetics in terms of H_2O_2 concentration. The effect of pH is small, yet statistically significant. The rate constant of step 2 is 13 times higher than that of step 1. Incorporation of chemisorbed oxygen at the nanocatalyst surface resulted in higher initial rate of H_2O_2 decomposition because more sites initiate their cyclic process in the faster step of the reaction. Particle size does not affect the kinetics of the reaction. This new molecular-scale understanding of the decomposition of H_2O_2 by platinum is expected to help advance many energy technologies that depend on the rate of H_2O_2 decomposition on nanocatalysts of platinum and other metals.

Relation Between Surface Structural And Chemical Properties Of Platinum Nanoparticles And Their Catalytic Activity In The Decomposition Of Hydrogen Peroxide

Rui Filipe Serra Maia

GENERAL AUDIENCE ABSTRACT

Platinum nanomaterials are indispensable to catalyze a variety of industrial and technological processes ranging from catalytic conversion of carbon monoxide (CO), hydrocarbons, and nitrogen oxides (NO_x) in modern automobiles to energy production by hydrogen fuel cells and thrust generation in steam propellers. These technological innovations have a tremendous impact in modern society, including the areas of transportation, energy supply, soil and water quality, environmental remediation and global climate change.

The decomposition of hydrogen peroxide (H_2O_2) to water (H_2O) and oxygen (O_2) on platinum nanomaterials is of particular importance because it affects the efficacy of many technological applications, such as hydrogen peroxide steam propellers and hydrogen fuel cells. However, the reaction pathway and kinetics of H_2O_2 decomposition on platinum were only partly understood. My goal was to understand how the reaction conditions and the nanocatalyst properties control the mechanism and kinetics of platinum-catalyzed hydrogen peroxide decomposition.

To do that we characterized the atomic scale structural and chemical properties of two different platinum nanocatalysts, known as platinum black and platinum nanopowder and evaluated the effect of their properties in their catalytic activity. Our characterization studies were used to understand the reactivity of these two platinum nanocatalysts in the decomposition of H_2O_2, which we evaluated separately in laboratory studies.

Establishing relationships between the catalyst properties and their activity, as we have done in this work for platinum nanocatalysts in the decomposition of hydrogen peroxide, has the potential to improve nanocatalyst design and performance for those applications.

Acknowledgements

After four and half years of intense work during this PhD project, writing this acknowledgement note is the finishing touch to my dissertation. These years have been a period of endless learning at a scientific and personal level, and at this moment I would like to reflect on people without whom this degree would not have been possible.

I would first like to thank my outstanding advisor, Dr. F. Marc Michel. Marc is extremely insightful and the most visionary person I have ever met. No wonder he is so successful at a professional and personal level. His guidance was instrumental in our scientific achievements and I completely look forward to collaborate with him in many other projects in the future.

I would also like to thank my other committee members, Dr. J. Donald Rimstidt, Dr. Christopher Winkler and Dr. Mitsuhiro Murayama for their support and scientific expertise. As Don once taught me *"The reason why you should listen to your committee members is because we have done many mistakes throughout our careers, and we are here to guide you so you don't do them yourself"*.

A lot of the characterization work I performed would not have been possible without the guidance and assistance of people at the NCFL, including Chris Winkler (also a member of my committee), Steve McCartney, Andrew Giordani and Jay Tuggle.

Several undergraduate students worked with me in this project, particularly performing rate measurements of H_2O_2 decomposition. Mentoring them was an absolute privilege and has allowed me to develop mentorship skills that I hope to apply in the future as a principal investigator. In particular I want to highlight Kevin Tranhuu, Ivy Bellier and Stephen Chastka. They are extremely skilled and hardworking students. I am sure they will be very successful in their endeavors.

Within the department I am sincerely thankful for the amazing faculty, students and staff I had the pleasure to spend time with during these years. In particular I want to thank

former and present graduate students of the Michel research group, Hannah King, Aly Hoeher, Karel Kleteschka, Allie Nagurney, McNeil Bauer and Bryan Raimbault for their friendship and insightful scientific discussions.

In Blacksburg (this amazing place I had the pleasure to live in for four and half years) I want to thank people that highly contributed for my happiness and well-being. In particular I want to name the folks with whom I played tennis and racquetball on a regular basis, Hannah King, McNeil Bauer, Kira Dickey, Addison Dalton and Bob Bodnar as well as the Portuguese community of Blacksburg. Thankfully the latter was only composed of a few people, so naming all of them is an easy task, but well deserved, Paulo Polanah, Rita Teixeira, Jorge Costa, João Monteiro, Iris Vilares and Alexandre Ribeiro. Our regular dinners/coffees were memorable and unique!

At the family level there are really a lot of people to thank and I will never be able to thank them enough. First and foremost, my wonderful wife, Temple, who puts up with me and makes my life much funnier and a lot more meaningful (even though we can never agree on the house temperature). We have the cutest dog in the world, Rascal, an endless source of fun and joy that makes everyday a lot more entertaining. Throughout these years my in-laws have been an infinite source of support, and I am very thankful for all the weekends and vacation Temple, Rascal and I have spent with them. Last but not least, my parents, siblings, cousins, nephews, nieces and other relatives. I am very proud of my parents, Rosa and Manuel Augusto, and I will be always amazed how two parents with only 4th grade of elementary school of education level, born and raised in a small and relatively isolated village in Portugal, Covelas in the municipality of Trofa, had the wisdom to guide all their five children (my four siblings and I) to obtain college degrees. Their hard work was an inspiration to always aim higher and better, without ever forgetting honesty, fairness and gratitude to people around us that in one way or another contributed to our achievements. On that note, my siblings, Armindo, Emília, Lino and João (all older than me) truly were an inspiration. For all these years they were a source of priceless help (of all kinds), without ever expecting any kind of retribution. If I made it to a PhD at this great University, Virginia Tech, I owe that to my family almost entirely.

Table of Contents

ABSTRACT ii
GENERAL AUDIENCE ABSTRACT iii
ACKNOWLEDGEMENTS iv
TABLE OF CONTENTS vi
LIST OF FIGURES ix
LIST OF TABLES xii
INTRODUCTION/OVERVIEW 1
Approach 3
Scientific Contribution 4
Background 5
Hydrogen Peroxide 5
Platinum 7
Surface platinum oxide species 7
Formation of platinum oxide films 8
Structure/organization of the Dissertation 9
CHAPTER 1 10
1. Abstract 11
2. Introduction 12
2.1 Platinum black 12
2.2 Platinum nanopowder 13
2.3 Impacts of nanosized platinum properties on catalytic activity 14
3. Materials and Methods 16
3.1 Samples 16
3.2 Microscale physical and chemical characterization by SEM 16
3.3 Bulk crystal structure and volume-weighted crystal size by x-ray diffraction (XRD) and small-angle x-ray scattering (SAXS) 16
3.4 Rietveld analysis 17
3.5 Specific surface area (SSA) by BET 18
3.6 Surface composition by XPS 18
3.7 Thermogravimetric analysis (TGA) 19
3.8 Transmission electron microscopy (TEM) and selected area electron diffraction (SAED). 19
3.9 Derivation of rate constants 20

4 Results and Discussion 21
4.1 Physical properties of Pt black and Pt nanopowder 21
4.2 Crystal structure, size and shape of as received and heated samples 24
4.3 Surface Chemical Properties 29
4.4 Impact of catalyst properties on catalytic activity 32
5 Conclusions 37
CHAPTER 2 38
1 Abstract 39
2 Introduction 40
3 Materials and Methods 44
3.1 Platinum black and platinum nanopowder 44
3.2 Rate measurements 44
3.3 Rate models 45
3.4 Concentrated H_2O_2 pretreatment 46
3.5 Heat treatment of catalysts 46
3.6 •HO detection 47
3.7 X-ray photoelectron spectroscopy (XPS) of heat treated catalysts 48
3.8 X-ray diffraction Rietveld analysis 48
3.9 Electrochemical analysis of Pt black and Pt nanopowder 49
4 Results and Discussion 50
4.1 Characterization of Pt black and Pt nanopowder 50
4.2 Catalytic activity of Pt black, Pt nanopowder and Pt-Liu-3nm 50
4.3 Effect of particle (crystallite) size on catalytic activity 55
4.4 Effect of chemisorbed oxygen on catalytic activity 58
5 Conclusions 67
CHAPTER 3 68
1 Abstract 69
2 Introduction 71
3 Materials and Methods 72
3.1 Platinum black and platinum nanopowder 72
3.2 Rate measurements 73
3.3 Data regression of H_2O_2 decomposition rates 74
3.4 Platinum black heat treatment 74
3.5 Particle size determination 75

3.6 Calibration of particle size of heated platinum nanocatalyst samples....76
3.7 Surface chemisorbed oxygen determination....77
3.8 Calibration of surface chemisorbed oxygen of heated platinum nanocatalyst samples....79
4 Results....81
4.1 Characterization of samples used for H_2O_2 decomposition rate measurements....81
4.2 Kinetics of H_2O_2 decomposition on platinum nanocatalysts....83
4.2.1 Constructing the rate equation....83
4.2.2 Regression model of H_2O_2 decomposition....85
5 Discussion....90
5.1 Correlation between particle size and surface Pt(O) for heated platinum black samples....90
5.2 Effect of surface Pt(O) on the catalytic decomposition of H_2O_2 by platinum nanocatalysts....90
5.3 Mechanistic role of surface Pt(O)....92
6 Conclusions....96
OUTLOOK AND FUTURE WORK....97
REFERENCES....99
APPENDIX....111
Appendix A Chapter 1....111
Acknowledgements....112
Supporting Information....113
Appendix B Chapter 2....126
Acknowledgements....127
Supporting Information....127
Evaluation of •HO in solution during the decomposition of H_2O_2 by Pt black....132
Cyclic voltammetry of Pt nanopowder and Pt black....133
Appendix C Chapter 3....136
Acknowledgements....137
Supporting Information....138

List of Figures

Figure 1. Structure of free H_2O_2 molecule 6

Figure 1.1. Electron micrograph of (a) low magnification Pt black deposited on lacey carbon grid, (b) high magnification Pt black deposited on continuous Si_3N_4, (c) high magnification Pt black deposited on lacey carbon grid – dotted lines outline nanoparticle boundaries based on contrast, (d) low magnification Pt nanopowder deposited on lacey carbon grid, (e) high magnification Pt nanopowder deposited on lacey carbon grid, (f) high magnification of Pt nanopowder deposited on lacey carbon grid featuring fused nanocrystals – dotted line contains area where two particles are fused.....22

Figure 1.2. Nanoparticle size distribution of Pt nanopowder by TEM 23

Figure 1.3. Crystal size (length and width) distribution of Pt black by TEM 24

Figure 1.4. X-ray diffraction spectra of (111) reflection. The y-axis is offset in increments of 0.05 between each curve.....25

Figure 1.5. Effect of crystal size on lattice dimension (Rietveld analysis) of Pt black and Pt nanopowder. Samples subjected to TGA heating are separated 1 nm apart in the x-axis for graphing purposes.....27

Figure 1.6. Volume-weighted particle size distribution of Pt nanopowder and Pt black from SAXS 29

Figure 1.7. Effect of O/Pt ratio and particle size in the rate constant (k) of Pt black (◊) and Pt nanopowder (○) samples 34

Figure 2.1. Regression model of log measured $\boldsymbol{R}$ vs log predicted $\boldsymbol{R}$ as function of $\boldsymbol{C_{H_2O_2}}$, a_{H^+} and $\frac{1}{T}$....53

Figure 2.2. Regression model of log measured $\boldsymbol{R}$ vs log predicted $\boldsymbol{R}$ as function of $\boldsymbol{C_{H_2O_2}}$, a_{H^+} and $\frac{1}{T}$ and d.....56

Figure 2.3. (a) Comparison of specific catalytic activity of Pt nanopowder-240 with Pt nanopowder as function of $\boldsymbol{C_{H_2O_2}}$, a_{H^+} and $\frac{1}{T}$. (b) Comparison of specific catalytic activity of Pt black-240 with Pt black as function of $\boldsymbol{C_{H_2O_2}}$, a_{H^+} and $\frac{1}{T}$. 60

Figure 2.4. Comparison between the rate of H_2O_2 decomposition of a) Pt nanopowder in the as supplied form and pretreated with concentrated H_2O_2 and b) Pt black in the as supplied form and Pt black pretreated with concentrated H_2O_2.....63

Figure 3.1. Rate measurements of H_2O_2 decomposition as function of $C_{H_2O_2}$, pH, temperature, particle size (d) and fraction of catalyst surface covered with chemisorbed oxygen (θ) for samples of as received platinum black (black ○) and as received platinum nanopowder (green □), platinum black heated in air (red ◊), platinum nanopowder heated in air (▭), platinum black heated in vacuum (blue ▽), platinum nanopowder heated in vacuum (blue ◘), platinum black pre-treated with concentrated H_2O_2 (pink ▷) and platinum nanopowder pre-treated with concentrated H_2O_2 (pink ◁) 86

Figure 3.2. Rate measurements of H_2O_2 decomposition as function of $C_{H_2O_2}$, pH, temperature and fraction of catalyst surface covered with chemisorbed oxygen (θ) for samples of as received platinum black (black ○) and as received platinum nanopowder (green □), platinum black heated in air (red ◊), platinum nanopowder heated in air (▭), platinum black heated in vacuum (blue ▽), platinum nanopowder heated in vacuum (blue ◘), platinum black pre-treated with concentrated H_2O_2 (pink ▷) and platinum nanopowder pre-treated with concentrated H_2O_2 (pink ◁).....88

Figure S1.1. Scanning electron microscopy (SEM) images of dry, as received, Pt black (a–b) and Pt nanopowder (c–d) 116

Figure S1.2 SAED (a) obtained with camera length of 120 mm and 20s of exposure time of an aggregate of Pt black-AsRec (c) and SAED (b) obtained with camera length of 120 mm and 20s of exposure time of an aggregate of Pt nanopowder-AsRec (d) 117

Figure S1.3. X-ray diffraction spectra of Pt nanopowder and Pt black. The y-axis of the plot is offset in increments of 0.05 between each curve 119

Figure S1.4. Full profile Rietveld analysis of a) Pt black-AsRec, b) Pt black-BET, c) Pt black-TGA, d) Pt nanopowder-AsRec, e) Pt nanopowder-BET and f) Pt nanopowder-TGA 121

Figure S1.5. High resolution XPS analysis of Pt black (a - c), Pt black-TGA (d - f), Pt nanopowder (g - i) and Pt nanopowder-TGA (j - l). 122

Figure S1.6. Thermogravimetric analysis of Pt black and Pt nanopowder in air 124

Figure S2.1. Oxygen reduction reaction mechanisms (reproduced with permission from ref[173]. (Copyright 2012 Royal Society of Chemistry)[173] 127

Figure S2.2. Transmission electron microscopy image of a small cluster of Pt nanopowder (a) and Pt black (b). Each cluster is formed by a few nanocrystals loosely attached 128

Figure S2.3. Cyclic voltammogram for Pt nanopowder (red) and Pt black (black) 133

Figure S2.4. Example of the initial rate method. The initial rate of H_2O_2 decomposition was determined by the derivative of the quadratic regression extrapolated to t=0. For a quadratic regression, that value is the coefficient of the term with power of 1. In the example of the figure the initial rate of H_2O_2 decomposition is 64.0 $\frac{mol_{H_2O_2}}{L \cdot min}$ 134

Figure S3.1. Correlation between surface chemisorbed oxygen abundance and particle size for platinum black samples heated in air 140

Figure S3.2. Surface θ and particle size of each set of samples used in the H_2O_2 decomposition rate study. As received platinum black (black ○) and as received platinum nanopowder (green □), platinum black heated in air (red ◊), platinum nanopowder heated in air (▭), platinum black heated in vacuum (blue △), platinum nanopowder heated in vacuum (blue ◘), platinum black pre-treated with concentrated H_2O_2 (pink ▷) and Pt nanopowder pre-treated with concentrated H_2O_2 (pink ◁) 141

Figure S3.3. Partial regression graphs of the rate measurements of H_2O_2 decomposition as function of a) temperature, b) a_{H^+}, c) $C_{H_2O_2}$, d) particle size (d) and e) surface θ for samples of as received platinum black (black ○) and as received platinum nanopowder (green □), platinum black heated in air (red ◊), platinum nanopowder heated in air (▭), platinum black heated in vacuum (blue ▽), platinum nanopowder heated in vacuum (blue ◘), platinum black pre-treated with concentrated H_2O_2 (pink ▷) and Pt nanopowder pre-treated with concentrated H_2O_2 (pink ◁). f) shows the residuals plot for Figure 3.1 143

Figure S3.4. Partial regression graphs of the rate measurements of H_2O_2 decomposition as function of a) temperature, b) pH, c) $C_{H_2O_2}$ and e) surface θ for samples of as received platinum black (black ○) and as received platinum nanopowder (green □), platinum black heated in air (red ◊), platinum nanopowder heated in air (▭), platinum black heated in vacuum (blue ▽), platinum nanopowder heated in vacuum (blue ◘), platinum black pre-treated with concentrated H_2O_2 (pink ▷) and Pt nanopowder pre-treated with concentrated H_2O_2 (pink ◁). f) shows the residuals plot for Figure 3.2 144

Figure S3.5. Rate measurements of H_2O_2 decomposition as function of $C_{H_2O_2}$, pH, temperature and particle size (d) for samples of as received platinum black (black ○) and as received platinum nanopowder (green □), platinum black heated in air (red ◊), platinum nanopowder heated in air (▭), platinum black heated in vacuum (blue ▽), platinum nanopowder heated in vacuum (blue ◘), platinum black pre-treated with concentrated H_2O_2 (pink ▷) and Pt nanopowder pre-treated with concentrated H_2O_2 (pink ◁) 145

Figure S3.6. Residuals plot for Figure S3.5 for samples of as received platinum black (black ○) and as received platinum nanopowder (green □), platinum black heated in air (red ◊), platinum nanopowder heated in air (▭), platinum black heated in vacuum (blue ▽), platinum nanopowder heated in vacuum (blue ◘), platinum black pre-treated with concentrated H_2O_2 (pink ▷) and Pt nanopowder pre-treated with concentrated H_2O_2 (pink ◁) 146

Figure S3.7. Rate measurements of H_2O_2 decomposition as function of $C_{H_2O_2}$, pH and temperature for samples of as received platinum black (black ○) and as received platinum nanopowder (green □), platinum black heated in air (red ◊), platinum nanopowder heated in air (▭), platinum black heated in vacuum (blue ▽), platinum nanopowder heated in vacuum (blue ◘), platinum black pre-treated with concentrated H_2O_2 (pink ▷) and Pt nanopowder pre-treated with concentrated H_2O_2 (pink ◁).....147

Figure S3.8. Residuals plot for Figure S3.7 for for samples of as received platinum black (black ○) and as received platinum nanopowder (green □), platinum black heated in air (red ◊), platinum nanopowder heated in air (▭), platinum black heated in vacuum (blue ▽), platinum nanopowder heated in vacuum (blue ◘), platinum black pre-treated with concentrated H_2O_2 (pink ▷) and Pt nanopowder pre-treated with concentrated H_2O_2 (pink ◁). 148

List of Tables

Table 1.1. XPS surface atomic chemical composition analysis of Pt black and Pt nanopowder 29

Table 1.2. High resolution XPS O1s peak area analysis 30

Table 1.3. Rate constant and activation energy of H_2O_2 decomposition by Pt nanocatalysts 33

Table 2.1. Proposed mechanisms of H_2O_2 decomposition on platinum group metal surfaces 41

Table 2.2. Physical properties of Pt black and Pt nanopowder. Uncertainties shown in parentheses 50

Table 2.3. Notation used 52

Table 2.4. Rietveld analysis of Pt nanopowder and Pt black heated at 240 ^{o}C for 24h 59

Table 3.1. List of samples used in the rate measurements 73

Table 3.2. Particle size and surface θ of the platinum nanocatalyst samples used to measure the effect of these two variables on the rate of H_2O_2 decomposition 82

Table 3.3. Notation used 84

Table 3.4. Summary of fitted coefficients for models regressed with different variables.....87

Table S1.1. Summary of previous studies that characterized platinum black.....113

Table S1.2. Summary of previous studies that report morphology and characterization of platinum nanoparticles obtained by chemical vapor deposition 115

Table S1.3. Selected area electron diffraction d-spacing measurements of Pt nanopowder and Pt black .118

Table S1.4. Selected results of Rietveld analysis. Uncertainties given in parentheses 120

Table S1.5. High res XPS Pt4f7/2 peak area analysis.....123

Table S1.6. Rate measurements for Pt black-BET, Pt black-air, Pt nanopowder-BET and Pt nanopowder-air at different conditions of $\boldsymbol{C_{H_2O_2}}$, pH and temperature.....125

Table S2.1. Rate measurements for Pt nanopowder and Pt black at different conditions of $\boldsymbol{C_{H_2O_2}}$, pH and temperature 129

Table S2.2. Rate measurements for Pt nanopowder and Pt black heated at 240 ^{o}C for 24h at different condition of $\boldsymbol{C_{H_2O_2}}$, pH and temperature 131

Table S2.3. Rate measurements for Pt nanopowder and Pt black submitted to H_2O_2 pre-treatment exposure. The conditions of $\boldsymbol{C_{H_2O_2}}$, pH and temperature were maintained constant for all runs 135

Table S3.1. Experimental particle size (d) of platinum black as function of heating time and heating temperature.....138

Table S3.2. Fraction of platinum black surface covered with chemisorbed oxygen sites (θ) as function of heating time and heating temperature 139

Table S3.3. Master Table with all rate measurements analyzed in this study, including rate measurements performed in the current study and rate measurements obtained in our previous studies[17-18]. For platinum black samples heated in air, particle size values *(d)* were determined using equation 2, and surface θ fraction was determined using equation 5 for heating T > 450 ^{o}C and

equation 6 for heating T < 450 ^{o}C. For all other samples particle size and surface θ were determined for each sample set 149

Introduction/Overview

Estimates are that at least 20% of all commercially produced chemical products involve heterogeneous catalysis at some point in the process of the manufacture[1]. In particular, platinum-based nanocatalysts are applied in a variety of industrial and technological processes ranging from catalytic converters to petroleum refineries, and to the oxidation of H_2 in the expanding industry of hydrogen fuel cells. These technological applications have had – and will continue to have – a tremendous impact in structural needs of our society at global scale[2].

Catalysts intervene by allowing a reaction to evolve through a different pathway that requires lower energy of activation, which increases the reaction rate[3-4]. In heterogeneous catalysis processes that involve solid state catalysts, surface chemistry is very important and challenging for several reasons. It takes place at the border between the catalyst and the surrounding medium and can be seen as the meeting place between condensed-matter and chemistry theory[5].

The vast application of platinum based catalysts in industrial processes has triggered a large volume of research in this field. One important reaction catalyzed by platinum is the decomposition of H_2O_2. One possible pathway to decompose H_2O_2 on platinum involves addition of electrons and hydrogen ions to yield H_2O as the only product. However, if the catalyst is not under an applied potential and no electrons and hydrogen ions are supplied, H_2O_2 decomposes via a non-electrochemical pathway, which yields H_2O and O_2 as final products. This pathway is known as H_2O_2 disproportionation and is purely chemical in nature (no overall gain or loss of electrons). This reaction is very important in technological applications, such as steam propulsion of miniaturized spacecrafts, military missiles and underwater vehicles[6-7]. Additionally, in hydrogen fuel cells H_2O_2 often forms as a byproduct of the oxygen reduction reaction and proceeds to decompose by disproportionation (parasitic reaction), which reduces the energetic yield of the fuel cell **(Figure S2.1)**.

A number of works have reported the effect of single variables in the catalytic decomposition of hydrogen peroxide on platinum surfaces. However, metal nanocatalysts are physicochemically and structurally complex, heterogeneous and modify with time. This complexity, mostly at the

surface, has important, yet poorly understood implications on the fundamental behavior of catalysts. In consequence, inconsistent catalytic activity behaviors are often reported, which kept previous studies from obtaining quantitative analysis of which variables affect more significantly the activity of platinum nanocatalysts in the decomposition of H_2O_2[8-10]. For these reasons the reaction mechanism of H_2O_2 decomposition on platinum has remained unresolved for more than 100 years[8, 11].

My overarching goal was to determine the mechanism for the H_2O_2 disproportionation reaction and to understand which variables controlled the kinetics of H_2O_2 decomposition on platinum nanocatalysts. To do that, I characterized two platinum nanocatalysts, known as platinum black and platinum nanopowder, with different physicochemical and structural properties and studied their catalytic effect on the decomposition of H_2O_2. I also studied the activity of these two nanocatalysts after they were subjected to select treatments before being used for rate measurements to increase the range of surface chemisorbed oxygen abundance and particle size of the samples. The catalytic activity of platinum black and platinum nanopowder samples was studied at variable conditions of hydrogen peroxide concentration, pH and reaction temperature. Rate measurements of H_2O_2 decomposition were used to quantify the effect of each variable and deconvolute the effect of correlated variables. By quantifying the effect of each variable on the catalyzed H_2O_2 decomposition I was able to infer the mechanism and rate limiting step of H_2O_2 decomposition on platinum. This knowledge was used to provide a quantitative understanding of the reaction kinetics at variable conditions and to deconvolute the effect of correlated variables that previously caused ambiguous and inaccurate ascribing of property-activity relationships[11-16].

Approach

This work was carried by performing thorough structural and chemical characterization of two commercial platinum nanocatalysts in the as received condition as well as after being subjected to different treatments. In parallel I performed rate measurements of H_2O_2 decomposition on the nanocatalysts to relate their structural and chemical properties to their catalytic activity. The full set of my characterization results allied to the rate models of H_2O_2 decomposition developed in this project were used to determine the mechanism and identify the rate limiting step of H_2O_2 decomposition at the surface of platinum nanocatalysts. This project was divided into three parts.

1) Abundance and speciation of surface oxygen on nanosized platinum catalysts and effect on catalytic activity. (published in *ACS AEM*)[17] The goal of this study was to characterize and compare the physicochemical and structural properties of platinum black and platinum nanopowder in the as received condition and after being heated at variable conditions. The main outcome of this study was to understand that particle size and surface oxygen abundance are affected by sample heating, which in turn affect the catalytic decomposition of H_2O_2.

2) Mechanism and kinetics of hydrogen peroxide decomposition on platinum nanocatalysts. (published in *ACS AMI*)[18] The goal of this study was to quantify the effect of reaction conditions and catalyst properties on the catalytic activity of platinum black and platinum nanopowder. The main outcome of this study was the development of rate models of H_2O_2 decomposition on platinum nanocatalysts, which were used to infer the mechanism and rate limiting step of the reaction.

3) Effect of platinum chemisorbed oxygen on catalytic activity of platinum nanocatalysts in the decomposition of hydrogen peroxide. (*in prep.* for submitting at *ACS Catalysis*). The goal of this study was to evaluate whether surface chemisorbed oxygen or particle size had the most important role in the catalytic decomposition of H_2O_2. The main outcome of this study was quantifying the significant role of surface chemisorbed oxygen on the catalytic rate of H_2O_2 decomposition on platinum, which allowed determining the individual rate constants of the partial steps of H_2O_2 decomposition on platinum.

Scientific Contribution

This work provides a mechanistic understanding of how hydrogen peroxide decomposes on platinum nanocatalysts under non-electrochemical conditions. The reaction model that we established reconciles previous results that were thought to be inconsistent. The rate models that we developed provide a quantitative understanding of the effect of reaction conditions and catalyst properties that affect the rate of H_2O_2 decomposition on platinum.

Equally important, this work establishes an effective approach and methodology that can be applied to study the reaction mechanism and kinetics of any chemical reactions catalyzed by platinum or other metal nanocatalysts in aqueous conditions.

Background

Hydrogen Peroxide

Hydrogen peroxide solutions are transparent, colorless and miscible with water. The density of pure H_2O_2 solution is 1.44 g/mL at a temperature of 25 ^oC and the molar mass is 34.01 g/mol. In the liquid state H_2O_2 is even more prone to form hydrogen bonding than H_2O[19]. These properties contribute to an ebullition point of 150.2 ^oC and freezing point of -0.43 ^oC. Pure H_2O_2 is chemically very unstable so it is usually not available. For scientific purposes 30% H_2O_2 solutions are generally used. For technologic applications that require high throughput of energy a mixture of 85% H_2O_2 and water is often required. At 20 ^oC the densities of these solutions are 1.11 and 1.36 g/mL, respectively[19]. H_2O_2 has a more acidic character than water, with $K_{20^oC} = 1.5 \times 10^{-12}$, where

$$H_2O_2 \Leftrightarrow H^+ + HO_2^-$$

Hydrogen peroxide is thermodynamically unstable and it decomposes to H_2O and O_2. The process is accelerated homogeneously by metal ions or heterogeneously by metallic surfaces. The decomposition of H_2O_2 is also found to be slightly enhanced in basic solutions[20].

$$H_2O_2 \Leftrightarrow H_2O + O_2 \qquad \Delta H = -99\ KJ \cdot mol^{-1}, \Delta S = 70.5\ J/(mol \cdot K)$$

The structure of free H_2O_2 molecule is shown in **Figure 1**.

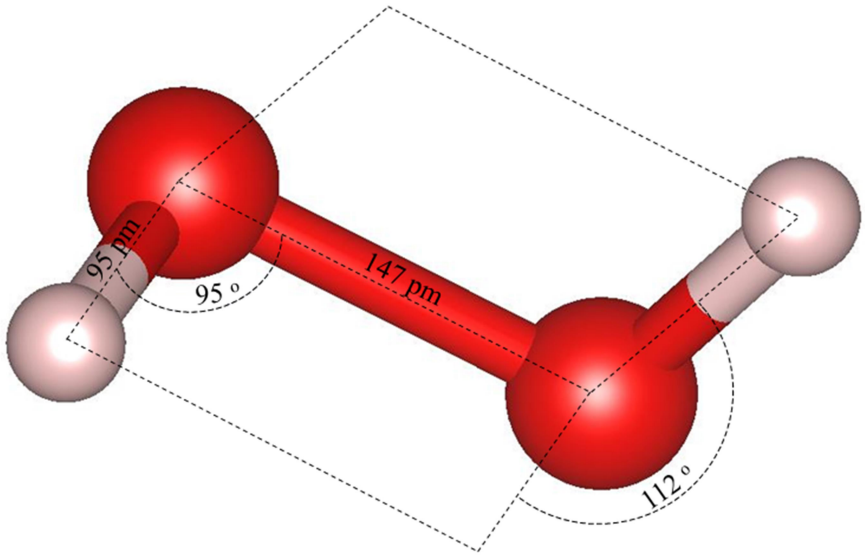

Figure 1. Structure of free H_2O_2 molecule.

Hydrogen peroxide is used in many commercial and household applications. Its main use is as a bleaching agent for textiles and paper production, which uses its strong oxidizing capacity generating only water and oxygen as by products that can be easily removed from the fabric or paper[21]. Diluted solutions of H_2O_2 are well tolerated by human tissue, but exhibit great antimicrobial activity, which makes it suitable for topical disinfection. For this reason H_2O_2 is also used as anti-bacterial agent in pharmaceutical products and for rapid sterilization of equipment in the dairy industry[22]. The ability to determine low concentrations of aqueous H_2O_2 has received great attention in atmospheric studies because it is believed to be involved in the oxidation of hydrogen sulfite ions in water at pH < 4.5, which results in the generation of sulfuric acid in cloud water droplets, thus contributing for the production of acid rain[23]. More importantly in the context of this dissertation, H_2O_2 is used as an energy source in aircraft jets, rockets, missiles and underwater vehicles[6, 24-25]. The chemical decomposition of H_2O_2 is also a parasitic reaction of the oxygen reduction reaction, which reduces the energy yield of hydrogen fuel cells[26-28].

Platinum

Platinum surfaces have the capacity to adsorb many species due to their electronic structure, which can be represented by $[Xe]s^2p^6d^9$. The d-orbital of platinum is partially unsaturated, which facilitates adsorption of compounds with non-bonded electron pairs. The presence of oxide species at the surface of platinum is very important because it affects the electronic properties of surface interface sites[29]. For many reactions it has been shown that the adsorbed species and other surface oxides are actively involved in several oxidation-reduction processes[30].

Surface platinum oxide species

Many important implications arise from the presence of oxide species at the surface of platinum catalysts[31]. Surface oxide species represent the activated state for several catalytic oxidation reactions, where the oxygen species is first delivered from the surface oxide followed by subsequent reforming of surface oxygen, instead of direct transference from bulk solution[32-33].

One important challenge to understand the effect of surface oxide species is the lack of knowledge of the mechanistic pathway of many chemical reactions. In some instances this produces contradictory results. For example, some studies showed that the existence of a thin oxide film on platinum enhances the catalytic activity of platinum for some reactions, but other studies showed that oxidation suppresses platinum catalysis[8, 11, 15, 34-37]. In this work we demonstrate that surface chemisorbed oxygen has an important role in the decomposition of hydrogen peroxide. For this reason, the next section expands on background information on the formation of surface platinum oxide films.

Formation of platinum oxide films

The oxidation of platinum surfaces can be electrochemically initiated in water at 0.75 V vs SHE[38],

$$Pt + H_2O \Leftrightarrow PtOH + H^+ + e^-$$

This reaction is followed by an electron transfer reaction to the medium, which leaves surface chemisorbed oxygen (Pt(O)) at the electrode surface[38]

$$PtOH \rightarrow Pt(O) + H^+ + e^-$$

The oxidation potential of H_2O_2 ($C_{H_2O_2} = 10^{-2}\ M$) in acidic conditions is 1.69 V (SHE)[39], which means that the oxidation of platinum with chemisorbed oxygen is very likely to happen when platinum is in the presence of H_2O_2. This is consistent with the formation of a similar surface platinum oxide film observed when platinum is immersed in H_2O_2[40]. These authors found that the reactions that occur at the surface of anodically reduced platinum surfaces immersed H_2O_2 solutions generated similar potentials to those observed in electrochemical oxidation of platinum, which suggests that the same reaction is generating the surface oxide film that forms at the surface of the catalyst[40]. Electrochemical studies indicate that many oxidation-reduction reactions occur at electrochemical potentials near those of surface Pt(O) formation, which indicates that Pt(O) is likely involved in many reactions on interest[31, 34].

Structure/organization of the Dissertation

This dissertation is divided in 3 major chapters. Each chapter has its own abstract, introduction, materials and methods, results, discussion, conclusions and appendix.

The appendix of each chapter is found in the last section of the overall dissertation and its number matches that of the chapter it refers to. For example Appendix B Chapter 2, is the appendix of chapter 2.

The supporting information (supporting figures, tables and complementary analyses) is provided in the appendix of each chapter.

The first digit of image and table numbers refers to the chapter number. For example, **Figure 3.5** refers to Figure 5 in chapter 3. In addition, images or figures in the supporting information (appendix) are numbered with an "S" before the number, which stands for "supporting information". For example, **Table S2.4** refers to Table 4 in the supporting information (appendix) of chapter 2.

For convenience to other researchers that may be interested to analyze the data collected in this PhD project, **Table S3.3** is a Master table. This table contains all H_2O_2 rate measurements, and respective independent variables, obtained in the course of the overall project. This includes rate measurements that were object of study in Chapter 1 **(Table S1.6)** and rate measurements that were object of study in Chapter 2 **(Table S2.1 and S2.2)**. The entire data set was object of study in chapter 3.

Notation is self-consistent within each chapter, but a few variables were defined differently in different chapters. This is particularly important for chapter 2 and chapter 3 because both contain a large number of variables. **Table 2.3** and **Table 3.3** provide the notation list and their units for their respective chapter.

The reference list is continuous in the whole dissertation. For example ref[13] in chapter 2 refers to the same publication of ref[13] in chapter 3. All references are found in the section "References"

Chapter 1

Abundance and Speciation of Surface Oxygen on Nanosized Platinum Catalysts and Effect on Catalytic Activity

Rui Serra-Maia [Ɨ], Christopher Winkler [±], Mitsuhiro Murayama [±, ‡], Kevin Tranhuu [Ɨ], F. Marc Michel [Ɨ]

[Ɨ] Department of Geosciences, Virginia Polytechnic Institute and State University, Blacksburg VA, USA

[‡] Department of Materials Science and Engineering, Virginia Polytechnic Institute and State University, Blacksburg VA, USA

[±] Institute of Critical Technology and Applied Science, Virginia Polytechnic Institute and State University, Blacksburg VA, USA

Author contributions: RS-M and KT performed rate measurements of H_2O_2 decomposition on platinum samples; RS-M performed most of the characterization of platinum black and platinum nanopowder. FMM performed small angle x-ray scattering analysis and wrote the materials and methods section referring to that technique. The paper was written by RS-M with input from CW, MM, KT and FMM.

Citation:

Serra-Maia R., Winkler C., Murayama M., Tranhuu K., Michel F.M. (2018) Abundance and Speciation of Surface Oxygen on Nanosized Platinum Catalysts and Effect on Catalytic Activity, *ACS Appl. Energy Mater.,* vol. 1, pp. 3255 – 3266.

1. Abstract

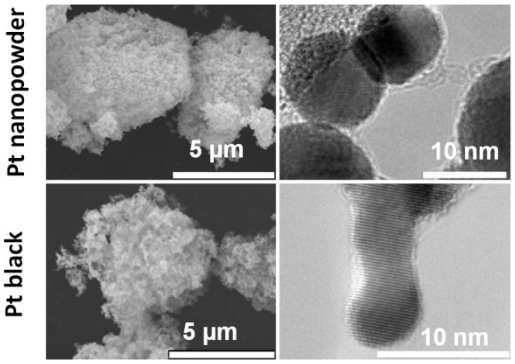

Oxygen at the surface of nanosized platinum has a direct effect on catalytic activity of oxidation-reduction chemical reactions. However, the abundance and speciation of oxygen remain uncertain for platinum with different particle size and shape characteristics, which has hindered the development of fundamental property-activity relationships. We have characterized two commercially available platinum nanocatalysts known as Pt black and Pt nanopowder to evaluate the effects of synthesis and heating conditions on the physical and surface chemical properties, as well as on catalytic activity. Characterization using complementary electron microscopy, x-ray scattering and spectroscopic methods showed that the larger average crystallite size of Pt nanopowder (23 nm) compared to Pt black (11 nm) corresponds with a 70% greater surface oxygen concentration. Heating the samples in air resulted in an increase in surface oxygen concentration for both nanocatalysts. Surface oxygen associated with platinum is in the form of chemisorbed oxygen and no significant amounts of chemically bonded platinum oxide were found for any of the samples. The increase in surface oxygen abundance during heating depends on the initial size and surface oxygen content. Hydrogen peroxide decomposition rate measurements showed that larger particle size and higher surface chemisorbed oxygen correlate with enhanced catalytic activity. These results are particularly important for future studies that aim to relate the properties of platinum, or other metal nanocatalysts, with surface reactivity.

2. Introduction

Understanding property-activity relationships for metal nanoparticles is one of the greatest challenges in the design of heterogeneous catalysts[41]. This includes colloidal forms of metallic nanocatalysts currently used in a wide range of applications[42-48]. Surface chemical composition is a critical factor in nanocatalyst reactivity because it directly affects the type and strength of chemical bonds that can be established with reactants in solution[49]. Crystallite size and shape are also important because of their effects on lattice strain and the work function of metal nanoparticles, which directly influence surface electronic properties[50]. The physical and surface chemical properties of metal nanocatalysts are initially determined by the conditions of synthesis. Further modifications of properties can occur from subsequent sample treatments, such as heating, or during chemical reactions due to the interaction of the particle surfaces with a surrounding medium[51-53]. However, these effects are not usually accounted for in experimental studies aimed at developing property-activity relationships. This has been the case for platinum (Pt), an important and effective nanocatalyst used in colloidal form in a wide variety of industrial and technical applications[42, 54-59]. Overall, the reported physicochemical properties of Pt nanocatalysts vary widely for different synthesis methods and studies, which has direct implications in their catalytic activity[60-63]. Here, we report detailed characterization results and compare the catalytic activity of two different types of commercially available unsupported Pt nanocatalysts. Selected background information is given for the samples that are the focus of the present study.

2.1. Platinum black

Platinum black (Pt black) is a form of synthetic nanosized Pt that has long been recognized for its outstanding catalytic activity[64-65]. It is typically synthesized by heating H_2PtCl_6 to approximately 450 ºC to form PtO_2 followed by hydrogenation in an aqueous suspension to form metallic Pt black[11, 64, 66-79]. Alternative synthesis routes involve reaction of H_2PtCl_6 or K_2PtCl_6 with formaldehyde in a potassium hydroxide solution[77]. To reduce loss of catalyst material, in applications such as fuel cells, electrochemical precipitation of Pt onto the surface of electrodes to form platinized platinum is also used [61, 71, 80-85]. When the deposited product has the

characteristic black color the term 'Pt black' is often used in place of platinized platinum[61, 66, 71]. A summary of synthesis methods, physicochemical characteristics, and uses of Pt black from selected studies is provided in **Table S1.1**.

Pt black aggregates are generally characterized by a dendritic morphology[61, 73, 80, 84] with rounded nanocrystals[78] and crystallite sizes ranging between 5 and 12 nm[78, 85]. The specific surface area (SSA) based on the Brunauer-Emmett-Teller (BET) method ranges from 10 to 30 m^2/g[63, 68, 70-72, 76, 85]. Sintering, crystallite growth, and the loss of fractal features has been reported for Pt black at temperatures as low as 360 ^oC[80, 85].

There is limited data and lack of consensus in the literature regarding the surface and bulk chemical compositions of Pt black. Early studies suggested that surface oxygen content varies from 2-20 % (mol_o/mol_{Pt}) [64-65]. More recent XPS analyses confirm the presence of oxygen at the surface of Pt black, but the speciation and concentration are seldom discussed[86-88].

2.2. Platinum nanopowder

Platinum 'nanopowder' and 'nanoparticles' (hereinafter referred to as Pt nanopowder) are Pt nanocatalysts with renowned catalytic activity. It is usually synthesized by chemical vapor deposition, due to high size and shape control [67], for uses such as proton exchange membrane (PEM) fuel cells[89], integrated circuits, and optical applications[90]. Pt nanopowder is typically lighter in color than the distinctive dark grey to black color of Pt black. A summary of synthesis methods, physicochemical characteristics, and applications of Pt nanopowder from selected studies is provided in **Table S1.2**.

The reported physical and chemical properties of Pt nanopowder vary widely for different studies. Crystallite sizes range from 1 to 30 nm[62, 91-95]. Specific surface area (SSA) values of 150 to 205 m^2/g have been reported for particle sizes ranging from 1 to 4.5 nm[62]. Particle morphologies vary from irregular[62, 93] to (pseudo) spherical[91-92, 96]. Increases in crystallite size have been reported when Pt nanopowder is subjected to temperatures of 600 ^oC or above[69, 97].

The concentration and speciation of surface oxygen on Pt nanopowder, as well as its dependence on particle size remains poorly understood[98-101]. Some studies have shown that surface oxygen concentration increases with decreasing particle size[98-99], Others reported that larger particle sizes correlated with higher oxygen content in the form of chemisorbed oxygen[100-101].

2.3. Impacts of nanosized platinum properties on catalytic activity

Prior research has focused mainly on the effect of a single physical or chemical property on catalyst performance[99, 102-108], such as effects of particle size on the oxygen reduction reaction[102], or facet-dependent catalytic activity on solar cell reduction reactions[109]. A limitation of these and other related studies on commercial samples[110-112] is that the reported property-activity relationships are restricted to only a specific set of conditions making it difficult or impossible to understand the studied processes at a mechanistic level. In addition, correlated effects of different physical, chemical and structural properties often induce incorrect ascribing of property-activity relationships for Pt and other metal nanoparticles[100]. For example, as the particle size of metal nanoparticles increases the work function decreases, which is linked to enhanced accumulation of surface chemisorbed oxygen[101]. Surface chemisorbed oxygen can also affect the catalytic activity of Pt nanoparticles[113-115].

Results from previous research on nanosized platinum reveal two important and currently unresolved questions: 1) what oxygen species are present at the surfaces of nanosized platinum and in what abundance, and 2) how does surface oxygen change as a function of different synthesis conditions, sample treatments such as heating, and reaction conditions. Questions regarding surface oxygen composition are important for explaining the enigmatic variability in catalytic performance that has been reported for Pt nanocatalysts synthesized at different conditions[6, 10]. For example, the formation of surface oxides due to heating[116-117] is known to affect the rate of reactions catalyzed by Pt[8, 11, 15]. New studies and detailed characterization of commercial Pt nanocatalysts are thus needed to determine fundamental properties of commercial Pt nanocatalysts, as well as how they change as a function of external conditions.

This study reports detailed characterization results for commercially sourced samples of Pt black and Pt nanopowder. The two catalysts were characterized in the 'as received' condition, as well as after being subjected to BET outgassing at 300 ^{o}C (Pt black-BET and Pt nanopowder-BET) and thermogravimetric analysis (TGA) in air (Pt black-TGA and Pt nanopowder-TGA). Heating was used to evaluate the effect of moderate to high temperature conditions on the initial properties of the two samples. Complementary electron microscopic imaging and small-angle x-ray scattering methods were used to quantify the crystal size, shape, and aggregation behavior of the samples. Powder x-ray and selected area electron diffraction were used to evaluate bulk atomic structural characteristics. X-ray photoelectron spectroscopy was used to quantify surface chemical composition, specifically the speciation and concentration of oxygen. Changes in particle size and surface oxygen due to heating were evaluated in terms of their impact on catalytic activity of H_2O_2 decomposition, which we have used here as a model reaction. The chemical decomposition of H_2O_2 is exothermic and is used for propulsion of miniaturized spacecraft and underwater vehicles[6, 24-25]. This reaction is also important in hydrogen fuel cells, where the decomposition of H_2O_2 through a non-electrochemical pathway (without addition of electrons from the anode) lowers the energetic efficiency of the oxygen reduction reaction. Although the surface of platinum is affected by the voltage between the anode and the cathode in fuel cells, our study provides a model to understand the kinetics of the parasitic non-electrochemical decomposition of H_2O_2 in these applications[26-28, 118].

Overall, the results significantly improve our understanding of commercial Pt nanocatalysts by addressing key questions regarding their physical and surface chemical properties, mainly regarding the presence of oxygen, as well as how these properties change during heating.

3. Materials and Methods

3.1. Samples

Pt nanopowder and Pt black were obtained from Sigma-Aldrich (St. Louis, MO USA). According to the manufacturer Pt nanopowder was synthesized by combustion chemical vapor condensation and its (TEM) particle size is < 50 nm. Pt black was derived from chemical reduction of H_2PtCl_6 to metallic Pt[65-66] and its reported average aggregate size is ≤ 20 µm. Pt black and Pt nanopowder were received as finely divided dry powders with colors ranging from dark gray to black. Samples were characterized in four different conditions: 1) 'as received' from the supplier (Pt black and Pt nanopowder), 2) heated in air at 240 ^{o}C for 24h, 3) subjected to heat in vacuum conditions at 300 ^{o}C for 22h during BET outgassing (Pt black-BET and Pt nanopowder-BET), and 4) subjected to TGA heating conditions in air from room temperature to 700 ^{o}C at a heating rate of 10 ^{o}C/min (Pt black-TGA and Pt nanopowder-TGA).

3.2. Microscale physical and chemical characterization by SEM

Scanning electron microscopy analysis was performed on dry powder samples loaded on double sided carbon conductive tape (Ted Pella, USA). Images were collected using a FEI Quanta 600 FEG operated at an accelerating voltage of 20 kV.

3.3. Bulk crystal structure and volume-weighted crystal size by x-ray diffraction (XRD) and small-angle x-ray scattering (SAXS)

Powder x-ray diffraction and small-angle x-ray scattering data were collected using a PANalytical Empyrean Nano Edition multi-purpose diffractometer equipped with a Cu source ($\lambda\ Cu_{K_\alpha}$ = 0.15406 nm) and Bragg-Brentano HD divergent beam optic with an energy resolution

of about 450 eV. Dry samples of Pt nanopowder and Pt black for powder XRD were loaded individually onto a 32 mm diameter low-background Si wafer sample holder with 0.2 mm well (PANalytical). Diffracted intensities from the samples were collected from 20 to 130° 2θ in approximately 0.007° increments using a GaliPIX^{3D} area detector system and exposure time of approximately 188 sec/point. The raw scattering data were processed in HighScore (PANalytical). Average crystal sizes for each sample were estimated using full profile Rietveld analysis. SAXS measurements were made using a Cu focusing mirror and 1/32° fixed diffraction slit. Dry samples were flat mounted between scotch tape and Mylar film and measured in a ScatterX[78] evacuated sample holder and beam path. Data processing and volume-weighted size distribution (D v(R)) analysis were performed using EasySAXS (PANalytical).

3.4. Rietveld analysis

Rietveld analysis of powder XRD data was performed using Profex 3.20.2[119]. A fundamental parameters approach (FPA) was used to calculate the instrumental weight function from the device configuration. A silicon NIST640d standard for line position and line shape was used to verify the instrumental weight function.

The initial unit cell parameter (a) and isotropic displacement parameters, and spacegroup $Fm\bar{3}m$ (no. 225) with Wyckoff value 4a for face-centered cubic (FCC) platinum were obtained from crystallographic information file (CIF) number 0011157 obtained from the AMCSD[120]. A pseudo-Voigt function (RP4) and spherical harmonics correction (SPHAR4) were used in all fits to model peak profiles. The displacement parameter for Pt was left fixed at the initial value (U=0.001). Two fitting strategies were tested to account for peak broadening and asymmetry. One strategy included fitting the data with two separate Pt phases having the same FCC structure. The unit cell dimension and peak profile parameters for size-induced broadening of the Lorentzian (B1) and Gaussian (k1) components were allowed to vary independently for each phase. The second strategy used a single Pt phase affected by size-induced broadening (B1) and anisotropic microstrain (k2). The unit cell dimension and B1 were first allowed to vary freely

and then k2 was added to the refinement. Further details regarding the fitting strategy for each sample are included in the Results section.

3.5. Specific surface area (SSA) by BET

The gas accessible surface area of Pt black and Pt nanopowder was determined by BET analysis with a Quantachrome Autosorb-1 using a 6 mm borosilicate sample cell and nitrogen as adsorbate. Two protocols for outgassing the samples at room temperature (23 ºC) or 300 ºC were used to evaluate the effects of heating on surface area. Samples outgassed at 300 ^{o}C were recovered for XRD analysis (Pt black-BET and Pt nanopowder-BET). Samples were analyzed in triplicate and outgassed for 22 hours followed by standard 11-point BET analysis in the P/P0 range of 0.05 to 0.35. Sample weight was obtained by subtracting the weight of the empty sample holder from that of the sample holder plus outgassed sample for each run. Weight determinations were obtained from the average of 5 consecutive measurements and SSA values were obtained from the analysis of three independent samples of each catalyst.

3.6. Surface composition by XPS

X-ray photoelectron spectroscopy quantitative surface chemical characterization of the samples was done using a PHI Quantera SXM scanning photoelectron spectrometer microprobe. Samples were deposited on double coated carbon conductive tape (Ted Pella, USA). High-energy resolution XPS data were collected for selected Pt, O, and C peaks with 0.1 eV of energy resolution at a pressure of 10^{-7} Pa. High resolution XPS was done on the C1s, O1s and Pt4f peaks. The raw spectroscopy data were processed using Phi Multipak software. High resolution XPS analysis with peak deconvolution and charge calibration was performed using CASA XPS. Charging was referenced to the C1 component of adventitious C1s peak at a binding energy of 284.8 eV for all samples. The O1s spectra were deconvoluted into four components for all samples (Figure S5). Component 1 and 2 relate to oxygen present in adventitious carbon, attributed as follows: O1 (532.6 eV, -C=O and C-OH), O2 (533.9 eV, -COOH structure)[121].

Component 3 and 4 reflect oxygen bonded to Pt in the form of Pt(O) - chemisorbed oxygen - at 531.60 eV[121-122] and in the form of PtO_x at 530.30 eV, respectively [122-123]. The C1s peak was deconvoluted into three symmetric components for Pt black and Pt nanopowder, attributed as follows: C1 (284.8 eV, C-C, C-H bonds), C2 (286.3 eV, C-O-C, C-O-H bonds), C3 (288.6 eV, C=O, O-C=O bonds). Two extra components C5 (284.4 eV, C=C structure) with its respective pi-pi* shake-up C6 at 290.79 eV were added for the fits to samples subjected to TGA heating to account for the presence of graphitic-like bonds[121]. The C1 component was used as a charging reference at a binding energy of 284.8 eV for all samples.

3.7. Thermogravimetric analysis (TGA)

Thermogravimetric analysis was performed in a TA Instruments Q5000 equipped with 100 µL capacity titanium pans. Samples were analyzed in triplicate (approximately 15 mg each) in air. The protocol included a 20 min isotherm at 90 ºC to minimize the weight loss associated with physisorbed water. Samples were then heated from 90 ºC to 700 ºC at 10 ºC/min. TGA samples were recovered for XPS and XRD analysis (Pt black-TGA, and Pt nanopowder-TGA).

3.8. Transmission electron microscopy (TEM) and selected area electron diffraction (SAED).

Transmission electron microscopy was performed on a JEOL 2100 equipped with a high-resolution pole piece and a thermionic emission gun operated at 200kV. Point-to-point resolution of this TEM is 0.23 nm. Samples were prepared by dispersing approximately 2 mg of dry sample in 2 mL of methanol (Fisher Scientific, USA), followed by a 2 min sonication. The dispersion was then filtered through a 0.22 µm pore size filter and 10-20 µL of filtrate was loaded onto a lacey carbon support film on a copper grid mesh (Ted Pella, USA) or a continuous film of amorphous Si_3N_4 on a silicon frame (Ted Pella, USA). SAED patterns were obtained at camera lengths of 80-150 mm and exposure times of 20-40 s. Gatan Digital Micrograph software was used for image processing and analysis. Diffraction patterns were analyzed with the Circular Hough Transform diffraction analysis script, an add-on to Gatan Digital Micrograph software

developed by David Mitchell (2007)[124]. Reciprocal space distances were obtained with rotational average of diffraction spots obtained from polycrystalline samples, improving the statistical significance and reducing the error associated with these measurements.

3.9. Derivation of rate constants

Rate constants of H_2O_2 decomposition were determined at 22 ^{o}C by multivariate linear regression analysis of the rate of H_2O_2 decomposition as function of $C_{H_2O_2}$, a_{H^+} (activity of H^+) and $\frac{1}{T}$ for each catalyst sample. Rate measurements were performed following the protocol described in ref[18] for Pt black-BET (6 data), Pt black-air$_{300}$ (8 data), Pt nanopowder-BET (4 data) and Pt nanopowder-air$_{300}$ (6 data). The measured rates for each set of reaction conditions can be found in **Table S1.6**. The rate constants of Pt black and Pt nanopowder in the as received condition, Pt black-air$_{240}$ and Pt nanopowder-air$_{240}$ were calculated from rate measurements reported in ref[18] for these four catalyst samples.

4. Results and Discussion

4.1. Physical properties of Pt black and Pt nanopowder

Scanning Electron Microscopy (SEM) imaging showed that the as received samples of Pt nanopowder and Pt black consist of porous and irregularly shaped aggregates of nanoparticles **(Figure S1.1)**. In comparison to Pt black, the aggregates of Pt nanopowder are more rounded and have smoother surfaces. Sizes of aggregates determined by SEM are similar for both samples and vary from less than 1 micrometer to approximately 50 micrometers. Individual crystallites were not discernable by SEM for either sample.

Nanoscale imaging by high-resolution transmission electron microscopy (TEM) of samples deposited on lacey carbon TEM grids showed that Pt nanopowder and Pt black consist of aggregates of nanosized crystallites **(Figure 1.1)**. Selected area electron diffraction (SAED) patterns show continuous rings, confirming that the aggregates are polycrystalline for both samples **(Figure S1.2)**. The average aggregate size of Pt black is 536 ± 412 (N=30) nm and Pt nanopowder is 458 ± 398 nm (N=32). Small aggregates consisting of only a few nanocrystals were frequently observed for both samples when mounted on continuous Si_3N_4 TEM grids.

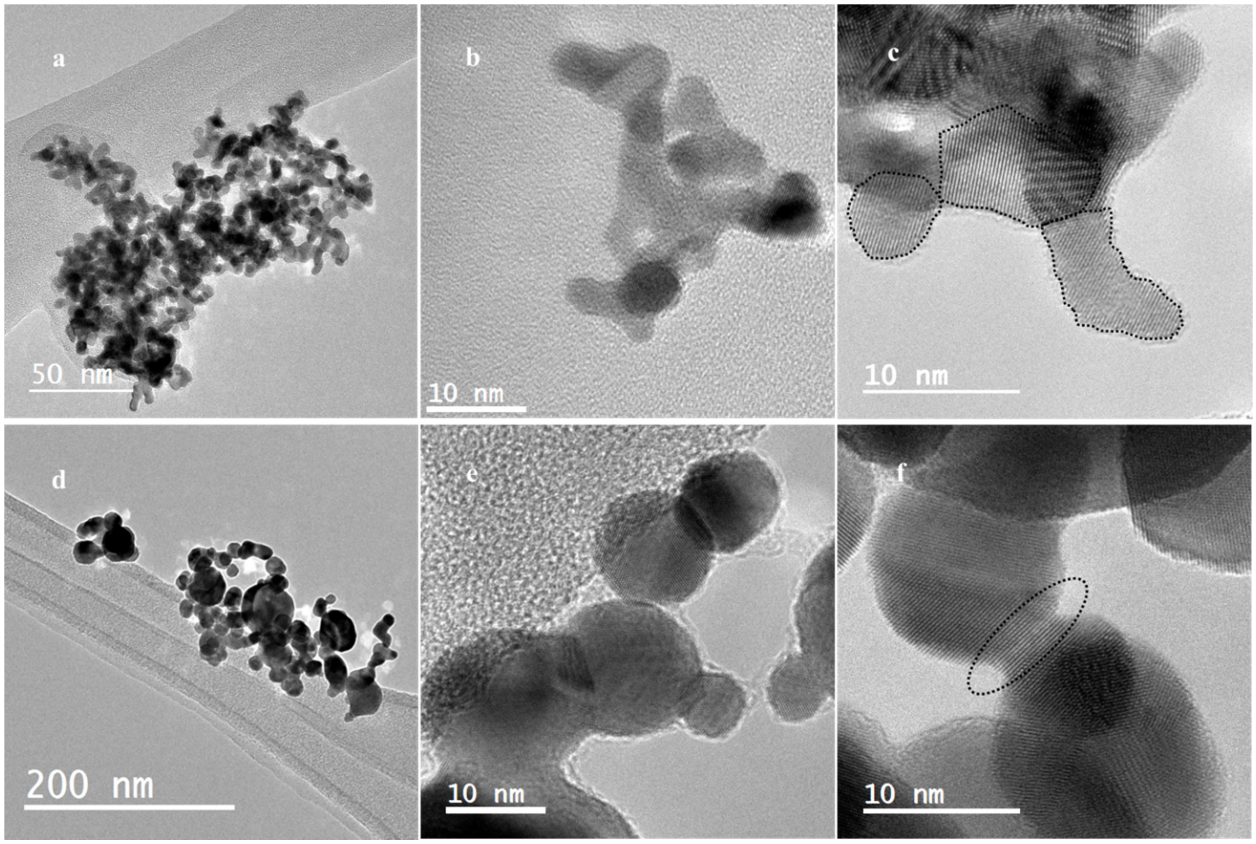

Figure 1.1. Electron micrograph of (a) low magnification Pt black deposited on lacey carbon grid, (b) high magnification Pt black deposited on continuous Si_3N_4, (c) high magnification Pt black deposited on lacey carbon grid – dotted lines outline nanoparticle boundaries based on contrast, (d) low magnification Pt nanopowder deposited on lacey carbon grid, (e) high magnification Pt nanopowder deposited on lacey carbon grid, (f) high magnification of Pt nanopowder deposited on lacey carbon grid featuring fused nanocrystals – dotted line contains area where two particles are fused.

Individual crystallites of Pt nanopowder observed by TEM were mostly pseudo-spherical **(Figure 1.1 d-f)**. Some exhibited surface facets (mostly hexagonal) while others appeared relatively smooth and featureless. In addition to individual and (loosely) aggregated nanoparticles, TEM imaging also showed fused crystallites in the case of Pt nanopowder **(Figure 1.1 f)**. Crystallite sizes of Pt nanopowder ranged mostly from 5 to 50 nm, but larger particles up to 150 nm were occasionally observed. The particle size distribution was up-tailed leading to an average value of 22 ± 19 nm and a median value of 16.6 nm **(Figure 1.2)**. These particle sizes

are consistent with previous reports for Pt nanopowder obtained by chemical vapor deposition, the same method used to synthesize the sample in this study[62, 94].

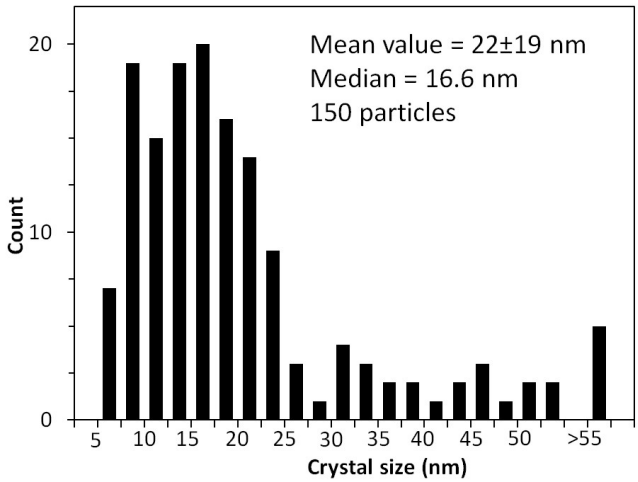

Figure 1.2. Nanoparticle size distribution of Pt nanopowder by TEM.

The majority of the Pt black crystallites were irregularly shaped **(Figure 1.1 a-c)**. Facets of different crystal terminations were observed on some nanocrystals but were less common than for Pt nanopowder. While most crystallites were elongated, nearly round ones were also observed **(Figure 1.1c)**. The elongation did not occur systematically along any specific Miller index. Crystallites ranged between 4 and 25 nm in length and between 2 and 12 nm in width, which is consistent with prior observations of Pt black synthesized by chemical reduction[68, 71, 75, 80]. The average length was 10 ± 4.7 nm, with median value of 8.93 nm and the average width was 5.9 ± 2.5 with a median value of 5.17 nm **(Figure 1.3)**. The average aspect ratio (obtained as the ratio of the longest dimension perpendicular to the widest dimension) was 1.97 ± 0.75 for Pt black, 73% larger than 1.14 ± 0.15 obtained for Pt nanopowder (p-value < 0.001).

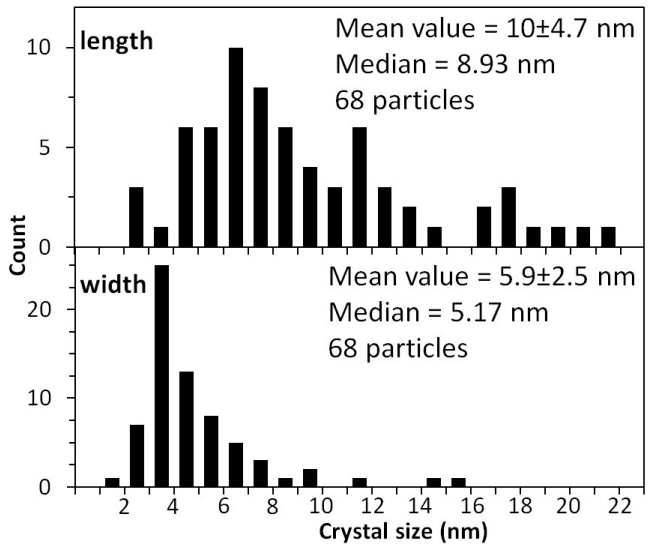

Figure 1.3. Crystal size (length and width) distribution of Pt black by TEM.

4.2. Crystal structure, size and shape of as received and heated samples

Samples were subjected to two different heat treatments in order to understand the effects of moderate to high temperature on the initial properties described above. Powder X-ray diffraction (XRD) profiles for the (111) reflection of Pt black and Pt nanopowder samples are shown in **Figure 1.4**. The full XRD spectra for all samples are characteristic of FCC Pt metal[120] **(Figure S1.3)**. No peaks associated with PtO_x or any impurity phases were detected. Qualitative comparison shows that peak full width at half maximum (FWHM) is inversely related to heating temperature. This trend, combined with an absence of structural defects observable by high resolution TEM, suggests that the reduced crystallinity of Pt black compared to Pt nanopowder is primarily size-induced[125-128].

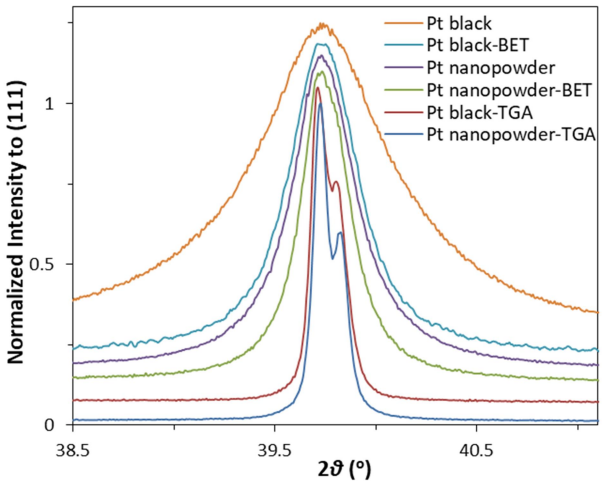

Figure 1.4. X-ray diffraction spectra of (111) reflection. The y-axis is offset in increments of 0.05 between each curve.

Full-profile Rietveld analysis was used to determine average crystallite sizes and assess size-induced lattice strain (see **Figure S1.4** and **Table S1.4** for full results). The fundamental parameters approach (FPA) was used to calculate the contribution of the instrument to the XRD peak widths and confirmed using a silicon standard. Therefore, any additional peak broadening for the Pt samples was assumed to be due to the effects of crystal size and/or microstrain.

The peak profile of both as received samples was best fit with isotropic size broadening. For Pt black, TEM imaging showed that the nanocrystals are elongated in comparison to Pt nanopowder. Taken together this indicates that the elongation does not correspond with a specific crystallographic direction. Thus, we expect no particular crystallographic plane be preferentially exposed at the particle surface. These results were corroborated by TEM crystallographic orientation analysis and suggest that the crystal size obtained through Rietveld refinement is the average for all directions. Pt nanopowder was also best fit with isotropic size induced broadening, which also indicates no preferential crystal orientation. The average crystal size of Pt nanopowder from Rietveld was twice as large as Pt black.

Powder XRD showed a small asymmetry in the peak profiles of Pt black and Pt black-BET towards larger d-spacings. The asymmetry may be due to lattice strain, which would be expected

for the range of particle sizes observed for Pt black and Pt black-BET. Previous studies of Pt have shown lattice contraction with decreasing size[115]. This is consistent with our results as the particle size distribution is up-tailed for these samples, which causes a peak asymmetry in the XRD peak profile towards larger d-spacings[114-115]. Including an anisotropic microstrain parameter during Rietveld analysis provided the best fit of the peak asymmetry for both Pt black and Pt black-BET. The refined values for microstrain correlated with the average particle sizes of Pt black and Pt black-BET. In contrast, the addition of a microstrain parameter did not improve the fits for Pt nanopowder and Pt nanopowder-BET. This is because little or no lattice strain would be expected for the comparatively large particle sizes of these samples.

The refined lattice dimension from Rietveld for each sample correlated well with average particle size (**Figure 1.5** and **Table S1.4**). Pt black and Pt nanopowder samples subjected to TGA heating did not show any size-induced broadening and thus their crystal sizes are assumed to be larger than 1 μm. The refined unit cell dimensions of these samples differed from the published value for the unit cell dimension of bulk Pt by $\leq 0.01\%$[129], indicating that the structure of both Pt black and Pt nanopowder becomes relatively unstrained when subjected to TGA heating due to the increase in crystal size. Crystal growth by sintering is highly dependent on the temperature to which the nanocatalysts are subjected[68, 75, 78, 85]. For example, Páal et al. (1989) showed by TEM analysis that the particle size of Pt black increased much faster when exposed to 633 K compared to 473 K for the same amount of time[78]. This result corroborates the enhanced effect of temperature (samples subjected to TGA heating) compared to exposure to lower temperatures for extended periods of time (samples subjected to BET heating) in our study.

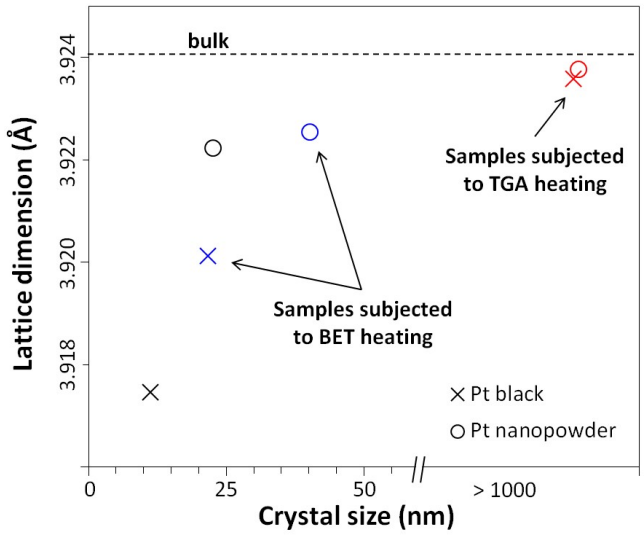

Figure 1.5. Effect of crystal size on lattice dimension (Rietveld analysis) of Pt black and Pt nanopowder. Samples subjected to TGA heating are separated 1 nm apart in the x-axis for graphing purposes.

Specific surface area (SSA) measurements were used to confirm that the increase in crystallinity during heating was due primarily to an increase in crystal size, rather than a decrease in the numbers of internal defects. The SSA of the as received Pt black and Pt nanopowder outgassed at room temperature in the BET was 35.5 ± 0.4 m^2 g^{-1} and 10.4 ± 1.0 m^2 g^{-1}, respectively. Outgassing at 300 ºC for 22 h resulted in a SSA of 11.5 ± 0.3 m^2 g^{-1} for Pt black-BET and 5.1 ± 0.1 m^2 g^{-1} for Pt nanopowder-BET, which corresponds to approximately 1/3 and 1/2 of the SSA of Pt black and Pt nanopowder, respectively. Heating the samples to 300 ºC during BET outgassing increased the crystal size by 1.77 and 1.92 times for Pt nanopowder and Pt black **(Table S1.4)**. These results suggest that the increase in crystallinity was due mainly to crystal growth since annealing defects (e.g., planar faults) would result in a negligible change in surface area.

Specific surface area determination by BET is common in characterization studies of metallic nanocatalysts, and many prior results were obtained on samples that were heated to moderate temperatures during outgassing. Our results show that heating at even moderate temperatures of 300 ºC, which is common in BET outgassing protocols, causes significant and detectable

changes in crystallite size and specific surface area. The effect was greater for Pt black, which has a smaller average particle size than Pt nanopowder. This observation is consistent with numerous studies showing that decreasing size reduces the temperature and time necessary to induce material coalescence during sintering[63, 70, 77, 80]. The possible effects of heating, even if only to moderate temperatures, should be considered in past and future studies of Pt and other metal nanocatalysts because size and surface area have a significant impact on nanocatalyst behavior.

The accessible surface area of both Pt black and Pt nanopowder was evaluated by comparing the SSA from BET with the geometric SSA calculated using crystallites sizes determined by Rietveld analysis. Assuming monodisperse particles, the geometric SSA of the as received Pt black and Pt nanopowder is 40.5 $m^2 g^{-1}$ and 12.7 $m^2 g^{-1}$, respectively. Comparing these sizes to the measured SSA for samples outgassed at room temperature in the BET suggests that the two nanocatalysts expose a similar fraction of their crystallite surfaces (81% for Pt nanopowder and 88% for Pt black). These results suggest that both nanocatalysts are partially aggregated, which was confirmed by small-angle x-ray scattering (SAXS) **(Figure 1.6)**. SAXS results indicate that the average particle size of as received Pt black and as received Pt nanopowder is 18.6 and 31.4 nm, approximately 1.5 times larger than the sizes from Rietveld analysis. The fractions of exposed surface for Pt black and Pt nanopowder determined in this study are significantly larger than estimates from previous studies, also comparing geometric surface area to BET surface area, which range between 20%-50%[78, 85]. This difference supports that the particle size of the samples in these previous studies may have been inadvertently affected by heating during BET outgassing.

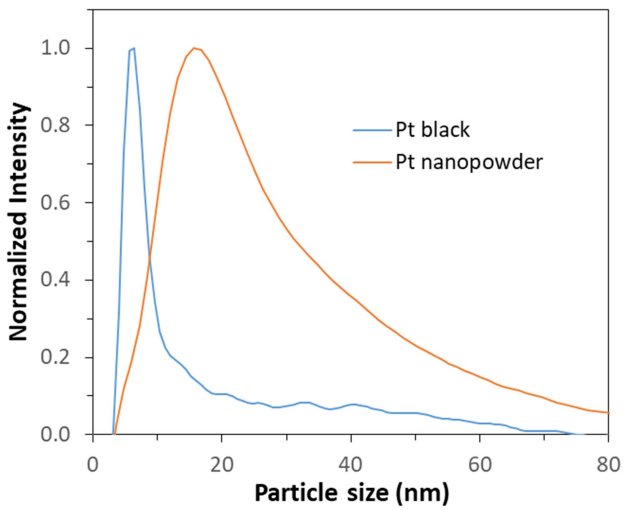

Figure 1.6. Volume-weighted particle size distribution of Pt nanopowder and Pt black from SAXS.

4.3. Surface Chemical Properties

X-ray photoelectron spectroscopy (XPS) was used to evaluate the surface chemical properties of the as received samples and to compare the effects of particle size and heating. XPS analysis of the as received samples showed that the surfaces are composed only of Pt, C and O **(Table 1.1)**. The concentrations of C and Pt are not statistically different between Pt black and Pt nanopowder (p-value=0.99 and p-value=0.10, respectively). In comparison, surface oxygen is 1.7 times higher on Pt nanopowder (p-value=0.01), which has a larger average particle size than Pt black **(Table S1.4)**.

Table 1.1. XPS surface atomic chemical composition analysis of Pt black and Pt nanopowder.

	C	O	Pt
Pt black	40.4 ± 0.9	7.2 ± 0.6	52.3 ± 0.9
Pt black-TGA	47.6 ± 4.1	11.3 ± 1.8	41.1 ± 3.1
Pt nanopowder	40.4 ± 1.9	12.3 ± 1.4	47.2 ± 3.2
Pt nanopowder-TGA	53.3 ± 5.6	14.5 ± 0.8	32.1 ± 6.0

High-resolution XPS analysis of the O1s peak was performed to evaluate the chemical speciation of oxygen present at the surface of both Pt black and Pt nanopowder **(Figure S1.5)**. In addition to having enhanced surface oxygen content, high-resolution XPS analysis of the O1s peak showed that the fraction of oxygen chemisorbed to Pt (O3 component) is 1.5 times higher for Pt nanopowder than for Pt black (p-value=0.03). The fraction of oxygen bonded to carbon (O1 + O2 component) is similar for both nanocatalysts (p-value=0.37) **(Table 1.2)**.

Table 1.2. High resolution XPS O1s peak area analysis.

	O1 + O2	O3	O4
Pt black	81.1 ± 7.7	16.1 ± 3.2	2.8 ± 3.0
Pt black-TGA	31.3 ± 5.0	67.1 ± 5.4	1.6 ± 2.7
Pt nanopowder	75.9 ± 2.4	23.8 ± 2.1	0 ± 0
Pt nanopowder-TGA	58.1 ± 11	40.2 ± 7.5	1.7 ± 1.5

The accumulation and speciation of oxygen on Pt surfaces has been a focus of debate in the literature due to its only partly understood relation to particle size[98-101] and effect on oxidation-reduction reactions[8, 130-131]. The present study shows that larger particle size corresponds with higher surface oxygen content and enhanced fraction of chemisorbed oxygen. This is consistent with results from previous studies also showing that the accumulation of chemisorbed oxygen is enhanced on larger Pt particles, compared to smaller ones[100-101]. The effect was attributed to larger particles having a lower work function, which favors the chemisorption of oxygen onto the surface[100-101]. As opposed to oxygen chemisorbed to the surface of Pt, the amounts of oxygen chemically bonded to Pt (PtO_x) were negligible for both Pt black and Pt nanopowder, i.e., within the measurement error (O4 component).

Surface chemical analysis of the samples subjected to TGA heating suggest that particle size is not the only factor that explains why surface chemisorbed oxygen is enhanced on Pt nanopowder compared to Pt black. Heating the samples to 700 ^{o}C during TGA in air caused an increase in surface oxygen content of 1.56 times for Pt black (p-value=0.047). The surface oxygen content of Pt-nanopowder increased 1.18 times, but the difference was not statistically significant (p-value=0.089), presumably because the surface oxygen content of as received Pt nanopowder was

already enhanced. The increase in surface oxygen concentration for Pt black correlated with a 4.1 times increase in the fraction of chemisorbed oxygen, Pt(O) (p-value<0.001). For Pt nanopowder, heating resulted in a 1.7 times increase in the fraction of Pt(O) (p-value=0.05). An increase in the amount of surface Pt(O) for heated samples has been observed in previous studies. Ono (2011) found that 10-20% surface oxygen was present on Pt nanoparticles exposed to temperatures of 430 ^{o}C in air[116].

The presence of Pt(O) at the surfaces of the as received samples may be related in part to synthesis conditions. Pt nanopowder is synthesized by chemical vapor deposition, which involves temperatures of 700 ^{o}C – 800 ^{o}C. Temperatures in this range are known to promote the incorporation of oxygen in the form of Pt(O)[116]. In contrast, synthesis of Pt black is done by chemical reduction of chloroplatinic acid to metallic Pt at room temperature. Based on our results, this produces a more chemically reduced (i.e., less Pt(O)) surface than Pt nanopowder. Our surface chemical analysis of the TGA heated samples is consistent with this hypothesis.

XPS also indicates the presence of carbon-bearing compounds at the surfaces of both nanocatalysts **(Figure S1.5)**. This is consistent with TEM observations showing the presence of a thin and irregular coating layer on the particle surfaces of both nanocatalysts **(Figure 1.1)**. The average thickness of the coatings is 1.8 ± 0.7 nm and 1.3 ± 0.7 nm for Pt black and Pt nanopowder, respectively. The C1s peak obtained for both Pt black and Pt nanopowder is characteristic of adventitious carbon[132-136]. The fraction of carbon bonded to oxygen became almost negligible when Pt black and Pt nanopowder were subjected to TGA heating (C2 + C3 components). This was accompanied by an increase in the fraction of carbon bonded to carbon or to hydrogen (C1 component). These spectra are characteristic of graphitic-like compounds, which is consistent with the conversion of aliphatic chains (adventitious carbon) into a graphitic carbon due to the materials being subjected temperatures above 450 ^{o}C, in a process known as coke formation[137-144].

4.4. Impact of catalyst properties on catalytic activity

Our characterization results showed that heating affects both particle size and abundance of chemisorbed oxygen at the surface of Pt nanocatalysts. This is important because particle size and surface chemistry directly affect the catalytic activity of Pt nanoparticles in a variety of chemical reactions, such (de)hydrogenation reactions[145], carbon monoxide oxidation[146], oxygen reduction reaction[98-99, 147-148], and decomposition of H_2O_2[8, 11, 15, 35]. Changes in particle size affect the position and shape of the valence band and consequently the surface work function[149]. Larger Pt nanoparticles exhibit lower work function values, which correlates with a lower oxidation potential and confers greater capacity to provide electron density to the reagents[150-151]. Heating Pt in the presence of oxygen promotes dissociative oxygen chemisorption onto its surface and decomposition of surface PtO_x species[116, 152]. This is important for the present study because weakly interacting surface oxygen species have been linked to enhanced activity in chemical reactions that involve transference of oxygen atoms[113, 147, 153].

The overall effect of particle size and surface oxides in the reaction kinetics depends on the reaction mechanism and conditions of reaction[8, 11, 15, 118]. To understand the interplay of average particle size ($\boldsymbol{d}$) and surface atomic oxygen to platinum ratio $(\boldsymbol{O/Pt})_{\boldsymbol{s}}$ in catalytic activity, we compared the rate constant *(**k**)* of H_2O_2 decomposition by Pt black and Pt nanopowder in the as received condition to that of samples heated at 300 ^{o}C for 22h in vacuum during BET outgassing (Pt black-BET and Pt-nanopowder-BET), samples heated at 300 ^{o}C for 22h in air (Pt black-air$_{300}$ and Pt nanopowder-air$_{300}$) and samples heated at 240 ^{o}C for 24h in air (Pt black-air$_{240}$ and Pt nanopowder-air$_{240}$) **(Table 1.3)**.

Table 1.3. Rate constant and activation energy of H_2O_2 decomposition by Pt nanocatalysts.

sample	$(O/Pt)_s$	d, nm	E_a, KJ.mol^{-1}	k, mol.m^{-2}.s^{-1}
Pt black	0.20±0.01	9.38±0.1	33±3	(3.3±0.7)×10^{-3}
Pt black-BET	0.21±0.03	18.7±0.1	34±5	(5.1±1.6)×10^{-3}
Pt black-air$_{240}$	0.24±0.07	10.2±0.9	29±4	(7.9±1.4)×10^{-3}
Pt black-air$_{300}$	0.26±0.02	9.2±0.1	32±4	(1.1±0.2)×10^{-2}
Pt nanopowder	0.32±0.02	21.7±0.1	26±3	(3.5±0.7)×10^{-2}
Pt nanopowder-BET	0.31±0.04	30.2±1.4	21±8	(4.2±1.2)×10^{-2}
Pt-nanopowder-air$_{240}$	0.30±0.04	21.3±0.7	20±8	(3.9±2.1)×10^{-2}
Pt-nanopowder-air$_{300}$	0.30±0.03	22.2±0.1	26±3	(3.3±3.6)×10^{-2}

Results show that the catalytic activity of Pt black correlates with the surface O/Pt ratio. The catalytic activity of Pt black increased 3 times (p-value<0.01) when the sample was heated in air, which corresponded with a 1.3 times increase in O/Pt. In comparison, the catalytic activity of Pt black heated in vacuum (absence of oxygen) only increased 1.5 times (90% confidence level, p-value=0.10). Since the surface oxygen concentration of Pt black and Pt black-BET are similar, we attribute this increase in catalytic activity to the larger particle size. In contrast, the rate constants of Pt nanopowder-BET and Pt-nanopowder heated in air (both at 240 ^{o}C and 300 ^{o}C) were similar to Pt nanopowder in the as received condition (p-value=0.89, p-value=0.70 and p-value=0.83, respectively). The similar rate constants obtained for all Pt nanopowder samples are consistent with the fact that these samples also have a similar surface O/Pt ratio. Overall, the results indicate catalytic activity increases with increasing particle size and surface oxygen abundance. We performed multi-variate analysis of the rate constant of the eight catalyst samples as function of O/Pt ratio and particle size to evaluate the contribution of each variable to the catalytic activity.

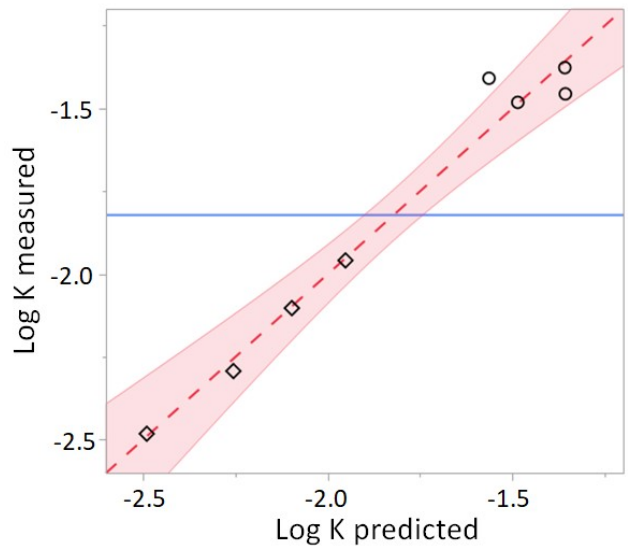

Figure 1.7. Effect of O/Pt ratio and particle size in the rate constant (k) of Pt black (◊) and Pt nanopowder (○) samples.

Figure 1.7 shows that the catalytic activity of Pt black and Pt nanopowder is well described by the combined effect of particle size and O/Pt ratio. All eight catalyst samples fall along one regression line with R^2=0.97 which suggests that particle size and O/Pt ratio explain the majority of variance of the rate constant within the range of studied conditions. The rate constant of H_2O_2 decomposition as function of particle size and O/Pt ratio on these Pt black and Pt nanopowder samples is given by

$$K = 10^{0.4\pm0.5}(d^{0.45\pm0.23})(o/Pt)_s^{4.76\pm0.58} \qquad (1)$$

From this it is clear that surface O/Pt ratio has a stronger effect than particle size on the catalytic activity of platinum in the decomposition of H_2O_2.

These results for Pt black and Pt nanopowder emphasize the importance of surface chemisorbed oxygen in the rate of H_2O_2 decomposition. Relatively weak interactions between Pt and O in chemisorbed oxygen (i.e., Pt(O)) can easily be reduced and re-oxidized[154]. In comparison, the stronger Pt-O bonds for PtO_x species would require larger energy to break, which is not possible given the chemical potentials of the reagents in many reactions[15, 102]. It is worthy to note that the

correlation between surface chemisorbed oxygen and catalytic activity has also been ascribed to a contraction of the surface atomic layer of Pt induced by oxygenated species, resulting in a downshift of the d-band center position[113]. The effect of particle size is explained by the fact that larger metallic nanoparticles exhibit a smaller oxidation potential, which causes more oxygen from H_2O_2 to react with Pt to form Pt(O)[150-151, 153, 155]. This is consistent with the correlation between lattice strain and activation energy of oxygen chemisorption on various Pt alloys, which again has been attributed to particle size effects on the d-band position of the surface Pt atoms[156-157].

We attribute the 10 times higher catalytic activity of Pt nanopowder compared to Pt black, as result of its 2 times larger particle size and 1.5 times higher surface chemisorbed oxygen abundance. However, it is possible that other factors may contribute to the relative lower catalytic activity of Pt black. For example, trace amounts of PtO_x in the Pt black structure due to incomplete reduction of its precursor (Adam's catalyst, PtO_2) may result in a fraction of the catalyst surface that is unreactive towards H_2O_2. Another possibility is that the smaller average particle size of Pt black results in a higher fraction of edges and corners, which are sites characterized by different steric and electronic properties compared to terrace surfaces[99, 116]. Pt atoms at edges and/or corners can establish stronger bonds with oxygen and/or hydroxyl species, which require more energy to be displaced[158]. As a result, Pt nanopowder more easily establishes metastatic interactions with oxidizing reactants, which is associated with enhanced catalytic properties[150].

In this study, a suite of complementary analytical characterization methods were used to quantify fundamental physical and chemical characteristics of two common types of commercial Pt nanocatalysts. Correlations were drawn between changes in particle size and surface chemistry, in particular the abundance of chemisorbed Pt(O). The availability of this information makes it possible to assess and interpret differences in the catalytic activity of these two materials, as demonstrated here by evaluating the effects of particle size and surface chemical composition on the rate of H_2O_2 decomposition. Developing a deeper and more predictive understanding of property-activity relationships in these and other nanocatalysts will improve the efficiency of existing catalysts and the design of future catalyst materials. This will have benefits in many

industrial and technological applications, such as petroleum cracking, catalytic conversion in modern automobiles, hydrogen peroxide sensors, and hydrogen fuel cells[61, 65, 68, 76, 159].

5. *Conclusions*

This study measured and compared the atomic structural, physical and chemical properties of two commercial platinum nanocatalysts both as received and after exposure to two common heating protocols used as part of standard characterization. Smaller average particle sizes corresponded with increased lattice strain and a lower abundance of surface oxygen. Oxygen associated directly with platinum at the surface of these nanocatalysts is in the form of chemisorbed oxygen and no significant amounts of chemically bonded oxygen (i.e., PtO_x) were found. The concentration of chemisorbed oxygen increases with increasing particle size, as well as due to heating of the nanoparticles in the presence of oxygen (air). Samples with smaller average particle sizes are more susceptible to the effect of heat both in terms of crystal growth and increased surface oxygen. Average particle size and surface composition directly affected the surface electronic properties of metallic nanoparticles and consequently their catalytic behavior, which was evaluated here in terms of H_2O_2 decomposition. Our results show that larger average particle size and higher surface chemisorbed oxygen abundance both correlated with enhanced activity toward the decomposition of H_2O_2.

In summary, this study highlights the inherent variability of commercial platinum nanocatalysts, particularly in terms of average particle size and surface oxygen abundance. The results also show how those differences affect their susceptibility to external conditions, such as mild heat exposure during, for example, BET outgassing. Surface oxygen plays an important role in oxidation-reduction reactions catalyzed by platinum nanocatalysts, such as H_2O_2 decomposition, which we used here as a model reaction to quantify and compare catalytic activity. These results are important for the development of more robust property-activity relationships of Pt and other metal nanocatalysts.

Chapter 2

Mechanism and Kinetics of Hydrogen Peroxide Decomposition on Platinum Nanocatalysts

Rui Serra-Maia [Ɨ], Marion Bellier [Ɨ], Stephen Chastka [Ɨ], Kevin Tranhuu [Ɨ], Andrew Subowo [Ɨ], J. Donald Rimstidt [Ɨ], Pavel M. Usov [¥], Amanda J. Morris [¥], F. Marc Michel [Ɨ]

[Ɨ] Department of Geosciences, Virginia Polytechnic Institute and State University, Blacksburg VA, USA

[¥] Department of Chemistry, Virginia Polytechnic Institute and State University, Blacksburg VA, USA

Author contributions: RS-M, MB, SC, KT and AS performed rate measurements of H_2O_2 decomposition; RS-M performed most characterization of platinum nanocatalysts. PMU performed cyclic voltammetry analysis. The paper was written by RS-M with input from MB, SC, KT, AS, JDR, PMU, AJM and FMM.

Citation:

Serra-Maia R., Bellier M., Chastka S., Tranhuu K., Subowo A., Rimstidt J.D., Usov P.M., Morris A.J., Michel F.M. (2018) Mechanism and Kinetics of Hydrogen Peroxide Decomposition on Platinum Nanocatalysts, *ACS Appl. Mater. Interfaces,* vol. 10, pp. 21224 – 21234.

1. Abstract

The decomposition of H_2O_2 to H_2O and O_2 catalyzed by platinum nanocatalysts controls the energy yield of several energy conversion technologies, such as hydrogen fuel cells. However, the reaction mechanism and rate limiting step of this reaction have been unsolved for more than 100 years. We determined both the reaction mechanism and rate limiting step by studying the effect of different reaction conditions, nanoparticle size and surface composition on the rates of H_2O_2 decomposition by three platinum nanocatalysts with average particle sizes of 3 nm, 11 nm and 22 nm.

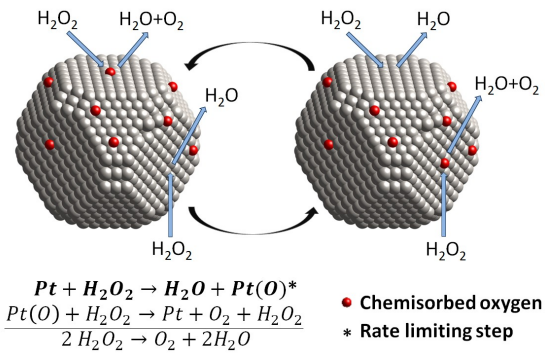

Rate models indicate that the reaction pathway of H_2O_2 decomposition is similar for all three nanocatalysts. Larger particle size correlates with lower activation energy and enhanced catalytic activity, explained by a smaller work function for larger platinum particles, which favors chemisorption of oxygen onto platinum to form Pt(O). Our experiments also showed that incorporation of oxygen at the nanocatalyst surface results in a faster reaction rate because the rate limiting step is skipped in the first cycle of reaction. Taken together these results indicate that the reaction proceeds in two cyclic steps and that step 1 is the rate limiting step.

Step 1	$\boldsymbol{Pt + H_2O_2 \rightarrow H_2O + Pt(O)}$
Step 2	$Pt(O) + H_2O_2 \rightarrow Pt + O_2 + H_2O$
Overall	$2\,H_2O_2 \rightarrow O_2 + 2\,H_2O$

Establishing relationships between the properties of commercial nanocatalysts and their catalytic activity, as we have done here for platinum in the decomposition of H_2O_2, opens the possibility of improving the performance of nanocatalysts used in applications. This study also demonstrates the advantage of combining detailed characterization and systematic reactivity experiments to understand property-behavior relationships.

2. *Introduction*

The decomposition of hydrogen peroxide (H_2O_2) catalyzed by platinum (Pt) through a non-electrochemical pathway (without addition of electrons from an anode) is an important reaction in many energy conversion applications ranging from miniaturized spacecraft to underwater vehicles[6, 24-25]. This reaction is also important in the oxygen reduction reaction (ORR) in hydrogen fuel cells, where it reduces efficiency by acting as a parasitic parallel pathway of the fully electrochemical conversion of O_2 to H_2O[26-28, 118] **(Figure S2.1)**. Despite its importance, the reaction pathway of H_2O_2 decomposition on both supported and colloidal Pt catalysts has been an unresolved question for more than 100 years[8-9, 11, 13, 15-16, 160]. This is due to a general lack of systematic studies that use multivariable analysis to simultaneously understand the effects of both catalyst properties and reaction conditions. The resulting knowledge gap has prevented scientists from explaining the enigmatic variable performance of Pt nanocatalysts in the decomposition of H_2O_2 and hindered the design of more efficient catalysts[6, 10, 24]. Our study aimed to establish how surface chemical and structural properties of colloidal forms of two commercial Pt nanocatalysts dictate their catalytic activity. For that, we used multivariable analysis to understand the effects of five key variables: nanocatalyst size, surface composition, reaction temperature, pH, and H_2O_2 concentration. These results lead to a better understanding of how surface chemical and physical properties of Pt and other Pt group element (PGE) catalysts relate to catalytic behavior.

Several different reaction pathways have been proposed to explain the decomposition of H_2O_2 on PGE surfaces **(Table 2.1)**[8-9, 11, 13, 15-16, 68, 160-164].

Table 2.1. Proposed mechanisms of H_2O_2 decomposition on platinum group metal surfaces.

Name/supporting references	Mechanism/reaction steps	Testable predictions
1) Oxygen-oxide mechanism[165]	$xPt + ½\ yO_2 = Pt_xO_y$ $Pt_xO_y + yH_2O_2 = xPt + yH_2O + yO_2$	Induction period for metallic surfaces[8]. Reaction rate does not increase for catalysts pretreated with H_2O_2.
2) Peroxide-oxide mechanism[4, 5,166]	$Pt + H_2O_2 = Pt(O) + H_2O$ $Pt(O) + H_2O_2 = Pt + O_2 + H_2O$	Surface oxygen concentration of catalysts pretreated with H_2O_2 depends on relative rates of step 1 vs step 2 and is independent of $C_{H_2O_2}$ [15] (see section 4.3). pH does not have a primary effect in the reaction rate[11, 167].
3) Perhydroxyl anion-oxide mechanism[8]	$H_2O_2 = O_2H^- + H^+$ $Pt(O) + O_2H^- = Pt + OH^- + O_2$ $Pt + O_2H^- = Pt(O) + OH^-$	Reaction rate is first order in terms of $a_{O_2H^-}$[8]. Reaction is first order in $C_{H_2O_2}$ if all active sites are covered with oxygen (PtO)[8]. For lower coverages reaction order increases[8].
4) Electrochemical mechanism[9, 11, 167-168]	$H_2O_2 + e^- = OH^- + \bullet OH$ $H_2O_2 = O_2H^- + H^+$ $O_2H^- = \bullet O_2H + e^-$ $\bullet O_2H = O_2^- + H^+$ $O_2^- + H_2O_2 + OH^- + \bullet OH + O_2$ $2\ \bullet OH = H_2O_2$	Lowering catalyst work function increases reaction rate[11]. Hydroxyl radicals are generated[9, 168]. Open circuit potential matches loss of an electron from platinum[169]. Less conductive surfaces are less catalytically active[117, 170]. Reaction rate does not change for catalysts pretreated with H_2O_2.
5)Eley-Rideal mechanism[164, 171][1]	$H_2 + 2Pt = 2Pt\text{-}H$ $½\ O_2 + Pt = Pt\text{-}O$ $Pt + OH^- = Pt\text{-}(OH)_{ads} + e^-$ $Pt\text{-}(OH)_{ads} + H_2O_2 = Pt\text{-}(OOH)_{ads} + H_2O$ $Pt\text{-}H + H_2O_2 + e^- = Pt + H_2O + OH^-$ $Pt\text{-}(OOH)_{ads} + Pt\text{-}(H)_{ads} = 2Pt + O_2 + H_2$ $Pt\text{-}O + 2Pt\text{-}H = Pt\text{-}H_2O + 2Pt$ $Pt\text{-}H_2O = Pt + H_2O$	Molecular H_2 and O_2 are present in solution[171]. Reaction rate is strongly affected by pH when platinum is used as catalyststt[171-172].

[1]The study performed in Ref[171] was done under corona discharging conditions.

In most cases, H_2O_2 decomposition on Pt is first order in terms of H_2O_2 concentration[8-9, 11, 15-16, 160, 163, 165, 171, 173] although exceptions have been observed for $C_{H_2O_2} < 10^{-4}\ M$. Low H_2O_2 concentrations resulted in inconsistent rate measurements and replicability issues, which were attributed to insufficient H_2O_2 to overcome the chemical potential necessary to convert PtO_x to Pt[15]. Increasing pH causes an increase in H_2O_2 decomposition rate to a maximum that was determined experimentally to be near pH 10.5[8, 11, 167]. Radical species have been detected when the decomposition of H_2O_2 is catalyzed by certain transition metals[13, 167, 174-175], but there currently is no evidence for radical species generation on Pt[167].

The catalytic activity of Pt in the decomposition of H_2O_2 is known to also depend on the structural and/or surface chemical properties of the catalyst[8, 11, 15, 35]. Higher concentrations of surface oxygen correlate with enhanced H_2O_2 decomposition rates, but a mechanistic understanding for this correlation has not yet been established[8, 11, 15, 35]. Higher H_2O_2 decomposition rates also match with enhanced cold-working of platinum catalysts. This effect was initially attributed to an increase in structural dislocations[10, 176], but was later ascribed to an enhancement of surface oxygen[8].

Particle size is another important factor in Pt reactivity because it influences the ability of metal nanoparticles to accept or donate charge[99, 103, 150]. However, this effect has never been studied for the decomposition of H_2O_2. Particle size effects are generally not well understood due to the complex interplay of multiple factors[50, 99, 116, 118, 177]. As the size of metal nanoparticles decreases, both the work function and the Pauling's electronegativity increase, which reduces their ability to provide charge[178]. For Pt, the ionization potential varies between 9.0 eV for a single atom and 5.3 eV for the bulk metal (i.e., the work function)[150]. With decreasing particle size the ratio of edges/corners to terraces increases as function of 1/d. These sites are more undercoordinated and form stronger bonds in comparison with atoms at terrace sites[150]. These differences are important as they result in variable binding energies of the reactants onto the catalyst surface[179]. The optimum activity is obtained for intermediate binding energy values, which represent a compromise between low activation energy for the reaction, and a surface with low reactant coverage[150, 180].

This paper reports the rates of H_2O_2 decomposition as a function of H_2O_2 concentration, pH and temperature by two common Pt nanocatalysts, known as Pt black and Pt nanopowder. Our characterization of these samples, which have different average crystal size and shape characteristics, revealed new information regarding the abundance and speciation of surface oxygen[17]. The results from that study showed that oxygen at the surfaces is primarily chemisorbed with platinum, and that its abundance increases with increasing particle size. Rate models obtained for both catalysts were used to infer the reaction pathway of H_2O_2 decomposition on Pt nanocatalysts and identify the rate limiting step of reaction, thus providing a molecular-scale understanding of the decomposition mechanism of H_2O_2 on Pt. The new and detailed understanding of the H_2O_2 decomposition mechanism on Pt nanocatalysts described here is crucial for improving current and future catalysts used in energy conversion technologies that depend on this reaction.

3. Materials and Methods

3.1. Platinum black and platinum nanopowder

Pt nanopowder is synthesized by combustion chemical vapor condensation and the particle size reported by the manufacturer is ≤ 50 nm. Pt black is derived from high temperature reduction of H_2PtCl_6 to metallic Pt[65, 159] and has an average aggregate size reported by the manufacturer of ≤ 20 μm. Pt black aggregates are composed of individual nanoparticles, despite occurring as micrometer-sized aggregates in the form of dry powder[17]. Pt black and Pt nanopowder are characterized by different average crystal size, shape, and surface oxygen concentration. Average values for crystal size, specific surface area, aspect ratio, lattice strain and surface O/Pt ratio of the two materials are given in **Table 2.2.**

3.2. Rate measurements

Hydrogen peroxide decomposition rate measurements were performed in well-stirred 1 L Erlenmeyer flasks. Data were collected over the concentration range of 100 μM < $C_{H_2O_2}$ < 1000 μM, the pH range of 2.7 < pH < 9.3 and the temperature range of 0 ^{o}C < T < 55 ^{o}C. For experiments carried at near 0 ^{o}C the reactor was immersed in an ice bath and temperature was allowed to equilibrate before initiating the experiments. For experiments carried at temperatures above room temperature the reactor was heated directly on a heating-stir plate. Experiments were conducted when the temperature variation was smaller than 0.4 ^{o}C / min. The temperature of the H_2O_2 solution was recorded at the start and at the end of each run, and the average of both measurements was used for data analysis.

For each run 6 mg of Pt black or Pt nanopowder were dispersed in 5 mL of H_2O at pH 11 and sonicated for 1 minute to enhance particle dispersion. This dispersion was added to the Erlenmeyer flask containing 1 L of H_2O_2 solution previously prepared at the concentration of H_2O_2, pH and temperature conditions specific to each run. The solution was sampled at 10 sec, 1, 2, 3, 4 and 5 mins. Each sample consists of a 1 mL aliquot that was filtered through a 0.22 μm

pore size syringe filter. The xylenol-orange spectrophotometric method[181] was used to determine the concentration of H_2O_2 of the solution samples. For that, 500 µL of filtrate were transferred into a spectrophotometer cuvette and immediately mixed with 250 µL of 100 mM of xylenol-orange and 250 µL of 250 mM ferrous ammonium sulfate in that order. This protocol was designed for a maximum concentration of H_2O_2 of 100 µM, so when higher concentrations of H_2O_2 were analyzed the filtered solutions were diluted. The cuvettes were then incubated in the dark for 30 mins and their absorbance was read at 560 nm against a blank containing 500 µL of water in place of the filtrate solution. The concentration of H_2O_2 was calculated from the absorbance of each aliquot. A new calibration curve was prepared each day.

The rate of H_2O_2 decomposition was determined using the initial rate method. The concentration of H_2O_2 was fitted as a function of time with a quadratic equation[182] **(Figure S2.4)**. The initial rate of decomposition was calculated from the slope of the curve at t=0.

3.3. Rate models

For each catalyst the specific rate of H_2O_2 decomposition was regressed against H_2O_2 concentration, pH and temperature **(see Table 1.3 for notation)**.

$$R = \frac{-dC_{H_2O_2}}{dt} = k \cdot C_{H_2O_2}^{n_1} \cdot a_{H^+}^{n_2} = (\mathrm{A} \cdot e^{\frac{E_a}{R \cdot T}}) \cdot C_{H_2O_2}^{n_1} \cdot a_{H^+}^{n_2} \quad (7)$$

This equation can be linearized by a log transformation.

$$log\, R = log\, k + n_1 \cdot log\, C_{H_2O_2} + n_2 \cdot log\, a_{H^+} = \log A - \frac{E_a}{2.303 \cdot R} \cdot \frac{1}{T} + n_1 \cdot \log\, C_{H_2O_2} - n_2 \cdot pH (8)$$

The generalized form of this equation has 4 fitting parameters (a, b, c and d).

$$log\, R = a + \frac{b}{T} + c \cdot log\, C_{H_2O_2} - d \cdot pH \quad (9)$$

Multi-variate linear regression analysis was applied to each data set, using JMP Pro 12.0.1 (SAS Institute Inc.), to obtain values for E_a, k, n_1 and n_2. The regression coefficients obtained were used to evaluate the contribution of each independent variable to the overall fit[183]. The p-value for each coefficient was used to evaluate the statistical significance of the contribution of each variable.

3.4. Concentrated H_2O_2 pretreatment

The catalytic activity of Pt black and Pt nanopowder pretreated with H_2O_2 was evaluated by reacting each nanocatalyst with a range of concentrated solutions of H_2O_2 ($C_{H_2O_2}^{pre}$) prior to the rate measurement. For each pretreatment 6 mg of Pt black or Pt nanopowder were reacted with 2 mL of H_2O_2 at a concentration ranging from 0.003% (v/v) to 3% (v/v) of H_2O_2. The suspensions were agitated for 20 seconds and then transferred to a falcon tube along with 5 mL of water at pH 11. The suspension was sonicated for 1 minute. The sonicated suspension was then added into a 1 L Erlenmeyer flask containing H_2O_2, and the rate of H_2O_2 decomposition was determined following the procedure for rate measurements described earlier. In these experiments $C_{H_2O_2}$, pH and temperature were maintained constant, and the only variable studied was $C_{H_2O_2}^{pre}$.

3.5. Heat treatment of catalysts

The rate of H_2O_2 decomposition by heated samples (in atmospheric conditions) of Pt black and Pt nanopowder was compared with the samples analyzed in the as received form. Pt nanopowder and Pt black were heated at 240 ^{o}C for 24h in atmospheric conditions. These samples are designated Pt nanopowder-240 and Pt black-240, respectively. Six rate measurements were performed for each heat-treated catalyst: $C_{H_2O_2} = 100\ \mu M, 300\ \mu M$ and $1000\ \mu M$ at room (~22°C) and high temperature (~50 ^{o}C) conditions. For all runs pH was ~5.9.

The rate of H_2O_2 decomposition by heat-treated Pt black and Pt nanopowder was evaluated in the same way as for samples in the as supplied condition (see section 3.2).

3.6. •HO detection

An attempt was made to detect hydroxyl radicals (•HO) in solution during the decomposition of H_2O_2 on Pt black following an established protocol[184]. In this experiment, 20 mL of 100 µM or 1000 µM H_2O_2 along with 50 mM DMSO (Sigma-Aldrich, St. Louis, MO USA) were added to a flask containing 80 mL of 3.7 mg of Pt black. Aliquots of a mixture of 80 mL containing 3.7 mg of Pt black plus 20 mL of 50 mM DMSO without H_2O_2 were used as blanks. Reaction of DMSO with •HO produces methane sulfinic acid that can be detected by a protocol developed by Babbs et al., 1986[185] with a theoretical sensitivity of 10 $nmol \cdot mL^{-1}$. A 1 mL aliquot of the aqueous mixture of DMSO, Pt particles and H_2O_2 was filtered through a 0.22 µm filter into a test tube containing 1 mL of 2 M sulfuric acid. Then 8 mL of butanol, previously added with 1 mL of 1 M sulfuric acid, was added to the sample and mixed for 30 s. The upper butanol phase was removed to a second clean tube containing 4 mL of sodium acetate buffer and mixed thoroughly. The two phases were allowed to separate for 3 min by gravity. Color development was initiated by transferring the lower aqueous phase into a third test tube containing 2 mL of 15 mM Fast Blue BB salt, freshly prepared, to form diazofulfone. The sample was subsequently incubated for 10 minutes at room temperature in the dark. Finally, 3.0 mL of 1:1 (v/v) toluene/butanol was mixed with the aqueous phase and the lower phase, containing unreacted diazonium salt, was discarded. The tube was centrifuged at 500 g for 3 min and the upper phase, which contains diazosulfones was transferred into a cuvette. The absorbance of the sample was determined at 420 nm against the blank. The calibration curve developed by Babbs et al., 1986[185] was used to determine the concentration of hydroxyl radicals in the samples analyzed in this study.

3.7. X-ray photoelectron spectroscopy (XPS) of heat treated catalysts

XPS analysis was done using a PHI Quantera SXM scanning photoelectron spectrometer microprobe. Pt catalysts preheated at 240 ^{o}C for 24 h in atmospheric conditions were deposited on double coated carbon conductive tape (Ted Pella, USA). High-resolution XPS data were collected for Pt4f, O1s, and C1s peaks with 0.1 eV of energy resolution at a pressure of 10^{-7} Pa. The raw data were processed using Phi Multipak software. Charging was referenced to the C1 component of adventitious C1s peak at a binding energy of 284.8 eV for all samples[137].

3.8. X-ray diffraction Rietveld analysis

Powder X-ray diffraction data were collected for all samples. Rietveld analysis was performed using Profex 3.20.2[119]. This software uses a fundamental parameters approach (FPA) to calculate the instrumental weight function from the device configuration. A silicon NIST640d standard for line position and line shape was used to verify the instrumental weight function. The data for silicon were fitted with a function (RP2) that had no specimen influence on line shapes. No spherical harmonics correction was used. Only the initial unit cell parameter (a), isotropic displacement (thermal) parameter, and scale factor were allowed to vary freely during the refinement. The initial unit cell parameter (a) and isotropic displacement parameters, and space group $Fm\overline{3}m$ (no. 225) for face-centered cubic (FCC) platinum with a Wyckoff value of 4a were used from crystallographic information file (CIF) number 0011157 obtained from the AMCSD[120]. A pseudo-Voigt function (RP4) to model peak profiles and spherical harmonics correction (SPHAR4) were used in all fits. The displacement parameter was left fixed at the initial value (U=0.001). The fitting strategy used a single Pt phase affected by size-induced broadening (B1) and anisotropic microstrain (k2). The unit cell dimension and B1 were first allowed to vary freely and then k2 was added to the refinement.

3.9. Electrochemical analysis of Pt black and Pt nanopowder

Cyclic voltammetry (CV) was used to compare the oxidation potential of Pt black and Pt nanopowder. The experiments were carried out on a BASi EC Epsilon potentiostat using a standard three-electrode cell. Glassy carbon disk (diameter = 3 mm) was used as a working electrode, while high surface area Pt mesh was used as a counter electrode and Ag/AgCl (saturated $KCl_{aq.}$) as a reference electrode. For the measurements, 0.1 M Na_2SO_4/H_2O or 0.5 M H_2SO_4/H_2O (prepared from Millipore water, 18.3 MΩ, and analytical grade reagents) were used as supporting electrolyte, which were bubbled with high purity argon for 15 min. The potential of the reference electrode was calibrated in each electrolyte using ferricyanide ($E_{1/2}([Fe(CN)_6]^{3-}/[Fe(CN)_6]^{4-})$ = 0.164 V vs Ag/AgCl). For the sample preparation, acetonitrile suspensions of Pt black and Pt nanopowder were deposited onto the working electrode. Upon evaporation of the solvent, a uniform layer of Pt particles was formed on the electrode surface. The voltammograms were collected at room temperature using 100 mV s^{-1} scan rate.

4. Results and Discussion

4.1. Characterization of Pt black and Pt nanopowder

High-resolution TEM analysis from our previous work showed that Pt black and Pt nanopowder consist of nanosized Pt particles[17]. Dilute suspensions of the samples resulted in small aggregates and isolated crystallites (nanoparticles) when deposited on continuous film SiN TEM grids **(Figure S2.2)**. Average values for crystal size, specific surface area, aspect ratio, lattice strain and surface O/Pt ratio of the two nanocatalysts are given in **Table 2.2**. The elongation observed on Pt black crystallites occurs along random directions and no particular crystallographic plane is preferentially exposed for either catalyst. When dispersed in aqueous solutions the crystallites of both catalyst samples are partly aggregated and the extent of aggregation is similar for both[17].

Table 2.2. Physical properties of Pt black and Pt nanopowder. Uncertainties shown in parentheses.

	Pt black	Pt nanopowder
Crystal size (XRD Rietveld), *nm*	11.31(4)	22.70(4)
Specific surface area (BET), $m^2 \cdot g^{-1}$	35.5(4)	10.4(9)
Aspect ratio (TEM)	1.9(8)	1.1(2)
Lattice strain, Reference to bulk Pt	-0.09 %	-0.02 %
O/Pt ratio (XPS)	0.14(1)	0.26(5)

4.2. Catalytic activity of Pt black, Pt nanopowder and Pt-Liu-3nm

The rate equations reported here are intended to model the rate of H_2O_2 decomposition as a function of different $C_{H_2O_2}$, pH, and temperature (see section 3.3 for derivation of rate model).

These variables are known to affect the rate of H_2O_2 decomposition on Pt[8-9, 11, 13, 15]. Previous work by Liu et al. (2014) on colloidal suspensions of 3 nm Pt nanoparticles (Pt-Liu-3nm)[13] were analyzed along with the results obtained in our study. For Pt nanopowder there are 36 data points, for Pt black there are 30 data points and for Pt-Liu-3nm there are 6 data points. **Table 2.3** gives the notation with units used in this paper. Data from rate measurements performed for Pt black, Pt nanopowder and Pt-Liu-3nm as function of $C_{H_2O_2}$, pH, and temperature are given in **Table S1**.

Table 2.3. Notation used.

R	Rate of H_2O_2 decomposition, $mol/m^2 \cdot s$
$C_{H_2O_2}$	Concentration of H_2O_2, mol/L
t	Time, sec
A	Pre-exponential constant in Arrhenius equation, $mol/m^2 \cdot s$
E_a	Activation energy, J/mol
R	Gas constant, 8.314 $J/mol \cdot K$
T	Temperature, K
a_{H^+}	Activity of H^+ ion
a, b, c, d	Fitted parameters from regression model
k	Rate constant, $mol/m^2 \cdot s$
n_i	Reaction order for species i
R^2	Coefficient of determination for regression model
d	Crystal size (diameter), m
$Pt(O)$	Chemisorbed oxygen on Pt
$A_{Pt(O)}$	Average fraction of surface covered with Pt(O)
A_{Pt}	Average fraction of metallic surface
θ	$A_{Pt(O)}/A_{Pt}$
v_i	Rate of reaction step i

The catalyzed rate of H_2O_2 decomposition for each of the three catalysts is shown in **Figure 2.1**.

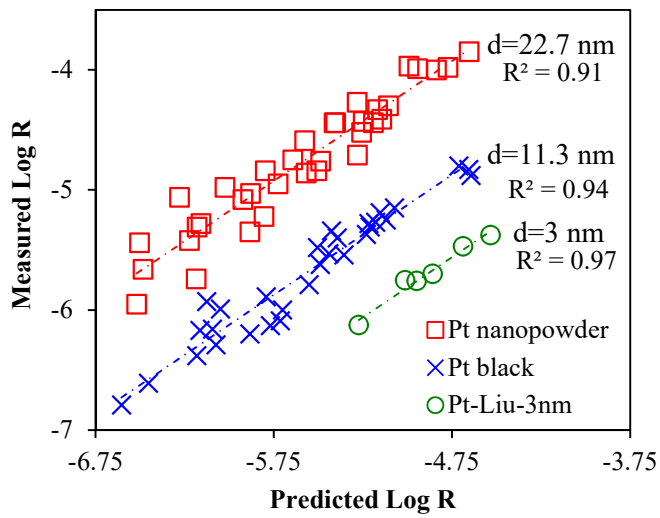

Figure 2.1. Regression model of log measured $\boldsymbol{R}$ vs log predicted $\boldsymbol{R}$ as function of $\boldsymbol{C_{H_2O_2}}$, a_{H^+} and $\frac{\mathbf{1}}{\boldsymbol{T}}$.

The rate of H_2O_2 decomposition as function of $C_{H_2O_2}$, a_{H^+}, and $\frac{1}{T}$ on Pt nanopowder is given by

$$R = 10^{2.81}(e^{-\frac{(26\pm3)10^3}{R}\cdot\frac{1}{T}})(C_{H_2O_2}^{0.94\pm0.07})(a_{H^+}^{-0.05\pm0.01})$$

On Pt black is given by

$$R = 10^{3.46}(e^{-\frac{(33\pm3)10^3}{R}\cdot\frac{1}{T}})(C_{H_2O_2}^{0.97\pm0.06})(a_{H^+}^{-0.02\pm0.01})$$

And on Pt-Liu-3nm is given by

$$R = 10^{-3.32}(C_{H_2O_2}^{1.08\pm0.1})(a_{H^+}^{-0.04\pm0.01})$$

The regression model indicates that the rate of H_2O_2 decomposition follows first order kinetics in terms of H_2O_2 concentration for all three nanocatalysts. Any differences in the order of reaction in terms of H_2O_2 concentration are not statistically significant (p-value = 0.48). This agrees with

previous studies[8-9, 11, 15-16, 160, 165, 171, 173] and indicates that in the rate limiting step of the reaction one molecule of H_2O_2 reacts with the active site[186]. The effect of pH is relatively small compared to $C_{H_2O_2}$, but is statistically significant for Pt black, Pt nanopowder, and Pt-Liu-3nm (p-value = 0.048, p-value < 0.001, and p-value=0.038, respectively) and similar for all three (p-value = 0.10). Contrary to these results, some previous studies have suggested that pH has a strong effect on the rate of H_2O_2 decomposition by Pt group metal catalysts[9, 11, 15]. However, this disparity may be simply a consequence of plotting the rate of H_2O_2 decomposition on a linear scale against a log-scale for pH. In any case, the effect of pH on catalytic activity is smaller than one log-unit over the range of 6 pH (log-scale) units for all three catalyst samples.

The small pH effect on the H_2O_2 decomposition rate is inconsistent with the perhydroxyl anion-oxide and the Eley-Rideal mechanisms **(Table 2.1)**. In the case of the perhydroxyl anion-oxide mechanism, if HO_2^- were to be the only active species that interacts with the catalyst surface, the decomposition of H_2O_2 should be first order in terms of $a_{HO_2^-}$ (directly correlated with a_{H^+}), which is not supported by our results. The Eley-Rideal mechanism, first proposed by Mededovic et al. (2006), depends on molecular hydrogen and oxygen formed via high-voltage aqueous-phase pulsed corona electrical discharge on Pt electrodes. Computational[171] and experimental[172] studies at analogous conditions showed that the H_2O_2 decomposition rate increases several orders of magnitude in the pH range 3.5 to 10.5. Unfortunately, this mechanism has been inadvertently used to explain the decomposition of H_2O_2 on Pt surfaces that were not actually subjected to electrical discharge conditions[24-25, 164]. Thus, the small pH effect on the H_2O_2 decomposition rate by Pt catalysts reported here indicates that the Eley-Rideal mechanism is not suitable to describe the decomposition of H_2O_2 on Pt surfaces that are not subjected to electrical discharges[171-172].

The effect of pH alone is not sufficient to reject the remaining three possible mechanisms (oxygen-oxide, peroxide-oxide and electrochemical)[11, 13, 15-16]. In the case of the mechanisms involving surface oxides (oxygen-oxide and peroxide-oxide mechanisms), the effect of pH is indirect as neither H^+ nor OH^- ions are directly involved. Bianchi et al. (1961) proposed that the lower rates of H_2O_2 decomposition on Pt surfaces at low pH values are caused by surface poisoning effects as H^+ ions sorb onto metal surfaces to fulfill their electron deficiency, thus preventing the formation of Pt(O)[15, 163]. This idea was corroborated by Ou et al. (2009) who used

first principle calculations to show that the chemisorption of O_2 on Pt (111) is slightly inhibited in the presence of hydrogen ions near the surface[187]. The known inhibition of H_2O_2 decomposition caused by Cl^- ions is also consistent with this explanation. Arruda et al. (2008) showed that Cl^- ions chemisorb to the surface of Pt nanoparticles (1-2 nm diameter), which is in direct competition with chemisorbed oxygen[188]. In the electrochemical mechanism, pH directly affects the concentration of H^+ and the balance between HO_2^- and H_2O_2, all of which are the active species that react with Pt at different stages. Based on the dissociation constants of H_2O_2 and HO_2^-, Weiss (1935) showed that it was possible to predict explicitly that the rate of H_2O_2 decomposition reaches its maximum at pH~10.5 (see derivation on Mckee et al., 1969)[9, 11, 168]. This is consistent with the fact that experimental values for the pH corresponding to maximum rate of H_2O_2 decomposition are not significantly affected by catalyst composition[11, 189]. In this mechanism the initial dissociation of the H_2O_2 molecule is thought to occur due to electron donation from the metal. According to Weiss (1935), H_2O_2 acts as the oxidizing agent to the metal and HO_2^- acts as reducing agent[9].

In summary, the effect of pH is sufficient to exclude the perhydroxyl anion-oxide and the Eley-Rideal mechanisms, but is consistent with the oxygen-oxide, peroxide-oxide, and electrochemical mechanisms. As discussed in sections 4.3 and 4.4, we found that Pt nanocatalysts with larger particle sizes and/or higher surface chemisorbed oxygen correlate with enhanced catalytic activity. Those results are not consistent with the electrochemical or the oxygen-oxide mechanisms and support that the H_2O_2 decomposition on Pt nanocatalysts occurs *via* the peroxide-oxide mechanism.

4.3. Effect of particle (crystallite) size on catalytic activity

For the range of conditions studied, the rate of H_2O_2 decomposition decreases with particle size in the order of Pt nanopowder (d=22.7 nm) > Pt black (d=11.3 nm) > Pt-Liu-3nm (d=3 nm). The catalytic activity of Pt nanopowder normalized to specific surface area is approximately 10 times greater than Pt black **(Figure 2.1)**, which is consistent with the 21% lower activation energy (see section 4.2) of Pt nanopowder compared to Pt black (p-value=0.039). The catalytic activity of Pt-

Liu-3nm is approximately six times lower than Pt black. The difference in activation energy could not be determined since the Liu et al. (2014) experiments were only done at a single temperature[13]. Changes in particle size could lead to differences in surface reactivity if certain surface sites become preferentially exposed. However, combined Rietveld and TEM analysis suggest that the direction of crystal elongation is random for Pt nanopowder and Pt black[17]. This means that preferential exposure of specific crystal faces (i.e., active sites) does not explain the 10-fold difference in catalytic activity between Pt nanopowder and Pt black.

A correlation between increasing particle size and enhanced catalytic activity has been observed previously for Pt nanocatalysts used in hydrocarbon oxidation reactions[50, 131] and the oxygen reduction reaction[98-99]. To evaluate whether catalytic activity is size-dependent for the samples in this study, the H_2O_2 decomposition rates of the three catalysts were regressed together as function of d in addition to $C_{H_2O_2}$, a_{H^+}, and $\frac{1}{T}$. This regression showed that the catalytic activity of the three Pt nanocatalysts fall along a unique linear regression curve with $R^2 = 0.95$ **(Figure 2.2)**.

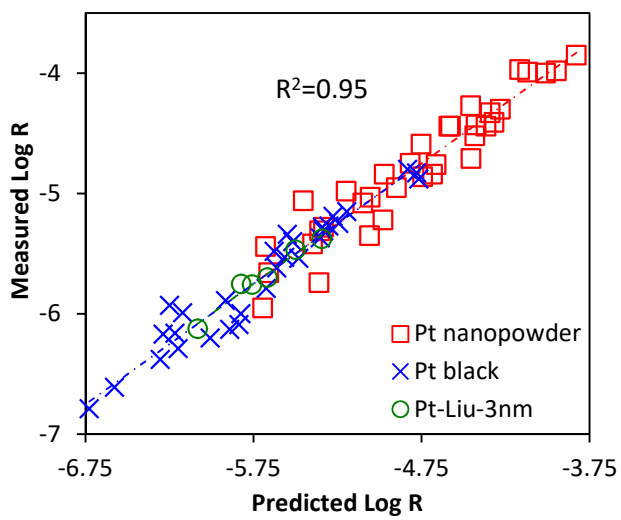

Figure 2.2. Regression model of log measured $\boldsymbol{R}$ vs log predicted $\boldsymbol{R}$ as function of $\boldsymbol{C_{H_2O_2}}$, a_{H^+} and $\frac{1}{T}$ and d.

The rate of H_2O_2 decomposition as a function of $C_{H_2O_2}$, a_{H^+}, $\frac{1}{T}$, and d normalized to surface area for the three nanocatalysts regressed together is given by

$$R = 10^{2.20}(e^{-\frac{28\pm2\times10^3}{R}\cdot\frac{1}{T}})(c_{H_2O_2}^{1.01\pm0.04})(a_{H^+}^{-0.04\pm0.01})(\mathrm{d}^{1.05\pm0.04})$$

The effect of pH and $C_{H_2O_2}$ observed for the three catalysts together is similar to the effect observed separately for each catalyst. Similarly, the activation energy is intermediate to the values for Pt black and Pt nanopowder (see section 4.2). Nanoparticle size resulted in first order kinetic effects on the specific catalytic activity of the three catalysts. Several different explanations for this behavior have been put forward. Early studies pointed out that the average coordination number of the surface atoms decreases with decreasing particle size. Calculations on perfect or quasi-perfect particle shapes showed that the proportions of low coordination number (edge and corner) atoms decreased and those of high coordination number atoms (in low-index planes) increased as size increased[50, 190]. The ratio of edges/corners to terraces increases proportionally to the inverse of the diameter[50]. Because atoms at the edges and corners are more undercoordinated than atoms at (planar) facets, the binding energy between reactants and catalyst for these sites shifts away from the peak of the so-called volcano plot[99, 116, 118, 177, 191], thus causing a reduction in reaction rates[179]. Alternative explanations attribute size-induced changes in behavior to variation in the electronic properties of surface atoms, such as formation of surface oxides[131].

More recently, the effect of the position and shape of the valence band on the work function of metals has been used to explain enhanced catalytic activity of metal nanoparticles as a function of particle size[149]. The Fermi level increases for larger particles, resulting in an effective reduction of the work function[149-150]. For metals, the work function varies linearly with the reciprocal of particle diameter in the range of particle sizes studied here[151], which is consistent with the observed correlation between catalytic activity and size (d). As a result of their lower work function, larger Pt nanoparticles have a greater capacity to provide electron density to the reagent, which happens in the first step of the peroxide-oxide mechanism[150-151]. This is corroborated further by the difference between the activation energies of Pt black and Pt nanopowder. The activation energy of the spontaneous decomposition of H_2O_2 in bulk solution is

about 75 kJ/mol[192]. We found that the catalytic effect of the samples reduced the activation energy to 26±3 kJ/mol for Pt nanopowder and 33±3 kJ/mol for Pt black. A correlation between particle size and the Fermi level (which correlates inversely with work function) is known to reduce the activation energy for the chemisorption of oxygen on larger Pt particles[100-101]. This is consistent with a rate limiting step that involves oxidation of metallic Pt sites to Pt(O) because the lower work function allows the chemisorption of oxygen to occur faster on larger Pt nanoparticles. Zhou et al. 2012 showed that the difference in the work function of particles with sizes similar to Pt nanopowder and Pt black could be up to 0.05 eV for isolated spheres or 0.02 eV for aggregated nanoparticles, where the smaller nanoparticles have the larger work function in both cases[151].

Considering the small difference between the activation energies of Pt black and Pt nanopowder, it appears unlikely that the effect of size is the only factor causing their 10-fold difference in the rate of H_2O_2 decomposition. This effect is well fitted in the multi-variate linear regression shown in **Figure 2.2**, but only three different particle sizes were considered and the effect may be subject to a large uncertainty. This is supported by the results shown in **Figure 2.3** and **Figure 2.4**, which suggest that surface chemisorbed oxygen also has a significant impact in the catalytic activity of Pt nanocatalysts in the decomposition of H_2O_2. Thus, we have also considered the effect of surface oxygen on the catalytic activity of Pt black and Pt nanopowder.

4.4. Effect of chemisorbed oxygen on catalytic activity

Rate measurements were performed on samples subjected to preheating in order to better understand the relationship between surface oxygen content and catalytic activity **(Table S2.2)**. Rietveld analysis showed that heating Pt black and Pt nanopowder at 240 ^{o}C for 24h in atmospheric conditions did not change their crystal sizes (**Table 2.4** and **Table 2.2**). In contrast, the O/Pt ratio of Pt black-240 increased approximately 30% (p-value=0.02) while the O/Pt ratio of Pt nanopowder-240 did not change (p-value=0.17).

Table 2.4. Rietveld analysis of Pt nanopowder and Pt black heated at 240 ^{o}C for 24h.

	Pt black-240	**Pt nanopowder-240**
Crystal size (XRD Rietveld), nm	10.20 ± 0.08	19.89 ± 0.07
Lattice strain, (XRD Rietveld) reference to bulk Pt	-0.04 %	-0.02 %
O/Pt ratio (XPS)	0.18 ± 0.07	0.24 ± 0.08

Rate measurements of the preheated samples show that the H_2O_2 decomposition reaction is faster on Pt nanocatalysts having greater surface oxygen content. The rate of H_2O_2 decomposition by Pt black-240 is approximately 2 times faster than Pt black in the as supplied state in the range of studied conditions **(Figure 2.3 b)**. In comparison, the rate H_2O_2 decomposition by Pt nanopowder-240 did not change compared to as-received Pt nanopowder **(Figure 2.3 a)**.

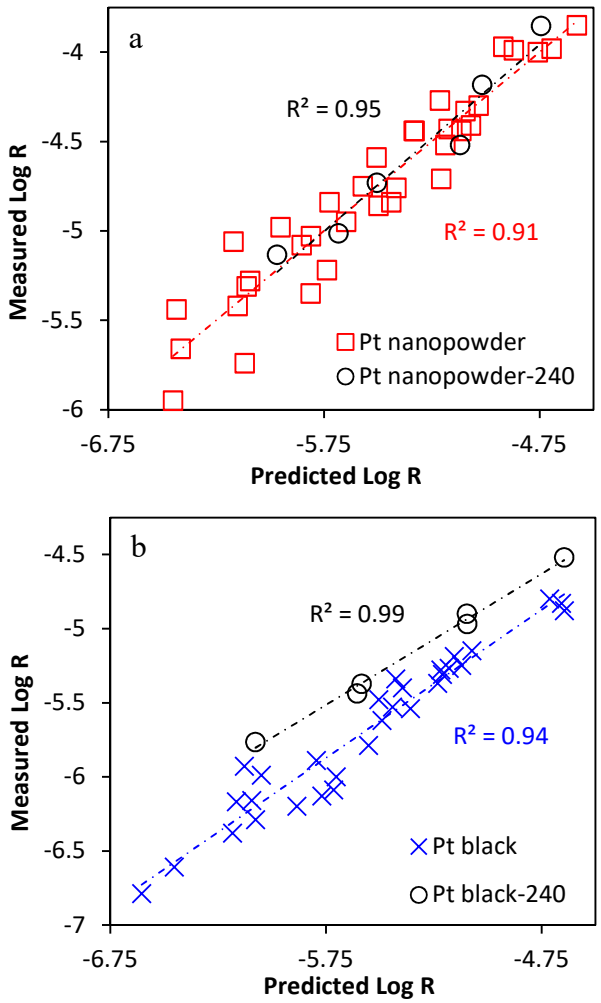

Figure 2.3. (a) Comparison of specific catalytic activity of Pt nanopowder-240 with Pt nanopowder as function of $\boldsymbol{C_{H_2O_2}}$, a_{H^+} and $\frac{1}{T}$. (b) Comparison of specific catalytic activity of Pt black-240 with Pt black as function of $\boldsymbol{C_{H_2O_2}}$, a_{H^+} and $\frac{1}{T}$.

The observed relation between increased surface oxygen content and enhanced catalytic activity is not consistent with an electrochemical mechanism because oxidized surfaces are characterized by larger work function values[117, 170]. This contradicts previous works on Pt that used electrochemical studies to claim that lowering the work function favors the rate of H_2O_2 decomposition and used that relationship to support the electrochemical mechanism **(Table 2.1)**[9, 11]. The effect observed in those studies is likely explained by the redox activity of H_2O_2. When

anodic potentials are applied the electrochemical decomposition of H_2O_2 driven by the external supply of electrons outweighs the catalytic effect of Pt. If the electrochemical mechanism truly represented this reaction, increasing surface Pt oxidation would reduce the number of active sites capable of exchanging electrons with H_2O_2 and consequently reduce the overall reaction rate, which is not observed in our results or in previous studies[8, 11]. Furthermore, the electrochemical mechanism would require the formation of hydroxyl radical species during the decomposition of H_2O_2. Hydroxyl radical generation has been suggested as a mechanism for the decomposition of H_2O_2 on Pt[13, 167, 174-175], although direct experimental evidence for this is lacking in this and in previous studies[167] (see supporting information).

The correlation between enhanced H_2O_2 decomposition rate and higher surface chemisorbed oxygen content supports that the rate limiting step of the reaction involves the oxidation of metallic Pt to Pt(O). The oxidation potential of Pt to Pt(O) observed by cyclic voltammetry for both samples at pH ~ 0 and pH ~ 6 is similar **(Figure S2.3)**. This suggests that this reaction does not depend on pH and is consistent with the trivial effect of pH on the rates of H_2O_2 decomposition for both catalysts. Thus, the reaction mechanism may be represented by reactions 10-12. Reaction 10 (bold) is the rate-limiting step of the reaction.

Step 1	$\boldsymbol{Pt + H_2O_2 \rightarrow H_2O + Pt(O)}$	(10)
Step 2	$Pt(O) + H_2O_2 \rightarrow Pt + O_2 + H_2O$	(11)
Overall	$2\,H_2O_2 \rightarrow O_2 + 2H_2O$	(12)

The presence of initially larger amounts of surface Pt(O) results in a mechanism of H_2O_2 decomposition where the oxidation of Pt to Pt(O) is skipped in the first cycle for the oxidized sites. Because H_2O_2 is also decomposed in reaction 11, and our rate measurements were performed through the initial rate method **(Figure S2.4)**, an increase in the initial number of Pt(O) sites (i.e., sites that skip the rate limiting step in their first cycle) results in a faster measured rate of H_2O_2 decomposition until the steady state of $\frac{[A_{Pt(O)}]}{[A_{Pt}]}$ is reached at the catalyst surface. This explains why Pt nanocatalysts with higher initial surface Pt(O) concentration exhibit enhanced catalytic activity in the decomposition of H_2O_2.

To support this mechanism, the effect of surface oxidation on the catalytic activity of Pt black and Pt nanopowder was also evaluated by pretreating Pt black and Pt nanopowder in the as-received state with different H_2O_2 concentrations ($C_{H_2O_2}^{pre}$) in the range of $9.8 \times 10^{-4}\ M < C_{H_2O_2}^{pre} < 9.8 \times 10^{-1}\ M$ before rate measurements **(Table S2.3)**. The catalytic activity of both Pt black and Pt nanopowder subjected to H_2O_2 pretreatment was similar, regardless of $C_{H_2O_2}^{pre}$ value being tested (p-value=0.12 and p-value=0.051, respectively). Interestingly, the catalytic activity of Pt nanopowder pretreated with concentrated H_2O_2 was similar to Pt nanopowder in the as supplied form (p-value=0.267) **(Figure 2.4 a)**. However, the catalytic activity of Pt black pretreated with concentrated H_2O_2 was approximately 3 times higher than Pt black in the as supplied form (p-value=0.03) **(Figure 2.4 b)**.

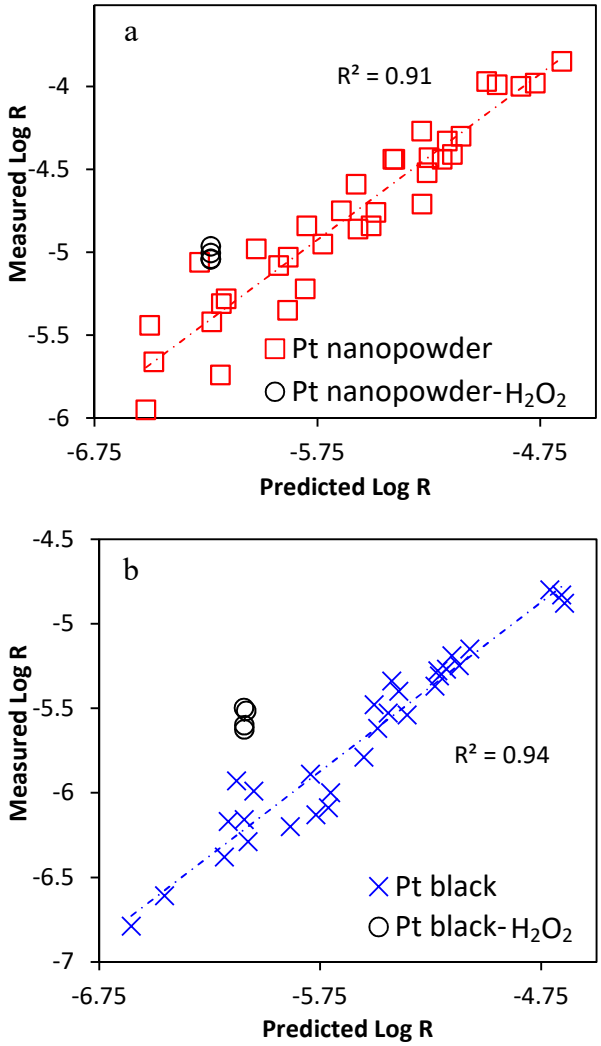

Figure 2.4. Comparison between the rate of H_2O_2 decomposition of a) Pt nanopowder in the as supplied form and pretreated with concentrated H_2O_2 and b) Pt black in the as supplied form and Pt black pretreated with concentrated H_2O_2.

The oxygen-oxide and the electrochemical mechanisms are both inconsistent with the enhanced rates of H_2O_2 decomposition obtained for Pt black pretreated with H_2O_2. In the oxygen-oxide mechanism, the catalytic activity of H_2O_2 pretreated Pt surfaces is expected to decrease due to an increase in the number of metallic sites generated during step 2 of the reaction with H_2O_2 **(Table 2.1)**. The addition of this step would result in longer induction periods, i.e., slower measured reaction rates. In the electrochemical mechanism, pretreating the catalyst surface with H_2O_2

should not have any effect on the catalyst properties and the catalytic activity should be similar. As H_2O_2 is an oxidizing compound, surface oxidation is plausible. However, as discussed above, in the electrochemical mechanism, increased surface oxidation should result in a reduction in overall catalytic activity, which is contradicted by our results.

The peroxide-oxide mechanism is consistent with the increase in catalytic activity observed for Pt black pretreated with H_2O_2, as well as the similar catalytic activity obtained for Pt nanopowder. This is demonstrated by deriving the ratio of oxidized Pt surface (θ) in the presence of H_2O_2 for this mechanism. From reactions 10-12, in steady state

$$v_{10} = v_{11} \qquad (13)$$

$$k_{10}[A_{Pt}][H_2O_2] = k_{11}[A_{Pt(O)}][H_2O_2] \qquad (14)$$

$$\frac{[A_{Pt(O)}]}{[A_{Pt}]} = \frac{k_{10}}{k_{11}} \qquad (15)$$

The ratio of $\frac{[A_{Pt(O)}]}{[A_{Pt}]}$ at the surface of Pt is only dependent on the ratio of the rate constants of reactions (10) and (11), and is totally independent from H_2O_2 concentration (reaction 15). As such, the concentration of H_2O_2 used in the pretreatment does not affect the surface Pt(O) concentration, which explains the similar effect of different $C_{H_2O_2}^{pre}$ on the catalytic activity of each nanocatalyst. This is further supported by previous studies showing that the open circuit potential of Pt electrodes immersed in H_2O_2 solutions is independent from the concentration of H_2O_2[163]. As discussed in section 4.3, the oxidation step of Pt → Pt(O) is favored for larger Pt nanoparticles and so one important consequence from equation 15 is that $\left(\frac{k_{10}}{k_{11}}\right)_{Pt\ nanopowder} > \left(\frac{k_{10}}{k_{11}}\right)_{Pt\ black}$, which results in $\frac{[A_{Pt(O)}]}{[A_{Pt}]}_{Pt\ nanopowder} > \frac{[A_{Pt(O)}]}{[A_{Pt}]}_{Pt\ black}$. Thus, in the steady state, the $\frac{[A_{Pt(O)}]}{[A_{Pt}]}$ ratio is higher for Pt nanopowder pretreated with concentrated H_2O_2 than for Pt black. This result is consistent with the greater catalytic activity observed for Pt nanopowder compared to Pt black when both were pretreated with H_2O_2 **(Figure 2.4)**. In support of this hypothesis, we note that the total number of surface Pt atoms in an experiment involving Pt black is approximately $2x10^{19}$. For the lowest concentration of H_2O_2 studied ($C_{H_2O_2} = 100\ \mu M$), the total

number of H_2O_2 molecules is $6x10^{19}$. Bianchi et al. (1962) showed that surface $\frac{[A_{Pt(O)}]}{[A_{Pt}]}$ on bulk Pt ranged between 0.54 – 0.58[15]. Assuming a $\frac{[A_{Pt(O)}]}{[A_{Pt}]}$ value in the same range for Pt black, on average each active site only has to go through three complete oxidation-reduction cycles (two molecules of H_2O_2 are decomposed per oxidation-reduction cycle) to decompose all of the H_2O_2. Increasing the initial $\frac{[A_{Pt(O)}]}{[A_{Pt}]}$ ratio would result in a significant increase in the initial rate of H_2O_2 decomposition because the rate limiting step of the reaction is skipped in Pt(O) sites. However, as shown in the present study, the effect of H_2O_2 pretreatment on Pt nanopowder was negligible, which suggests that the Pt(O) coverage on as received Pt nanopowder is close to the Pt(O) coverage that results from pretreating Pt nanopowder with H_2O_2.

Although limited in number, theoretical studies of H_2O_2 decomposition on platinum are in general agreement with the peroxide-oxide mechanism[193-194]. *Ab initio* calculations indicate that when hydrogen peroxide comes in contact with surface Pt atoms it becomes unstable and dissociates into two hydroxyls or a water molecule and atomic oxygen[191, 194]. If two hydroxyls are initially formed, one hydrogen atom is transferred to the adjacent hydroxyl to form H_2O and a surface Pt(O)[193]. To our knowledge, no studies have considered the subsequent interaction of Pt(O) with more H_2O_2. Oxygen chemisorption studies show that increased chemisorbed oxygen concentration leads to enhanced electrostatic repulsion, which hinders the chemisorption of more oxygen[195]. This supports the idea that H_2O_2 molecules are more prone to react with Pt(O) sites to regenerate their metallic character, instead of alternative pathways involving the generation of adjacent surface oxidized sites from adsorbed H_2O_2.

Multiple factors may be important for explaining the observed increase in the amount of oxygen at the surface of Pt nanopowder compared to Pt black in the as received condition and after pretreatment with H_2O_2. Pt nanopowder in the as supplied state incorporates more surface oxygen than Pt black, which is consistent with an enhanced stability of chemisorbed oxygen on larger catalysts. In addition to size, the differences in synthesis conditions for these two catalysts may be important. Synthesis of Pt black involves hydrogenation in aqueous suspension at 450 ^{o}C. These conditions are known to chemically reduce the surface of metal nanoparticles to levels below equilibrium with atmospheric oxygen[65, 159]. Residual surface oxygen after hydrogenation

is likely strongly bonded to Pt, presumably in the form of PtO or PtO_2. However, these phases are known to be inert species in the decomposition of H_2O_2[15]. Pt nanopowder, in comparison, is synthesized by chemical vapor condensation, which involves temperatures in the range of 700 ^oC – 800 ^oC. These synthesis conditions favor enhanced accumulation of chemisorbed oxygen at the surface[116].

Our results provide compelling evidence that the decomposition of H_2O_2 on Pt surfaces proceeds *via* peroxide-oxide mechanism. This mechanism, with the rate limiting step involving Pt → Pt(O), is also consistent with the fact that some previous studies reported an induction period for the decomposition of H_2O_2 on Pt. The catalysts in these studies were subjected to reducing conditions in order to obtain nearly perfect metallic surfaces[8-9]. Under such conditions the initial reaction rate is the rate limiting step, as virtually all active sites must go through the oxidation of Pt → Pt(O). In this case the rate constant will increase until surface $\frac{[A_{Pt(O)}]}{[A_{Pt}]}$ reaches steady state. Therefore surfaces that originally contain a lower than steady state $\frac{[A_{Pt(O)}]}{[A_{Pt}]}$ exhibit an induction period after exposure to H_2O_2. This is corroborated by another study that found that the rate constant of a freshly cleaved platinum surface increased asymptotically with time of contact with hydrogen peroxide[10]. Thus, the induction period depends on the surface chemical properties of the original catalyst surface. The majority of studies have used different catalysts, pretreatments and reaction conditions, all of which play a role in determining surface properties. This explains many of the inconsistencies between different studies, which resulted in a lack of scientific consensus regarding the mechanism of H_2O_2 decomposition[8, 11].

5. *Conclusions*

The decomposition of hydrogen peroxide on Pt nanocatalysts occurs *via* the peroxide-oxide mechanism. In the first step of this cyclic mechanism H_2O_2 reacts with the surface of Pt nanocatalysts to form Pt(O) releasing one molecule of H_2O. In the second step, a second molecule of H_2O_2 reduces Pt(O) to metallic Pt releasing a second molecule of H_2O and O_2. Particles that incorporate more Pt(O) at the surface exhibit a faster rate of H_2O_2 decomposition because the rate limiting step of the reaction is skipped in the first cycle. The catalytic activity is enhanced for larger Pt nanoparticles due to their lower work function, which increases the rate at which surface Pt atoms react with H_2O_2 to form Pt(O) (rate limiting step). For the samples in this study, the enhanced catalytic activity of Pt nanopowder compared to Pt black results from the combined effect of higher surface chemisorbed oxygen and lower activation energy due to its larger particle size. The reaction mechanism established here rationalizes previous studies that reported inconsistent results in terms of the induction periods of Pt nanocatalysts in the decomposition of H_2O_2. The multivariate analysis utilized in this work highlights the integrated effect of particle size, surface chemistry and the reaction conditions in the catalytic activity of Pt nanocatalysts in the decomposition of H_2O_2. This approach presents a pathway for unveiling the mechanism of other chemical reactions at the atomic level in order to improve the performance of platinum or other metal nanoparticles used to catalyze them.

Chapter 3

Effect of platinum chemisorbed oxygen on catalytic activity of platinum nanocatalysts in the decomposition of hydrogen peroxide

1. Abstract

We quantified the role of particle size (d) and surface chemisorbed oxygen (Pt(O)) abundance by studying the rate of H_2O_2 decomposition on platinum black and platinum nanopowder samples treated at different conditions to generate sample sets for which particle size and surface chemisorbed oxygen abundance were not correlated.

Rates of H_2O_2 decomposition were measured on platinum black and platinum nanopowder as received (35 and 36 data), platinum black and platinum nanopowder heated in air (69 and 12 data), platinum black and platinum nanopowder heated in vacuum (13 and 4 data), and platinum black and platinum nanopowder reacted with concentrated H_2O_2 (4 and 4 data). Hydrogen peroxide decomposition rate measurements were performed for solutions with H_2O_2 in the concentration range of $100\ \mu M < C_{H_2O_2} < 1000\ \mu M$, the pH range of $2.7 < pH < 9.3$ and the temperature range of $0\ ^oC < T < 55\ ^oC$. Catalyst particle size ranged from $8.8\ nm < d < 41\ nm$ and Pt(O) abundance – quantified as the fraction of catalyst surface covered with chemisorbed oxygen – ranged from $0.21 < \theta < 0.69$. The H_2O_2 decomposition rate (**R**) ($mol \cdot m^{-2} \cdot s^{-1}$) on platinum nanocatalysts was best fit by

$$R = 10^{2.9}\left(e^{\frac{(24\pm1.6)10^3}{R\cdot T}}\right)\left(C_{H_2O_2}^{0.92\pm0.03}\right)\left(a_{H^+}^{0.04\pm0.01}\right)\left(\theta^{0.83\pm0.03}\right)$$

This rate model explains 91% of the variance of the rate and indicates that θ has a nearly first order effect on the rate of H_2O_2 decomposition. The effect of particle size was found to be negligible. This result is consistent with a reaction mechanism for H_2O_2 decomposition on platinum that involves two cyclic steps, where step 1 is the rate limiting step.

Step 1	$Pt + H_2O_2 \xrightarrow{k = 0.0036} H_2O + Pt(O)$
Step 2	$Pt(O) + H_2O_2 \xrightarrow{k = 0.0412} Pt + O_2 + H_2O$
Overall	$2\ H_2O_2 \xrightarrow{k = 0.0370} O_2 + 2\ H_2O$

Our results showed that the rate constant (k) of step 2 is approximately 13 times faster than the rate constant of step 1. Reactions rates are faster on samples with more surface Pt(O) sites because in those sites the reaction skips the rate limiting step in the first cycle of decomposition.

2. *Introduction*

The chemical decomposition of hydrogen peroxide (H_2O_2) to water (H_2O) and molecular oxygen (O_2) catalyzed by platinum (Pt) nanocatalysts is technologically very important, particularly in the field of energy. This reaction is used to generate thrust in new generation aircraft jets, rockets, missiles and underwater vehicles[6, 24-25]. In hydrogen fuel cells H_2O_2 can be formed as an intermediate of the oxygen reduction reaction (ORR) and then decompose chemically, which reduces the energy yield of the process. Despite its importance, understanding the kinetics of this reaction has been hindered due to strongly correlated catalyst properties, which has produced ambiguous assessments of property-activity relationships.

Our previous study suggested that the catalyzed rate of H_2O_2 decomposition is enhanced on platinum nanocatalysts with larger particle size as well as enhanced surface chemisorbed oxygen (Pt(O)) abundance[17-18]. However these two variables are strongly correlated because larger platinum nanoparticles generally have enhanced Pt(O) levels. This has been attributed to the fact that larger particles have lower work functions, which increases their ability to provide electron density to stabilize oxygen at their surface[150-151, 155, 178].

The goal of this study is to determine whether particle size or surface chemisorbed oxygen is the most important factor that controls the rate of H_2O_2 decomposition on platinum nanocatalysts. To do that we analyzed the rates of hydrogen peroxide decomposition on platinum nanocatalysts having a variety of particle size and surface chemisorbed oxygen abundance. Rate models were used to confirm the mechanism of H_2O_2 decomposition on heated platinum nanocatalyst samples and deconvolute the effect of Pt(O) and particle size on the rate of H_2O_2 decomposition on platinum nanocatalysts.

3. Materials and Methods

3.1. Platinum black and platinum nanopowder

Platinum black and platinum nanopowder were obtained commercially (Sigma Aldrich, USA). Platinum black is synthesized by heating H_2PtCl_6 at 450 ^oC to form PtO_2 (known as Adam's Catalyst) followed by chemical reduction by hydrogenation in aqueous dispersion[196]. Platinum black is characterized by rounded nanoparticles with an average aggregate size, reported by the manufacturer of < 50 μm. Platinum nanopowder, also commonly referred to as platinum "nanoparticles" is synthesized by chemical vapor deposition and is characterized by nearly spherical particles with a manufacturer reported particle size of < 50 nm. In a recent publication we showed that the average particle (crystallite) sizes of platinum black and platinum nanopowder determined by TEM are 10 ± 4.7 nm and 22 ± 19 nm, respectively. Both samples expose approximately 85% of their geometric surface area due to a small extent of particle aggregation. Average values of particle size (Rietveld analysis), specific surface area (BET), aspect ratio, lattice strain, and surface chemical composition of the two materials are reported in our recent publication in ACS AEM[17].

In the current study we used samples of platinum black and platinum nanopowder in the as received condition, as well as subjected to different treatments, for H_2O_2 decomposition rate experiments **(Table 3.1).**

Table 3.1. List of samples used in the rate measurements.

Sample	Treatment	Graphing marker
Platinum black	as received	Black (○)
	heated in air, 95 °C < T < 525 °C, 60 s < t < 86400 s	Red (◊)
	heated in vacuum, 300 °C, t = 79200 s	Blue (▽)
	pre-treated with concentrated H_2O_2, 9.8×10^{-4} M < $C^{pre}_{H_2O_2}$ < 9.8×10^{-1} M	Pink (▷)
Platinum nanopowder	as received	Green (□)
	heated in air, 240 °C < T < 300 °C, 60 s < t < 86400 s	Orange (▭)
	heated in vacuum, 300 °C, t = 79200 s	Blue (▯)
	pre-treated with concentrated H_2O_2, 9.8×10^{-4} M < $C^{pre}_{H_2O_2}$ < 9.8×10^{-1} M	Pink (◁)

3.2. Rate measurements

The rate of H_2O_2 decomposition was determined on platinum nanocatalyst samples that were in the as received condition, heated in air or in vacuum, or reacted with concentrated H_2O_2. The treatments affected the particle size (d) and the surface fraction covered with chemisorbed oxygen (θ) of the samples in different ways. Samples had particle diameters in the range of 8.8 nm < d < 41 nm and surface chemisorbed oxygen coverage in the range of 0.21 < θ < 0.69. Detailed properties for each sample are given in the results section.

The rate of hydrogen peroxide decomposition was measured following the protocol utilized in a previous study. In this study we obtained 61 H_2O_2 decomposition rates for platinum black heated in air and 7 rates for platinum black heated in vacuum. These data were analyzed together with 24 H_2O_2 decomposition rate data for platinum black and platinum nanopowder heated in air and heated in vacuum conditions published in ref[17], as well as 65 data for platinum black and platinum nanopowder in the as received condition, 12 data for platinum black and platinum nanopowder heated in air and 8 data for platinum black and platinum nanopowder reacted with concentrated H_2O_2 before being used in the rate measurements, published in ref[18].

The experiments covered the following ranges for the independent variables: 100 μM < $C_{H_2O_2}$ < 1000 μM, 2.7 < pH < 9.3 and 0 °C < T < 55 °C. For each experiment, 6 mg of catalyst were

dispersed in 5 mL of water at pH 11, sonicated for 1 minute and subsequently added in the form of a dispersion to an Erlenmeyer flask reactor containing 1 L of H_2O_2 solution at the selected conditions for the run. The solution was sampled six times with 1 mL aliquots at regular intervals for the first 5 minutes. Each aliquot was filtered through a 0.22 μm pore size syringe filter. The concentration of H_2O_2 at each time point in time was calculated from the absorbance based on the xylenol-orange spectrophotometric method[181]. A new calibration curve was prepared each day.

The rate of H_2O_2 decomposition was determined using the initial rate method by taking the derivative at t = 0 of a second order polynomial fit of H_2O_2 concentration as function of time[182].

3.3. Data regression of H_2O_2 decomposition rates

The rate of H_2O_2 decomposition was regressed against H_2O_2 concentration $\left(C_{H_2O_2}\right)$, activity of hydrogen ion $\left(a_{H^+}\right)$, reaction temperature $\left(\frac{1}{T}\right)$, average catalyst particle size (d) and fraction of catalyst surface covered with chemisorbed oxygen (θ) (see **Table 3.3** for full notation list). Multi-variate linear regression analysis was applied to the whole data set of rate measurements from this and previous studies , using JMP Pro 12.0.1 (SAS Institute Inc.) to obtain values for the coefficients of each variable, A, E_a, n_1, n_2, n_3 and n_4 (see equation 8). The regression coefficients obtained were used to evaluate how much each variable contributed to the overall fit[183, 197-198]. The p-value for each coefficient was used to evaluate the statistical significance of the contribution of each variable at a level of confidence of 95%.

3.4. Platinum black heat treatment

Platinum black was heated in air in a thermoelectric furnace model F-1415T (Fisher Scientific, USA) at selected temperatures in the range of 95 ^{o}C < T < 525 ^{o}C. The temperature of the furnace was allowed to equilibrate until it changed less than 0.1 ^{o}C·min^{-1} before each sample was introduced into the furnace. The samples were placed in the furnace in an open glass vial for

selected periods of time and removed to ambient conditions at the end of the heat treatment time. The furnace allows gas exchanges with the atmosphere so the O_2 partial pressure was 0.21 atm. The temperature of the furnace at the end of the heating period was recorded and used as the "heating temperature" for data analysis purposes. Vacuum heated samples were produced by heating platinum black in a BET outgassing station at 300 ºC for 22 h.

3.5. Particle size determination

The average particle size of platinum black in the as received condition as well as heated samples was determined by Rietveld analysis of powder X-ray diffraction patterns. Powder x-ray diffraction data were collected using a benchtop X-ray diffraction Miniflex™ II (Rigaku Americas Corporation, TX) equipped with a Cu K_α source (λ = 0.15418 nm) and graphite monochromator.

Dry samples of as received and heated platinum black and platinum nanopowder were loaded individually onto a zero background round flush Si510 holder with M5x0.2 mm well (Rigaku). Diffracted intensities from the samples were collected by scanning from 35 to 88° 2θ in 0.02° increment steps and with an exposure time of 5 sec.

The raw scattering data were processed in using Profex 3.20.2126. This software uses a fundamental parameters approach (FPA) to calculate the instrumental weight function from the device configuration. The initial unit cell parameter (a), isotropic displacement parameters (U), and spacegroup $Fm\bar{3}m$ (no. 225) for face-centered cubic (FCC) platinum were used from crystallographic information file (CIF) number 0011157 obtained from the AMCSD[129]. A pseudo-Voigt function (RP4) to model peak profiles and spherical harmonics correction (SPHAR4) were used in all fits. The displacement parameter was left fixed at the initial value (U = 0.001). The fitting strategy used one single platinum phase with size-induced broadening and anisotropic microstrain. The unit cell dimension (a) and size induced broadening of Laurentzian component (B1) were first allowed to vary freely and then the microstrain parameter

(k2) was added to the refinement. The B1 parameter was used to calculate the average particle size (d) of each sample, which is an output of the software at the end of the refinement.

3.6. Calibration of particle size of heated platinum nanocatalyst samples

The particle size of heated platinum black samples used in H_2O_2 decomposition rate measurements was not directly determined for each sample. For that reason we modeled the particle size of platinum black as function of heating temperature and time in order to calibrate the particle size of platinum black samples subjected to heat treatment before being used in H_2O_2 decomposition rate measurements.

The extent of particle growth is well correlated with average particle size of a given sample, which makes this an easy and reliable way to track particle growth produced by sample heating[199]. There are 46 particle size data for platinum black samples that were subjected to heat treatment in the temperature range of $95^{o}C < T < 700\ ^{o}C$ and for periods of time in the range of $60\ s < t < 86400\ s$.

Previous studies have shown that the growth of platinum nanoparticles subjected to a constant temperature is asymptotic with an exponential component that depends on temperature. When particle size approaches the asymptotic value particles neither grow nor shrink and their size reaches a constant value (commonly referred to as critical radius)[200-201]. Both the rate of particle size growth and the critical radius increase with increasing temperatures[202]. For these reasons the average particle size of the heat treated platinum black was fit as a function of temperature and time to equation 1.

$$d(T,t) = mT + b - (mT + b + d_0)\left(e^{-\frac{at}{T}}\right), \text{for } d > d_0 \quad (1)$$

Here d is the average particle diameter (nm) after heat treatment, T is temperature (K), d_0 is the particle diameter (nm) before heat treatment, t is time (s) and m, b and a are fitting parameters. The average particle (crystallite) diameter of platinum black in the as received condition (d_0)

determined by X-ray diffraction Rietveld analysis is 8.8 ± 0.1 nm, similar to previously reported values[71-72, 78, 85, 196].

Non-linear regression (equation 1) of the 46 particle size data as function of heating temperature and time **(Table S3.1)** produced the following relationship

$$d(T,t) = 0.634T - 450 - (0.634T - 450 + 8.80)\left(e^{-\frac{6.34t}{T}}\right), \text{for } d > 8.80 \text{ nm} \quad (2)$$

This equation is valid when $d > d_0$, which in the case of platinum black corresponds to heat treatment at T > 450 °C. For T < 450 °C the particle size of platinum black remains unchanged at 8.8 ± 0.5 nm. The R^2 of this fit is 0.78. Equation 2 was used to predict the particle size of the platinum black samples heated in air used for H_2O_2 decomposition rate measurements **(Table S3.3, sample key A1)**. The particle size of the other samples (as supplied or subjected to other treatments) was determined directly through X-ray diffraction Rietveld analysis of samples subjected to the same treatment conditions.

3.7. Surface chemisorbed oxygen determination

The surface chemisorbed oxygen abundance on the platinum nanocatalysts was determined by quantitative surface chemical X-ray photoelectron spectroscopy (XPS) analysis using CASA XPS. XPS characterization of the dry samples was done using a PHI Quantera SXM scanning photoelectron spectrometer microprobe. Samples were deposited on double coated carbon conductive tape (Ted Pella, USA). High resolution XPS data were collected on the C1s, O1s and Pt4f peaks with 0.1 eV of energy resolution at a pressure of 10^{-7} Pa and data was processed using Phi Multipak software. Peak deconvolution and area analysis of high resolution data was performed using CASA XPS. The C1 component from the C1s carbon peak referring to adventitious carbon was used as a charging reference at a binding energy of 284.8 eV for all samples. High resolution peak deconvolution was performed following the strategy that we used for platinum nanocatalyst samples in a previous publication[17]. Briefly, the O1s peak was deconvoluted into four components. Component 1 and 2 (532.6 eV and 533.9 eV) are attributed

to oxygen bonded to carbon[121]. Component 3 and 4 refer to oxygen bonded to Pt in the form of Pt(O) – chemisorbed oxygen – at 531.6 eV[121, 203] and in the form of PtO, PtO_2 and Pt_3O_4 at 530.3 eV[203-204]. The C1s peak was deconvoluted into three symmetric components. Component 1 refers to C-C and C-H bonds (284.8 eV), component 2 refers to single C-O bonds (286.3 eV) and component 3 refers to double C=O bonds (288.6 eV).

For each sample three individual spots were analyzed independently and the average fraction of oxygen in the form of chemisorbed oxygen $\left(O_{Pt(O)}\right)$ and the atomic fractions of oxygen (S_O), platinum (S_{Pt}) and carbon (S_C) were assigned to that sample. Hydrogen peroxide decomposes on both metallic surface and on surface with chemisorbed oxygen (see section 5.3). Because of this, discussing the quantified effect of surface chemisorbed oxygen becomes more meaningful in terms of the fraction of catalyst surface covered with chemisorbed oxygen (θ) and the fraction of metallic surface $(1-\theta)$. The mean escape path of XPS photoelectrons from platinum is estimated to be 2 nm[205] and there are approximately 4 layers of platinum per nm[102]. Assuming that the attenuation of XPS signal by adventitious carbon and surface oxygen is negligible compared to platinum, on average only 1/8 of the surface atomic fraction of platinum determined by XPS is at the outermost surface layer and therefore the fraction of catalyst surface covered with chemisorbed oxygen can be determined from the ratio of surface atomic fraction of oxygen chemisorbed onto platinum to one eighth of the surface atomic fraction of platinum, determined by XPS (equation 3).

$$\theta = \frac{(O_{Pt(O)})(S_O)}{\frac{1}{8}\cdot S_{Pt}} = \frac{(S_{Pt(O)})}{\frac{1}{8}\cdot S_{Pt}} \qquad (3)$$

Here, θ is the fraction of nanocatalyst surface covered with chemisorbed oxygen, $O_{Pt(O)}$, is the fraction of surface oxygen in the form of chemisorbed oxygen determined by XPS, S_O is the surface atomic fraction of oxygen determined by XPS, S_{Pt} is the surface atomic fraction of platinum determined by XPS and $S_{Pt(O)}$ is the surface atomic fraction of chemisorbed oxygen.

3.8. Calibration of surface chemisorbed oxygen of heat treated platinum nanocatalyst samples

The fraction of catalyst surface covered with chemisorbed oxygen (θ) of heat treated platinum nanocatalyst samples used for H_2O_2 decomposition rate measurements could not be determined directly for each sample. For that reason we calibrated the surface θ values of those samples by modeling how the surface θ of heated platinum black samples changes as function of heating temperature and time. There are 50 surface θ data for platinum black samples that were subjected to heat treatment in the temperature range of 95 ^{o}C < T < 700 ^{o}C and for periods of time in the range of 60 s < t < 86400 s **(Table S3.2)**. Surface θ of heated platinum black correlates with particle size for heat treated samples **(Figure S3.1)**[202]. For this reason we modeled surface θ as function of heating temperature and time with an equation of the same form of equation 1. The average values of surface θ for heated platinum black samples were fit to equation 4, for heating temperatures for which $d > d_0$.

$$\theta(T,t) = mT + b - (mT + b + \theta_0)\left(e^{-\frac{at}{T}}\right) \qquad (4)$$

Here θ is the fraction of catalyst surface covered with chemisorbed oxygen, θ_0 is the fraction of catalyst surface covered with chemisorbed oxygen at t = 0, T is temperature (K), t is time (s) and m, b and a are fitting parameters. The surface θ on as received platinum black determined by XPS is 0.21 ± 0.02.

Fitting the surface θ as function of heating temperature and heating time to equation 4 for 50 data produced the following relationship.

$$\theta(T,t) = 0.0095 \cdot T - 6.7 - (0.0095 \cdot T - 6.7 + 0.21)\left(e^{-\frac{2.6t}{T}}\right), \text{ for } T > 450\ ^{o}C \qquad (5)$$

The R^2 of this fit is 0.87. Equation 5 was used to predict the surface θ of heat treated platinum nanocatalyst samples used in H_2O_2 decomposition rate measurements **(Table S3.3)**.

Equation 4 shows that samples heated for long periods of time reach a steady state surface θ that depends on temperature. The steady state value is dictated by $mT + b$, as it corresponds to $t \rightarrow \infty$. However, this is only valid for samples that experience particle size growth (due to the correlation between surface θ and d for samples heated in air, see **Figure S3.1**), which for the case of platinum black corresponds to T > 450 ^{o}C. For heat treated platinum black samples that do not experience particle size growth (T < 450 ^{o}C) the steady state θ does not change with temperature and its average value is 0.31 ± 0.03. As such, for platinum black heated at T < 450 ^{o}C, in equation 4 $mT + b$ must be substituted by 0.31, giving rise to equation 6.

$$\theta(T,t) = 0.31 - (0.31 + 0.21)\left(e^{-\frac{2.61t}{T}}\right), \text{for } 95\ ^{o}\text{C} < T < 450\ ^{o}C \qquad (6)$$

4. Results

4.1. Characterization of samples used for H_2O_2 decomposition rate measurements

Our results show that when platinum black is heated in air at T > 450 ^oC both particle size and surface θ increase. For samples heated at 95^oC < T < 450 ^oC surface θ increases but particle size remains the same (**Table S3.1** and **Table S3.2**). In the range of temperature (95 ^oC < T 525 ^oC) surface θ and particle size are correlated for samples that are heated in air **(Figure S3.1)** (R^2=0.89, p-value < 0.01).

In order to determine whether particle size or surface θ has the most important effect on the rate of H_2O_2 decomposition on platinum nanocatalysts we studied the rate of H_2O_2 decomposition on platinum samples that do not follow the heat induced correlation between particle size and surface θ. For that the rates of H_2O_2 decomposition on samples of platinum black heated in air were studied along with samples prepared at other conditions (see section 3.1). **Table 3.2** shows the characterization of the samples used in H_2O_2 rate experiments in terms of their surface θ and their average particle size (d) as well as the number of rate measurements for each sample set.

Table 3.2. Particle size and surface θ of the platinum nanocatalyst samples used to measure the effect of these two variables on the rate of H_2O_2 decomposition.

	Particle size, nm	Surface θ	No. of rate measurements
Platinum black heated in air at 95 $^oC < T < 450\ ^oC$ that reached steady state d and θ	8.80	0.31 ± 0.03	59
Platinum black heated in air 250 $^oC < T < 525\ ^oC$ that did <u>not</u> reach steady state d and θ	8.80 – 40.9	0.30 – 0.65	10
As received platinum black	8.80	0.21 ± 0.02	35
As received platinum nanopowder	19.9	0.66 ± 0.03	36
Platinum nanopowder heated in air 240 $^oC < T < 300\ ^oC$	19.9	0.66 ± 0.02	12
Platinum black heated in vacuum	19.3	0.23 ± 0.01	13
Platinum nanopowder heated in vacuum	29.9	0.61 ± 0.02	4
Platinum black pre-treated with concentrated H_2O_2	8.8	0.39 ± 0.03	4
Platinum nanopowder pre-treated with concentrated H_2O_2	19.9	0.69 ± 0.02	4

The particle size of the samples ranges from 8.80 nm < d < 40.9 nm and the fraction of catalyst surface covered with chemisorbed oxygen ranges from $0.21 < \theta < 0.69$. **Figure S3.2** shows a visualization of the surface θ and particle size (d) ranges of the samples. A linear regression of surface θ vs d had an R^2=0.43 and the slope of the line has p-value=0.26. This indicates that the overall sample set does not have a strong correlation between surface θ and d.

4.2. Kinetics of H_2O_2 decomposition on platinum nanocatalysts

4.2.1. Constructing the rate equation

The rate of H_2O_2 decomposition on the various platinum nanocatalysts was measured at variable conditions of $C_{H_2O_2}$, pH and reaction temperature (T)[9, 11, 13, 15, 160]. Particle size (d) and fraction of catalyst surface covered with chemisorbed oxygen (θ) were evaluated by measuring the rate of H_2O_2 decomposition for the various sample sets used in this study also as function of d and θ and these two variables were included in the regression model. **Table 3.3** gives the notation with units used in this article.

Table 3.3. Notation used.

R	Rate of H_2O_2 decomposition, mol/m^2·s
$C_{H_2O_2}$	Concentration of H_2O_2, mol/L
t	Time, s
A	Pre-exponential constant in Arrhenius equation, mol/m^2·s
E_a	Activation energy, J/mol
R	Gas constant, 8.314 J/mol·K
T	Temperature, K
a_{H^+}	Activity of H^+ ion
k_i	Rate constant of reaction i, mol/m^2·s
n_i	Reaction order for species i
R^2	Coefficient of determination for regression model
d	Crystal size (diameter), nm
$O_{Pt(O)}$	Fraction of surface oxygen in the form of chemisorbed oxygen determined by XPS
S_O,S_{Pt}, S_C	Surface atomic fraction of oxygen, platinum or carbon, respectively, determined by XPS
$S_{Pt(O)}$	$O_{Pt(O)} \times S_O$, surface atomic fraction of chemisorbed oxygen
θ	$\frac{S_{Pt(O)}}{\frac{1}{8} \cdot S_{Pt}}$, fraction of catalyst surface covered with chemisorbed oxygen $(Pt(O))$ sites
1 – θ	Fraction of catalyst surface exposing metallic platinum (Pt) sites
v_i	Rate of reaction step i

As a first step, I hypothesized that the rate of H_2O_2 decomposition is function of H_2O_2 concentration, a_{H^+}, $\frac{1}{T}$, catalyst particle size (d) and fraction of catalyst surface covered with chemisorbed oxygen (θ).

$$\boldsymbol{R} = \frac{-dC_{H_2O_2}}{dt} = k \cdot \left(C_{H_2O_2}^{n_1}\right)\left(a_{H^+}^{n_2}\right)(\theta^{n_3})(d^{n_4}) \qquad (7)$$

For variable temperature the rate is

$$\boldsymbol{R} = \left(\mathrm{A} \cdot e^{\frac{E_a}{R \cdot T}}\right)\left(C_{H_2O_2}^{n_1}\right)\left(a_{H^+}^{n_2}\right)(\theta^{n_3})(d^{n_4}) \qquad (8)$$

This equation can be linearized by a log transformation.

$$log\,\boldsymbol{R} = \log A - \frac{E_a}{2.303 \cdot R} \cdot \frac{1}{T} + n_1 \cdot \log\, C_{H_2O_2} - n_2 \cdot pH + n_3 \cdot \log\theta + n_4 \cdot log\, d \qquad (9)$$

This equation has six fitting parameters (A, E_a, n_1, n_2, n_3 and n_4), five independent variables $\left(\frac{1}{T}, C_{H_2O_2}, a_{H^+}, \theta, d\right)$ and (**R**) is the dependent variable being studied.

The values of the regression parameters (A, E_a, n_1, n_2, n_3 and n_4) were determined using the multiple linear regression module from JMP. The values of the regression parameters along with their errors and p-values are given in **Table 3.4**.

4.2.2. Regression model of H_2O_2 decomposition

In the current study we performed 61 H_2O_2 decomposition rate measurements on platinum black heated in air and 7 H_2O_2 decomposition rate measurements on platinum black heated in vacuum. These data were analyzed together with 24 H_2O_2 decomposition rate measurements for platinum black and platinum nanopowder heated in air and heated in vacuum conditions published in ref[17], as well as 65 rate measurements for platinum black and platinum nanopowder in the as received condition, 12 rate measurements for platinum black and platinum nanopowder heated in air and 8

rate measurements for platinum black and platinum nanopowder reacted with concentrated H_2O_2 before being used in the rate measurements, published in ref[18]. The rates of H_2O_2 decomposition for all samples are given in **Table S3.3**. **Figure 3.1** shows a comparison of the predicted and measured values of log **R** for this model. The partial regression graphs and residuals plot of H_2O_2 decomposition as function of $C_{H_2O_2}$, a_{H^+}, $\frac{1}{T}$, d and θ are shown in **Figure S3.3**.

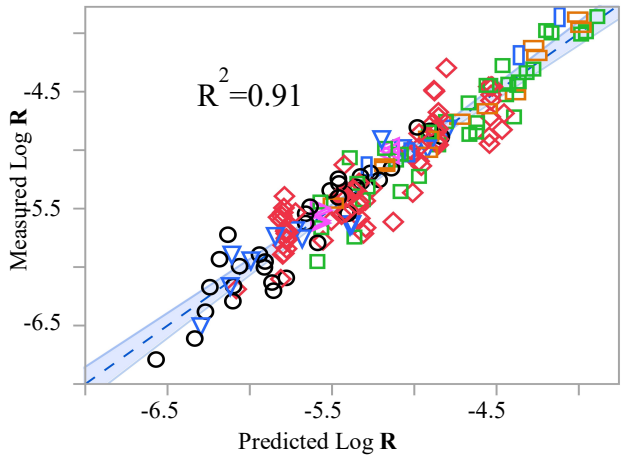

Figure 3.1. Rate measurements of H_2O_2 decomposition as function of $C_{H_2O_2}$, pH, temperature, particle size (d) and fraction of catalyst surface covered with chemisorbed oxygen (θ) for samples of as received platinum black (black ○) and as received platinum nanopowder (green □), platinum black heated in air (red ◊), platinum nanopowder heated in air (▭), platinum black heated in vacuum (blue ▽), platinum nanopowder heated in vacuum (blue ◘), platinum black pre-treated with concentrated H_2O_2 (pink ▷) and platinum nanopowder pre-treated with concentrated H_2O_2 (pink ◁).

To assess the role of particle size and surface θ on the catalytic decomposition of H_2O_2 by platinum nanocatalysts we evaluated the impact of removing each of these two variables from the regression model presented in equation 8. **Table 3.4** provides a summary of the regression coefficients and their p-value for the different scenarios.

Table 3.4. Summary of fitted coefficients for models regressed with different variables.

Variables considered in the model	Removed variable(s)	A, mol/m^2·s	E_a, $\frac{KJ}{mol}$	n_1	n_2	n_3	n_4	R^2
$C_{H_2O_2}$, a_{H^+}, $\frac{1}{T}$, d, θ	N/A	$10^{1.2\pm0.9}$ p-value=0.17	23.9±1.6 p-value<0.01	0.92±0.03 p-value<0.01	0.04±0.01 p-value<0.01	0.89±0.05 p-value<0.01	-0.09±0.04 p-value=0.06	0.91
$C_{H_2O_2}$, a_{H^+}, $\frac{1}{T}$, θ	d	$10^{2.9\pm0.3}$ p-value<0.01	24.3±1.6 p-value<0.01	0.92±0.03 p-value<0.01	0.04±0.01 p-value<0.01	0.83±0.03 p-value<0.01	N/A	0.91
$C_{H_2O_2}$, a_{H^+}, $\frac{1}{T}$, d	θ	$10^{12.1\pm1.2}$ p-value<0.01	22.8±2.9 p-value<0.01	0.92±0.06 p-value<0.01	0.04±0.02 p-value=0.01	N/A	0.57±0.06 p-value<0.01	0.71
$C_{H_2O_2}$, a_{H^+}, $\frac{1}{T}$	θ, d	$10^{0.74\pm0.7}$ p-value=0.26	16.7±3.56 p-value<0.01	0.92±0.07 p-value<0.01	0.04±0.02 p-value=0.06	N/A	N/A	0.54

The rate model without removing any variables indicates that the catalytic activity of H_2O_2 decomposition by platinum nanocatalysts is strongly affected by the fraction of catalyst surface covered with chemisorbed oxygen (θ) (p-value < 0.01). The effect of particle size is small and not statistically significant (p-value = 0.06) **(Table 3.4, first entry)**. The negligible effect of particle size in the rate of H_2O_2 decomposition is further reinforced by the fact that the R^2 of the regression is the same (R^2 = 0.91) when particle size is removed as a regression variable **(Table 3.4, first entry** and **second entry)**. **Figure 3.2** shows the regression model of catalytic H_2O_2 decomposition on platinum nanocatalysts without considering particle size as a regression variable. The partial regression graphs and residuals plot of H_2O_2 decomposition as function of $C_{H_2O_2}$, a_{H^+}, $\frac{1}{T}$ and θ for this fit are shown in **Figure S3.4**.

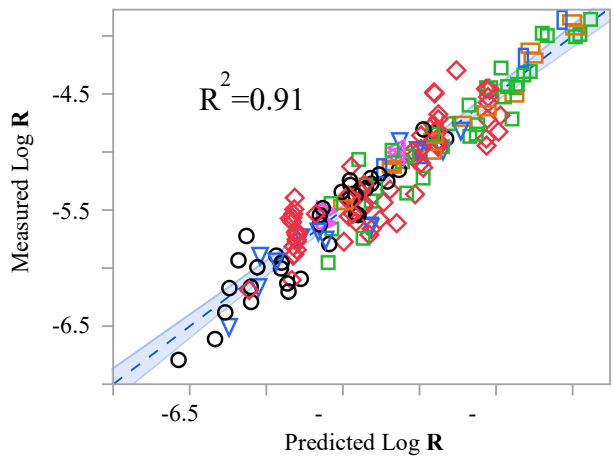

Figure 3.2. Rate measurements of H_2O_2 decomposition as function of $C_{H_2O_2}$, pH, temperature and fraction of catalyst surface covered with chemisorbed oxygen (θ) for samples of as received platinum black (black ○) and as received platinum nanopowder (green □), platinum black heated in air (red ◊), platinum nanopowder heated in air (▭), platinum black heated in vacuum (blue ▽), platinum nanopowder heated in vacuum (blue ◘), platinum black pre-treated with concentrated H_2O_2 (pink ▷) and platinum nanopowder pre-treated with concentrated H_2O_2 (pink ◁).

The R^2 of the fit without considering particle size as a regression variable is 0.91, which indicates that $C_{H_2O_2}$, a_{H^+}, $\frac{1}{T}$, and θ explain the 91% of data variance from the H_2O_2 decomposition rate data. The residuals plot of this regression **(Figure S3.4 f)** shows that the distribution of the measured rates around the line of predicted rates is symmetrical and homogeneous for all catalyst samples in the full spectrum of measured rates, which indicates that this regression model is good in the range of tested conditions.

The primary effect of surface chemisorbed oxygen is further elucidated by regressing the rate of H_2O_2 decomposition without surface θ **(Table 3.4, third entry)**. The regression model for this scenario is shown in **Figure S5**. The R^2 of this regression is 0.71. This value is significantly lower than the R^2 value when surface θ was considered. This shows that removing θ as a regression variable results in worse fit to the data, which indicates that the effect of surface θ is a lot more important to explain the variance of the data than the effect of particle size.

These results indicate that surface chemisorbed oxygen plays a key role in the rate of H_2O_2 decomposition and particle size has a small or negligible effect. The log transform of the regression equation produces the following rate equation

$$\boldsymbol{R} = 10^{2.9}\left(e^{\left(\frac{(24\pm1.6)10^3}{R\cdot T}\right)}\right)\left(C_{H_2O_2}^{0.92\pm0.03}\right)\left(a_{H^+}^{0.04\pm0.01}\right)\left((\theta)^{0.83\pm0.03}\right) \qquad (10)$$

This model indicates that the decomposition of H_2O_2 on platinum nanocatalysts follows approximately first order kinetics in $C_{H_2O_2}$ and the effect of pH is small (equation 10). This agrees with previous studies[15-16, 18, 165]. The activation energy is 24 ± 1.6 kJ·mol^{-1}, which is similar to what we previously reported for commercial platinum nanocatalysts that were not subjected to any treatments[18]. We attempted to model the rate measurements with a rate model that allowed the activation energy of the reaction to correlate with particle size. Notably the regression model always tended to a fixed activation energy value, equal to that on equation 10, which indicates that particle size effects are not significant on the activation energy of H_2O_2 decomposition on platinum.

If neither the effect of surface θ nor particle size is considered in the regression model, rate measurements for each of the catalyst samples are strongly offset from each other, which is diagnostic of different rate constant values **(Figure S3.8)**. This difference is clearer than when particle size is considered as one of the regression variables **(Figure S3.6)**. This happens because in the latter case the strong effect surface θ is partially captured when particle size is added to the regression due to the correlation between particle size and surface θ for heated platinum black samples (see section 4.1).

5. Discussion

5.1. Correlation between particle size and surface chemisorbed oxygen coverage for heated platinum black samples

The correlation between particle size and surface chemisorbed oxygen on heat treated platinum nanocatalysts is important in order to recognize and quantify correlated effects of surface θ and particle size on the catalytic activity of H_2O_2 decomposition by platinum nanocatalysts. To do that, in this work we analyzed samples whose levels of surface θ deviate from that correlation **(Table 3.2 and Figure S3.2)**. Platinum black is depleted in terms surface chemisorbed oxygen compared to platinum black samples heated in air. On the contrary platinum nanopowder samples exhibit enhanced surface chemisorbed oxygen abundance compared to platinum black samples heated in air. The different surface chemical composition of these two catalysts owes to their synthesis methods and has been discussed in a previous publication[17]. The other samples evaluated in this study were subjected to heat treatment at variable conditions or reacted with concentrated H_2O_2, which generates catalyst surfaces with different chemisorbed oxygen fractions (θ) and different particle sizes (d). The rates of H_2O_2 decomposition of the different nanocatalyst sample sets were analyzed to find whether particle size or surface θ was most important to explain differences in the rate constant of H_2O_2 decomposition by platinum nanocatalysts with different characteristics.

5.2. Effect of surface chemisorbed oxygen on the catalytic decomposition of H_2O_2 by platinum nanocatalysts

The fact that when θ is removed from being a regression variable causes samples to have different rate constants supports that the differently prepared samples used in this study do not exhibit a strong correlation between θ and d. If this were the case, the effect of surface θ on the rate of H_2O_2 decomposition would be fully captured by particle size, as it would happen if only samples of platinum black heated in air were used in this study (see section 4.1). This is a key

attribute of the entire sample set, indispensable for separating the effect of these two variables on the rate of H_2O_2 decomposition by platinum nanocatalysts.

The similar effect of the reaction conditions on all platinum nanocatalyst samples indicates that differences in the rate constant of these samples can be attributed to differences in the number of reactive sites, rather than changes in the mechanism of reaction.

The effect of surface chemisorbed oxygen (Pt(O)) abundance – quantified if the form of surface θ – on the rate of H_2O_2 decomposition is strong, which confirms the idea that surface chemisorbed oxygen plays a key role in the catalytic pathway of H_2O_2 on platinum nanocatalysts[18].

The R^2 of the regression model without considering particle size as one of the regression variables was the same as that of the regression model also taking particle size as a regression variable **(Table 3.4).** This means that particle size has a negligible contribution for explaining the variance of our rate measurements. If the effect of particle size was real, larger particles were also expected to have lower activation energy, because of size induced effects on the oxidation potential of the particles[17, 100-101], which our results did not support.

The rates of H_2O_2 decomposition on samples subjected to heat in vacuum are consistent with the negligible role of particle size on the catalytic activity of platinum nanocatalysts in the decomposition of H_2O_2. Although the particle size of platinum black heated in vacuum almost doubled and that of platinum nanopowder increased more than 1.5 times, their surface chemisorbed oxygen remained practically the same, which corresponded with a similar catalytic activity compared to that of samples in the as received condition.

In comparison, the catalytic activity of platinum black and platinum nanopowder subjected to concentrated H_2O_2 followed the increase in surface θ observed in both samples. This result also supports that surface chemisorbed oxygen exerts a causation effect and not an artifact correlated effect caused by sample heating. This is corroborated by the fact that the samples of platinum black heated in air at 95 $^{o}C < T < 450$ that reached steady state θ exhibit similar catalytic rates of H_2O_2 decomposition. This happens because surface chemisorbed oxygen is the actual property

that affects catalytic activity, regardless of the conditions used to change the abundance of chemisorbed oxygen. If the role of surface θ was simply an artifact correlation from the heat treatments, samples heated at different conditions would exhibit distinct rate constants, but they do not because the steady state θ is the same for samples heated at 95 ^{o}C < T < 450.

The fact that differences in the rate constants of all studied samples are almost entirely accounted by differences in surface chemisorbed oxygen abundance explains the distinct catalytic activity of as received platinum nanopowder and platinum black[18]. While the catalytic activity of platinum nanopowder is approximately 10 times higher than platinum black, this difference owes to their different chemisorbed oxygen abundance. Therefore, if platinum black is modified by action of a treatment, such as heating, to acquire a similar chemisorbed oxygen coverage to that of platinum nanopowder, their catalytic activity of H_2O_2 decomposition will be alike, as our results demonstrate.

5.3. Mechanistic role of surface chemisorbed oxygen (Pt(O))

The role of surface Pt(O) on the rate of H_2O_2 decomposition by platinum nanocatalysts is related to the mechanism but it has never been quantified and discussed in that context. In a previous study we provided evidence that the decomposition of H_2O_2 on platinum nanocatalysts proceeds *via* cyclic oxidation and reduction of surface Pt to Pt(O)[18] (equation 11-13). Step 1 (equation 11) is the rate limiting step of the reaction.

Step 1	$Pt + H_2O_2 \rightarrow H_2O + Pt(O)$	(11)
Step 2	$Pt(O) + H_2O_2 \rightarrow Pt + O_2 + H_2O$	(12)
Overall	$2\,H_2O_2 \rightarrow O_2 + 2\,H_2O$	(13)

Hydrogen peroxide decomposes on both surface metallic sites (step 1) and on sites with surface chemisorbed oxygen (step 2). Because of this, the quantified effect of surface chemisorbed oxygen on the rate of H_2O_2 decomposition is more appropriately discussed in terms of the percentage of catalyst surface covered with chemisorbed oxygen sites (θ) and the percentage of surface exposing metallic platinum sites ($1 - \theta$).

At any given point in time the overall rate of H_2O_2 decomposition is given by the sum of the rate of H_2O_2 decomposition through step 1 (equation 11) plus step 2 (equation 12). Thus, equation 8 assumes the form of equation 14.

$$\boldsymbol{R} = \frac{-dC_{H_2O_2}}{dt} = k_{13}(\theta^{n_3})\left(C_{H_2O_2}^{n_1}\right)\left(a_{H^+}^{n_2}\right) = k_{11}(1-\theta)\left(C_{H_2O_2}^{n_1}\right)\left(a_{H^+}^{n_2}\right) + k_{12}(\theta)\left(C_{H_2O_2}^{n_1}\right)\left(a_{H^+}^{n_2}\right) = \left(k_{11}(1-\theta) + k_{12}(\theta)\right)\left(C_{H_2O_2}^{n_1}\right)\left(a_{H^+}^{n_2}\right) \quad (14)$$

Re-arranging this equation to obtain an equation with θ as the independent variable we obtain

$$\boldsymbol{R} = \left(k_{11}(1-\theta) + k_{12}(\theta)\right)\left(C_{H_2O_2}^{n_1}\right)\left(a_{H^+}^{n_2}\right) = (k_{13})(\theta^{n_3})\left(C_{H_2O_2}^{n_1}\right)\left(a_{H^+}^{n_2}\right) \quad (15)$$

$$\frac{\boldsymbol{R}}{\left(C_{H_2O_2}^{n_1}\right)\left(a_{H^+}^{n_2}\right)} = (k_{12} - k_{11})(\theta) + k_{11} = k_{13}(\theta^{n_3}) \quad (16)$$

And therefore

$$k_{13}(\theta^{n_3}) = (k_{12} - k_{11})(\theta) + k_{11} \quad (17)$$

$$\theta^{n_3} = \left(\frac{k_{12}-k_{11}}{k_{13}}\right)(\theta) + \frac{k_{11}}{k_{13}} \quad (18)$$

Where $\left(\frac{k_{12}-k_{11}}{k_{13}}\right)$ and $\frac{k_{11}}{k_{13}}$ are respectively the slope and the origin of a linear regression that relates θ^{n_3} to θ. At T = 295 K, from equation 10, $n_3 = 0.83$ and $k_{13} = 10^{2.9}e^{\frac{24.3\times10^3}{R\cdot295}} = 0.0370$ mol/m^2·s. This results in $k_{12} = 0.0412$ mol/m^2·s and $k_{11} = 0.0036$ mol/m^2·s.

Thus equation 10 can be written with respect to the individual rate constants

$$\boldsymbol{R} = 0.044(\theta^{0.83})\left(C_{H_2O_2}^{0.92}\right)\left(a_{H^+}^{0.04}\right) = \left(0.0035(1-\theta) + (0.0435)(\theta)\right)\left(C_{H_2O_2}^{0.92}\right)\left(a_{H^+}^{0.04}\right) \quad (19)$$

These results are consistent with the reaction mechanism in equations 11-13. The rate constant of step 2 (reaction 12) is 13 times faster than that of step 1 (reaction 11). Samples with greater surface chemisorbed oxygen coverage (enhanced surface chemisorbed oxygen) have more sites that start their first cycle in step 2, which results in a significantly faster rate of H_2O_2 decomposition until steady state θ is reached, which ultimately results in a higher measured reaction rate, determined by the initial rate method, used in this study. Because $\boldsymbol{R} \propto \theta^{0.83}$, even small changes in θ affect $\boldsymbol{R}$ in a significant way. For example, if θ increases 5 times, the initial rate of H_2O_2 decomposition will increase approximately 4 times.

As explained in previous publications[11, 15], from equations 11-13, when steady state is reached

$$v_{11} = v_{12} \qquad (20)$$

$$k_{11}(1-\theta)\left(C_{H_2O_2}\right) = k_{12}(\theta)\left(C_{H_2O_2}\right) \qquad (21)$$

Given that step 1 (equation 11) is the rate limiting step of the reaction, from equation 21 we can conclude that in steady state the rate model can be represented by equation 22.

$$\boldsymbol{R} = \frac{-dC_{H_2O_2}}{dt} = 2 \cdot k_{11}(1-\theta)\left(C_{H_2O_2}^{0.92}\right)\left(a_{H^+}^{0.04}\right) \qquad (22)$$

My results illustrate the fundamental role of surface Pt(O) for controlling the rate of H_2O_2 decomposition. They reconcile many previous studies that reported differences in catalytic performance for differently prepared platinum nanocatalysts[8, 11]. When the initial surface Pt(O) coverage is lower than the coverage at steady state, the overall rate constant for the reaction will increase until steady state is reached. On the contrary, when the initial surface Pt(O) coverage is higher than the steady state coverage, the rate constant of the reaction will decrease until steady state is reached.

These results are important for many technological applications such as steam propellers fueled by H_2O_2, which make use of the decomposition of H_2O_2 to H_2O and O_2 on platinum, or other metal nanocatalysts, to generate thrust[6, 24-25]. This reaction is also important in hydrogen fuel

cells. Hydrogen fuel cells operate at temperatures up to 200 ^{o}C, and pressure conditions usually above atmospheric pressure, which likely affect the surface chemisorbed oxygen abundance of platinum nanocatalysts used in the reaction[206]. The chemical decomposition of H_2O_2, here studied, is a parasitic reaction of the oxygen reduction reaction and therefore the results of this study are directly related to the yield of the oxygen reduction reaction in hydrogen fuel cells.

This study also elucidates the potential of combining thorough structural and chemical characterization of nanocatalysts produced at different conditions allied with reaction rate measurements performed in series. The role of multi-variate rate analysis is particularly important in this approach as it allows quantifying the relative effect of different variables and deconvoluting the effect of correlated catalyst properties. By combining characterization and reaction rate studies I was able to establish property – activity relationships that were key for determining the mechanism and identify the rate limiting step of H_2O_2 decomposition at the surface of platinum nanocatalysts.

6. Conclusions

In this study we developed a methodology to deconvolute the effect of correlated variables in the two-step chemical reaction of H_2O_2 decomposition catalyzed by platinum nanocatalysts. The results show how surface chemisorbed oxygen plays a key role controlling the rate of H_2O_2 decomposition. The effect of particle size is negligible.

The overall platinum catalyzed H_2O_2 decomposition mechanism is a two-step reaction where the first step $Pt + H_2O_2 \rightarrow Pt(O) + H_2O$ is the rate limiting step. The second step of this cyclic reaction $Pt(O) + H_2O_2 \rightarrow Pt + H_2O + O_2$ is 13 times faster. Differences in the rate of H_2O_2 decomposition by platinum catalysts prepared at different conditions owe entirely to different density of surface catalyst sites covered with chemisorbed oxygen that skip the rate limiting step (step 1) in the first cycle of the reaction.

The multivariate analysis utilized in this work is a powerful tool to deconvolute the effect of correlated variables on the rate of reaction. This approach has a particularly great potential to improve our understanding of the mechanism and kinetics of other two-step chemical reactions with similar characteristics.

Outlook and Future Work

The decomposition of hydrogen peroxide on platinum is important in several energy conversion chemical reactions in modern society. However the prohibitive prices of platinum drive a demand for cheaper catalytic materials in these reactions. Silver nanoparticles in particular have shown activity in many reactions for which platinum is still the most used catalyst. For these reasons it is important to investigate the mechanism of H_2O_2 decomposition on silver nanoparticles and compare it with the mechanism on platinum. We anticipate that the approach that we used in the present work could be used to generate similar data sets that can be used to infer the mechanism and understand the kinetics of this reaction on silver nanoparticles. This work would allow redesigning silver nanocatalysts, as well as other metal nanocatalysts, in order to enhance their catalytic activity in a variety of energy conversion reactions.

From a methodology point of view, the work here developed can be applied to many other reactions of interest. For example, the conversion of methane to methanol at near room temperature is of great scientific interest because it would reduce the delivery cost of natural gas and make it economically competitive with liquid fossil fuels.

Recently methane was successfully oxidized to methanol in the temperature range of 30 ^{o}C < T < 95 ^{o}C using AuPd nanocatalysts and H_2O_2 as an oxidant[207-209]. However, achieving good methanol selectivity and productivity has been challenging and the actual role of the catalyst remains uncertain. For example, since hydroxyl radicals activate the molecule of methane by hydrogen abstraction, iron-based Fenton's type catalysts should also catalyze this reaction, however experimental tests have shown that they do not[209]. Developing a deeper understanding of the nanocatalyst role in the reaction is therefore essential to improve the efficiency and reduce the costs of this process. This study can be performed by measuring the rates of methane conversion to the reaction products. A mechanistic analysis similar to that developed in this study would allow quantifying the role of different factors in the selectivity and productivity of the reaction. This knowledge is of key importance because it can be used by engineers to improve catalyst design.

The kinetics of H_2O_2 dissociation on AuPd nanoparticles are very important in the conversion of methane to methanol because the presence of H_2O_2 is necessary in order for the reaction to occur.

$$H_2O_2 \xrightarrow{AuPd} 2\,(\bullet OH) \qquad \text{step 1}$$

$$\underline{CH_4 + 2\,(\bullet OH) \xrightarrow{AuPd} CH_3OH + H_2O} \qquad \text{step 2}$$

$$H_2O_2 + CH_4 \rightarrow CH_3OH + H_2O \qquad \text{overall}$$

Reaction byproducts: CH_3OOH; $HCOOH$; CO_2; H_2O; O_2

One of the challenges with this process is the parasitic H_2O_2 decomposition reaction (2 $H_2O_2 \rightarrow 2\ H_2O + O_2$) catalyzed by AuPd. This reaction leads to overconsumption of H_2O_2, which results in prohibitive costs for industrial applications. To address this challenge it is crucial to enhance the reaction of hydroxyl radicals with methane, which initiates the radical-chain reaction that converts methane to methanol[209]. For that it is mandatory to reduce/eliminate the parasitic reaction of H_2O_2 self-decomposition to H_2O and O_2. To understand what factors control the rate of hydroxyl radical generation derived from H_2O_2 we must study the overall rate of H_2O_2 decomposition on AuPd nanoparticles. In a second step, similar experiments should be carried to study the kinetics of H_2O_2 decomposition in the presence of a hydroxyl radical quenching reagent. The difference between the rates of H_2O_2 decomposition in the presence and in the absence of a quenching reagent is the rate of hydroxyl radical generation derived from H_2O_2 on the AuPd nanocatalysts. By applying the data analysis methods used in the current work it will be possible to understand hydroxyl radical generation on AuPd nanoparticles and to minimize the rates of parasitic H_2O_2 self-decomposition to ultimately maximize the reactivity of hydroxyl radicals with methane.

References

(1) Maxwell, I. E. Driving forces for innovation in applied catalysis. In Studies in Surface Science and Catalysis; Joe W. Hightower, W. N. D. E. I.; Alexis, T. B., Eds.; Elsevier: 1996; pp 1-9.

(2) Comninellis, C.; Chen, G. Electrochemistry for the Environment, Springer New York: 2009.

(3) ŗskov, J. K. N. Ã.; Studt, F.; Abild-Pedersen, F.; Bligaard, T. Fundamental Concepts in Heterogeneous Catalysis, Wiley: 2014.

(4) Ross, J. R. H. Heterogeneous Catalysis: Fundamentals and Applications, Elsevier: 2012.

(5) Nørskov, J. K.; Abild-Pedersen, F.; Studt, F.; Bligaard, T. Density functional theory in surface chemistry and catalysis. Proceedings of the National Academy of Sciences 2011, 108 (3), 937-943.

(6) Krejci, D.; Woschnak, A.; Scharlemann, C.; Ponweiser, K. Structural impact of honeycomb catalysts on hydrogen peroxide decomposition for micro propulsion. Chemical Engineering Research and Design 2012, 90 (12), 2302-2315.

(7) Baumgartner, H. J.; Hood, G. C.; Monger, J. M.; Roberts, R. M.; Sanborn, C. E. Decomposition of concentrated hydrogen peroxide on silver I. Low temperature reaction and kinetics. Journal of Catalysis 1963, 2 (5), 405-414.

(8) Eley, D. D.; Macmahon, D. M. The decomposition of hydrogen peroxide catalysed by palladium-gold alloy wires. Journal of Colloid and Interface Science 1972, 38 (2), 502-510.

(9) Weiss, J. The catalytic decomposition of hydrogen peroxide on different metals. Transactions of the Faraday Society 1935, 31, 1547-1557.

(10) Garwig, P. L. Hetetogeneous decomposition of hydrogen peroxide by inorganic catalysis. A literature survey; FMC corp. Princeton NJ: 1966.

(11) McKee, D. W. Catalytic decomposition of hydrogen peroxide by metals and alloys of the platinum group. Journal of Catalysis 1969, 14 (4), 355-364.

(12) Kamal, F.; Yann, B.; Charles, K.; Marie, T. Decomposition of hydrogen peroxide: influence of the shape of catalyst support. In 46th AIAA/ASME/SAE/ASEE Joint Propulsion Conference & Exhibit; American Institute of Aeronautics and Astronautics: 2010.

(13) Liu, Y.; Wu, H.; Li, M.; Yin, J.-J.; Nie, Z. pH dependent catalytic activities of platinum nanoparticles with respect to the decomposition of hydrogen peroxide and scavenging of superoxide and singlet oxygen. Nanoscale 2014, 6 (20), 11904-11910.

(14) Vetter, T. A.; Colombo, D. P. Kinetics of Platinum-Catalyzed Decomposition of Hydrogen Peroxide. Journal of Chemical Education 2003, 80 (7), 788.

(15) Bianchi, G.; Mazza, F.; Mussini, T. Catalytic decomposition of acid hydrogen peroxide solutions on platinum, iridium, palladium and gold surfaces. Electrochimica Acta 1962, 7 (4), 457-473.

(16) Roy, C. B. Catalytic decomposition of hydrogen peroxide on some oxide catalysts. Journal of Catalysis 1968, 12 (2), 129-133.

(17) Serra-Maia, R.; Winkler, C.; Murayama, M.; Tranhuu, K.; Michel, F. M. Abundance and Speciation of Surface Oxygen on Nanosized Platinum Catalysts and Effect on Catalytic Activity. ACS Applied Energy Materials 2018.

(18) Serra-Maia, R.; Bellier, M.; Chastka, S.; Tranhuu, K.; Subowo, A.; Rimstidt, J. D.; Usov, P. M.; Morris, A. J.; Michel, F. M. Mechanism and Kinetics of Hydrogen Peroxide Decomposition on Platinum Nanocatalysts. ACS Applied Materials & Interfaces 2018.

(19) Cotton, A. F.; Wilkinson, G.; Bochmann, M.; Murillo, C. A. Advanced inorganic chemistry, Wiley: 1999.

(20) Easton, M. F.; Mitchell, A. G.; Wynne-Jones, W. F. K. The behaviour of mixtures of hydrogen peroxide and water. Part 1.—Determination of the densities of mixtures of hydrogen peroxide and water. Transactions of the Faraday Society 1952, 48 (0), 796-801.

(21) Schumb, W. C.; Satterfield, C. N.; Wentworth, R. L. Hydrogen Peroxide. By W.C. Schumb ... Charles N. Satterfield ... Ralph L. Wentworth, New York: Pp. xiii. 759. Reinhold Pub. Corp.:, 1955.

(22) D'souza, N.; Mawson, A. Membrane cleaning in the dairy industry: a review. Critical reviews in food science and nutrition 2005, 45 (2), 125-134.

(23) Penkett, S. A.; Jones, B.; Brich, K.; Eggleton, A. E. The importance of atmospheric ozone and hydrogen peroxide in oxidising sulphur dioxide in cloud and rainwater. Atmospheric Environment (1967) 1979, 13 (1), 123-137.

(24) Chen, B.; Garland, N. T.; Geder, J.; Pruessner, M.; Mootz, E.; Cargill, A.; Leners, A.; Vokshi, G.; Davis, J.; Burns, W.; Daniele, M. A.; Kogot, J.; Medintz, I. L.; Claussen, J. C. Platinum Nanoparticle Decorated SiO_2 Microfibers as Catalysts for Micro Unmanned Underwater Vehicle Propulsion. ACS Applied Materials & Interfaces 2016, 8 (45), 30941-30947.

(25) Marr, K. M.; Chen, B.; Mootz, E. J.; Geder, J.; Pruessner, M.; Melde, B. J.; Vanfleet, R. R.; Medintz, I. L.; Iverson, B. D.; Claussen, J. C. High Aspect Ratio Carbon Nanotube Membranes Decorated with Pt Nanoparticle Urchins for Micro Underwater Vehicle Propulsion via H_2O_2 Decomposition. ACS Nano 2015, 9 (8), 7791-7803.

(26) Hammerschmidt, A.; Domke, W. D.; Nolscher, C.; Suchy, P., PEM fuel cell. Google Patents: 2000.

(27) Li, X.; Ge, S.; Hui, C.; Hsing, I.-M. Well-dispersed multiwalled carbon nanotubes supported platinum nanocatalysts for oxygen reduction. Electrochemical and solid-state letters 2004, 7 (9), A286-A289.

(28) Li, Y.; Yang, J.; Song, J. Structure models and nano energy system design for proton exchange membrane fuel cells in electric energy vehicles. Renewable and Sustainable Energy Reviews 2017, 67, 160-172.

(29) Gilroy, D. Oxide formation in the oxygen evolution region at Pt electrodes in M H2SO4. Journal of Electroanalytical Chemistry and Interfacial Electrochemistry 1977, 83 (2), 329-339.

(30) Bucher, J.; Buttet, J.; Van der Klink, J.; Graetzel, M. Electronic properties and local densities of states in clean and hydrogen covered Pt particles. Surface Science 1989, 214 (3), 347-357.

(31) Lingane, J. J.; Lingane, P. J. Chronopotentiometry of hydrogen peroxide with a platinum wire electrode. Journal of Electroanalytical Chemistry (1959) 1963, 5 (6), 411-419.

(32) E., R. R.; C., J. D. Fast-pulsed amperometric detection at electrodes: A study of oxide formation and dissolution at platinum in 0.1 M NaOH. Electroanalysis 1994, 6 (3), 193-199.

(33) Breiter, M. Anodic oxidation of formic acid on platinum—I. Adsorption of formic acid, oxygen, and hydrogen in perchloric acid solutions. Electrochimica Acta 1963, 8 (6-7), 447-456.

(34) Anson, F. C.; Lingane, J. J. Anodic Chronopotentiometry with Platinum and Gold Electrodes. The Iodide-Iodine-Iodate System. Journal of the American Chemical Society 1957, 79 (5), 1015-1020.

(35) Bliznakov, G.; Lazarov, D. Surface heterogeneity of metals of the copper group in the catalytic decomposition of hydrogen peroxide. Journal of Catalysis 1969, 14 (2), 187-192.

(36) Hickling, A.; Wilson, W. The anodic decomposition of hydrogen peroxide. Journal of the Electrochemical Society 1951, 98 (11), 425-433.

(37) Baker, B. B.; MacNevin, W. M. The Effect of Pre-polarization of a Platinum Anode on the Current Obtained in the Controlled Potential Oxidation of Iron and of Arsenic. Journal of the American Chemical Society 1953, 75 (6), 1476-1477.

(38) Conway, B. E.; Gottesfeld, S. Real condition of oxidized platinum electrodes. Part 2.—Resolution of reversible and irreversible processes by optical and impedance studies. Journal of the Chemical Society, Faraday Transactions 1: Physical Chemistry in Condensed Phases 1973, 69, 1090-1107.

(39) Latimer, W. M. Oxidation Potentials Prentice-Hall. Inc. Englewood Cliffs. NJ 1952.

(40) Lee, J.; Adams, R. N.; Bricker, C. Studies of gold, platinum and palladium indicating electrodes in strongly oxidizing aqueous solutions. Analytica Chimica Acta 1957, 17, 321-328.

(41) Wieckowski, A.; Savinova, E. R.; Vayenas, C. G. Catalysis and electrocatalysis at nanoparticle surfaces, CRC Press: 2003.

(42) Narayanan, R.; El-Sayed, M. A. Effect of Colloidal Nanocatalysis on the Metallic Nanoparticle Shape: The Suzuki Reaction. Langmuir 2005, 21 (5), 2027-2033.

(43) Wilson, O. M.; Knecht, M. R.; Garcia-Martinez, J. C.; Crooks, R. M. Effect of Pd Nanoparticle Size on the Catalytic Hydrogenation of Allyl Alcohol. Journal of the American Chemical Society 2006, 128 (14), 4510-4511.

(44) Dejhosseini, M.; Aida, T.; Watanabe, M.; Takami, S.; Hojo, D.; Aoki, N.; Arita, T.; Kishita, A.; Adschiri, T. Catalytic cracking reaction of heavy oil in the presence of cerium oxide nanoparticles in supercritical water. Energy & Fuels 2013, 27 (8), 4624-4631.

(45) Alkhaldi, S.; Husein, M. M. Hydrocracking of heavy oil by means of in situ prepared ultradispersed nickel nanocatalyst. Energy & Fuels 2013, 28 (1), 643-649.

(46) Popczun, E. J.; McKone, J. R.; Read, C. G.; Biacchi, A. J.; Wiltrout, A. M.; Lewis, N. S.; Schaak, R. E. Nanostructured Nickel Phosphide as an Electrocatalyst for the Hydrogen Evolution Reaction. Journal of the American Chemical Society 2013, 135 (25), 9267-9270.

(47) Popczun, E. J.; Read, C. G.; Roske, C. W.; Lewis, N. S.; Schaak, R. E. Highly active electrocatalysis of the hydrogen evolution reaction by cobalt phosphide nanoparticles. Angewandte Chemie 2014, 126 (21), 5531-5534.

(48) Callejas, J. F.; Read, C. G.; Roske, C. W.; Lewis, N. S.; Schaak, R. E. Synthesis, Characterization, and Properties of Metal Phosphide Catalysts for the Hydrogen-Evolution Reaction. Chemistry of Materials 2016, 28 (17), 6017-6044.

(49) Sylvestre, J.-P.; Poulin, S.; Kabashin, A. V.; Sacher, E.; Meunier, M.; Luong, J. H. T. Surface Chemistry of Gold Nanoparticles Produced by Laser Ablation in Aqueous Media. The Journal of Physical Chemistry B 2004, 108 (43), 16864-16869.

(50) Bond, G. C. The origins of particle size effects in heterogeneous catalysis. Surface Science 1985, 156, 966-981.

(51) Gupta, A. K.; Gupta, M. Synthesis and surface engineering of iron oxide nanoparticles for biomedical applications. Biomaterials 2005, 26 (18), 3995-4021.

(52) Narayanan, R.; El-Sayed, M. A. Shape-Dependent Catalytic Activity of Platinum Nanoparticles in Colloidal Solution. Nano Letters 2004, 4 (7), 1343-1348.

(53) Zak, A. K.; Abrishami, M. E.; Majid, W. H. A.; Yousefi, R.; Hosseini, S. M. Effects of annealing temperature on some structural and optical properties of ZnO nanoparticles prepared by a modified sol–gel combustion method. Ceramics International 2011, 37 (1), 393-398.

(54) Narayanan, R.; El-Sayed, M. A. Changing catalytic activity during colloidal platinum nanocatalysis due to shape changes: electron-transfer reaction. Journal of the American Chemical Society 2004, 126 (23), 7194-7195.

(55) Xie, R.; Cao, X.; Pan, Y.; Gu, H. Synthesis of Pt nanocatalysts for selective hydrogenation of ortho-halogenated nitrobenzene. Science China Chemistry 2015, 58 (6), 1051-1055.

(56) Ye, L.; Zheng, J.; Tian, T.; Gao, Y.; Li, P. In Preparation and Performance Study of an Unsupported Pt Catalyst for Proton Exchange Membrane Fuel Cell, Meeting Abstracts, The Electrochemical Society: 2015; pp 1590-1590.

(57) Tian, X. L.; Wang, L.; Deng, P.; Chen, Y.; Xia, B. Y. Research advances in unsupported Pt-based catalysts for electrochemical methanol oxidation. Journal of Energy Chemistry 2017.

(58) Gralec, B.; Lewera, A. Catalytic activity of unsupported Pd-Pt nanoalloys with low Pt content towards formic acid oxidation. Applied Catalysis B: Environmental 2016, 192, 304-310.

(59) Tian, X. L.; Xu, Y. Y.; Zhang, W.; Wu, T.; Xia, B. Y.; Wang, X. Unsupported Platinum-Based Electrocatalysts for Oxygen Reduction Reaction. ACS Energy Letters 2017, 2 (9), 2035-2043.

(60) Chi, N. Deposition and kinetics studies of platinum nanoparticles on highly oriented pyrolytic graphite. 香港大學學位論文 2000, 1-0.

(61) Kicela, A.; Daniele, S. Platinum black coated microdisk electrodes for the determination of high concentrations of hydrogen peroxide in phosphate buffer solutions. Talanta 2006, 68 (5), 1632-1639.

(62) Kim, H.; Moon, S. H. Chemical vapor deposition of highly dispersed Pt nanoparticles on multi-walled carbon nanotubes for use as fuel-cell electrodes. Carbon 2011, 49 (4), 1491-1501.

(63) Stonehart, P.; Ross, P. N. The commonality of surface processes in electrocatalysis and gas-phase heterogeneous catalysis. Catalysis Reviews 1975, 12 (1), 1-35.

(64) McDonald, D.; Hunt, L. B. A History of Platinum and its Allied Metals, Johnson Matthey: 1982.

(65) Voorhees, V.; Adams, R. The use of the oxides of platinum for the catalytic reduction of organic compounds. I. Journal of the American Chemical Society 1922, 44 (6), 1397-1405.

(66) Mills, A. Final Analysis: Porous Platinum Morphologies: Platinised, Sponge and Black. Platinum Metals Review 2007, 51 (1), 52-52.

(67) Larminie, J.; Dicks, A.; McDonald, M. S. Fuel cell systems explained, J. Wiley Chichester, UK: 2003; Vol. 2.

(68) McKee, D. Catalytic Activity and Sintering of Platinum Black. Kinetics of Propane Cracking. The Journal of Physical Chemistry 1963, 67 (4), 841-846.

(69) Simonsen, S. B.; Chorkendorff, I.; Dahl, S.; Skoglundh, M.; Sehested, J.; Helveg, S. Direct observations of oxygen-induced platinum nanoparticle ripening studied by in situ TEM. Journal of the American Chemical Society 2010, 132 (23), 7968-7975.

(70) Tseung, A. C. C.; Dhara, S. C. Loss of surface area by platinum and supported platinum black electrocatalyst. Electrochimica Acta 1975, 20 (9), 681-683.

(71) Bett, J.; Lundquist, J.; Washington, E.; Stonehart, P. Platinum crystallite size considerations for electrocatalytic oxygen reduction—I. Electrochimica Acta 1973, 18 (5), 343-348.

(72) Lundquist, J. T.; Stonehart, P. Platinum crystallite size effects on oxide formation and reduction parameters—II. Electrochimica Acta 1973, 18 (5), 349-354.

(73) Mills, A. Instrumental Note: Platinized Platinum, Platinum Sponge and Platinum Black. Bulleting-Scientific Instrument Society 2006, 89, 35.

(74) Adams, R.; Garvey, B. S. selective Reduction of Citral By Means of Platinum-oxide Platinum Black and a Promoter. Journal of the American Chemical Society 1926, 48 (2), 477-482.

(75) Stonehart, P.; Zucks, P. A. Sintering and recrystallization of small metal particles. Loss of surface area by platinum-black fuel-cell electrocatalysts. Electrochimica Acta 1972, 17 (12), 2333-2351.

(76) Bregoli, L. J. The influence of platinum crystallite size on the electrochemical reduction of oxygen in phosphoric acid. Electrochimica Acta 1978, 23 (6), 489-492.

(77) Paál, Z.; Tétényi, P. The mechanism of aromatization on platinum black catalyst; dehydrocyclization of hexadienes and hexatrienes. Journal of Catalysis 1973, 30 (3), 350-361.

(78) Paál, Z.; Zimmer, H.; Günter, J. R.; Schlögl, R.; Muhler, M. Sintering of platinum-black in hydrogen: Morphology and catalytic activity. Journal of Catalysis 1989, 119 (1), 146-160.

(79) Vogel, W.; Lundquist, L.; Ross, P.; Stonehart, P. Reaction pathways and poisons—II. Electrochimica Acta 1975, 20 (1), 79-93.

(80) Ilic, B.; Czaplewski, D.; Neuzil, P.; Stanczyk, T.; Blough, J.; Maclay, G. J. Preparation and characterization of platinum black electrodes. Journal of Materials Science 2000, 35 (14), 3447-3457.

(81) Teshima, N.; Genfa, Z.; Dasgupta, P. K. Catalytic decomposition of hydrogen peroxide by a flow-through self-regulating platinum black heater. Analytica Chimica Acta 2004, 510 (1), 9-13.

(82) Patel, P. R.; Gibson, M. D.; Ludwig, K. A.; Langhals, N. B. In Electrochemical sensing via selective surface modification of iridium microelectrodes to create a platinum black interface, Neural Engineering (NER), 2013 6th International IEEE/EMBS Conference on, IEEE: 2013; pp 961-964.

(83) Rosenbaum, M.; Schröder, U.; Scholz, F. Investigation of the electrocatalytic oxidation of formate and ethanol at platinum black under microbial fuel cell conditions. Journal of Solid State Electrochemistry 2006, 10 (10), 872-878.

(84) Fernandez, R. E.; Koklu, A.; Mansoorifar, A.; Beskok, A. Platinum black electrodeposited thread based electrodes for dielectrophoretic assembly of microparticles. Biomicrofluidics 2016, 10 (3), 033101.

(85) Baird, T.; Paal, Z.; Thomson, S. J. Sintering studies on platinum black catalysts. Part 1.-Effect of pretreatment and reaction on particle size. Journal of the Chemical Society, Faraday Transactions 1: Physical Chemistry in Condensed Phases 1973, 69 (0), 50-55.

(86) Watkins, J. J.; Blackburn, J. M.; McCarthy, T. J. Chemical fluid deposition: reactive deposition of platinum metal from carbon dioxide solution. Chemistry of Materials 1999, 11 (2), 213-215.

(87) Paál, Z.; Muhler, M.; Schlögl, R. Platinum black by XPS. Surface Science Spectra 1996, 4 (2), 119-124.

(88) Rodriguez, N. M.; Anderson, P. E.; Wootsch, A.; Wild, U.; Schlögl, R.; Paál, Z. XPS, EM, and Catalytic Studies of the Accumulation of Carbon on Pt Black. Journal of Catalysis 2001, 197 (2), 365-377.

(89) Escobar Morales, B.; Gamboa, S. A.; Pal, U.; Guardián, R.; Acosta, D.; Magaña, C.; Mathew, X. Synthesis and characterization of colloidal platinum nanoparticles for electrochemical applications. International Journal of Hydrogen Energy 2010, 35 (9), 4215-4221.

(90) Stepanov, A.; Golubev, A.; Nikitin, S. Synthesis and Applications of Platinum Nanoparticles: A Review. In Nanotechnology Vol. 2: Synthesis and Characterization; Studium Press LLC India: 2013; pp 173-199.

(91) Singal, S.; Srivastava, A. K.; Biradar, A. M.; Mulchandani, A.; Rajesh. Pt nanoparticles-chemical vapor deposited graphene composite based immunosensor for the detection of human cardiac troponin I. Sensors and Actuators B: Chemical 2014, 205, 363-370.

(92) Oljaca, M.; Xing, Y.; Lovelace, C.; Shanmugham, S.; Hunt, A. Flame synthesis of nanopowders via combustion chemical vapor deposition. Journal of materials science letters 2002, 21 (8), 621-626.

(93) Komiyama, M.; Kobayashi, J. i.; Morita, S. Structure of platinum ultrafine particles in Pt/C catalyst observed by scanning tunneling microscopy. Journal of Vacuum Science & Technology A: Vacuum, Surfaces, and Films 1990, 8 (1), 608-609.

(94) Kim, H.; Robertson, A. W.; Kim, S. O.; Kim, J. M.; Warner, J. H. Resilient high catalytic performance of platinum nanocatalysts with porous graphene envelope. ACS nano 2015, 9 (6), 5947-5957.

(95) Eppell, S.; Chottiner, G. S.; Scherson, D. A.; Pruett, G. Scanning tunneling microscopy of platinum deposits on the basal plane of highly oriented pyrolytic graphite. Langmuir 1990, 6 (7), 1316-1319.

(96) Lewis, L. N.; Stein, J.; Gao, Y.; Colborn, R. E.; Hutchins, G. Platinum catalysts used in the silicones industry. Platinum Metals Review 1997, 41 (2), 66-75.

(97) Lee, S.; Permana, H.; Ng, K. S. Effects of annealing and gas treatment on the morphology of platinum cluster size on highly oriented pyrolytic graphite by scanning tunneling microscopy. Catalysis letters 1994, 23 (3-4), 281-292.

(98) Antoine, O.; Bultel, Y.; Durand, R. Oxygen reduction reaction kinetics and mechanism on platinum nanoparticles inside Nafion®. Journal of Electroanalytical Chemistry 2001, 499 (1), 85-94.

(99) Shao, M.; Peles, A.; Shoemaker, K. Electrocatalysis on Platinum Nanoparticles: Particle Size Effect on Oxygen Reduction Reaction Activity. Nano Letters 2011, 11 (9), 3714-3719.

(100) Han, B. C.; Miranda, C. R.; Ceder, G. Effect of particle size and surface structure on adsorption of O and OH on platinum nanoparticles: A first-principles study. Physical Review B 2008, 77 (7), 075410.

(101) Jaeger, N. I.; Jourdan, A. L.; Schulz-Ekloff, G. Effect of the size of platinum particles on the chemisorption of oxygen. Journal of the Chemical Society, Faraday Transactions 1991, 87 (8), 1251-1257.

(102) Mukerjee, S. Particle size and structural effects in platinum electrocatalysis. Journal of Applied Electrochemistry 1990, 20 (4), 537-548.

(103) Kinoshita, K. Particle size effects for oxygen reduction on highly dispersed platinum in acid electrolytes. Journal of The Electrochemical Society 1990, 137 (3), 845-848.

(104) Halperin, W. P. Quantum size effects in metal particles. Reviews of Modern Physics 1986, 58 (3), 533-606.

(105) Subramanian, V.; Wolf, E. E.; Kamat, P. V. Catalysis with TiO_2/Gold Nanocomposites. Effect of Metal Particle Size on the Fermi Level Equilibration. Journal of the American Chemical Society 2004, 126 (15), 4943-4950.

(106) Watanabe, M.; Sei, H.; Stonehart, P. The influence of platinum crystallite size on the electroreduction of oxygen. Journal of Electroanalytical Chemistry and Interfacial Electrochemistry 1989, 261 (2, Part 2), 375-387.

(107) Solliard, C.; Flueli, M. Surface stress and size effect on the lattice parameter in small particles of gold and platinum. Surface Science 1985, 156 (Part 1), 487-494.

(108) Masson, A.; Bellamy, B.; Romdhane, Y. H.; Che, M.; Roulet, H.; Dufour, G. Intrinsic size effect of platinum particles supported on plasma-grown amorphous alumina in the hydrogenation of ethylene. Surface Science 1986, 173 (2), 479-497.

(109) Zhang, B.; Wang, D.; Hou, Y.; Yang, S.; Yang, X. H.; Zhong, J. H.; Liu, J.; Wang, H. F.; Hu, P.; Zhao, H. J. Facet-dependent catalytic activity of platinum nanocrystals for triiodide reduction in dye-sensitized solar cells. Scientific reports 2013, 3.

(110) Scheele-Ferreira, E. M.; Scott, C. E.; Perez-Zurita, M. J.; Pereira-Almao, P. R. Influence of the preparation variables on the synthesis of nanocatalyst for in-situ upgrading applications. Industrial & Engineering Chemistry Research 2017.

(111) Zimicz, M. G.; Lamas, D. G.; Larrondo, S. A. $Ce_{0.9}Zr_{0.1}O_2$ nanocatalyst: Influence of synthesis conditions in the reducibility and catalytic activity. Catalysis Communications 2011, 15 (1), 68-73.

(112) Yaripour, F.; Shariatinia, Z.; Sahebdelfar, S.; Irandoukht, A. The effects of synthesis operation conditions on the properties of modified γ-alumina nanocatalysts in methanol dehydration to dimethyl ether using factorial experimental design. Fuel 2015, 139 (Supplement C), 40-50.

(113) Stamenkovic, V. R.; Fowler, B.; Mun, B. S.; Wang, G.; Ross, P. N.; Lucas, C. A.; Marković, N. M. Improved Oxygen Reduction Activity on $Pt_3Ni(111)$ via Increased Surface Site Availability. Science 2007, 315 (5811), 493-497.

(114) Jiang, Q.; Liang, L. H.; Zhao, D. S. Lattice Contraction and Surface Stress of fcc Nanocrystals. The Journal of Physical Chemistry B 2001, 105 (27), 6275-6277.

(115) Deshpande, S.; Patil, S.; Kuchibhatla, S. V.; Seal, S. Size dependency variation in lattice parameter and valency states in nanocrystalline cerium oxide. Applied Physics Letters 2005, 87 (13), 133113.

(116) Ono, L. K.; Croy, J. R.; Heinrich, H.; Roldan Cuenya, B. Oxygen Chemisorption, Formation, and Thermal Stability of Pt Oxides on Pt Nanoparticles Supported on SiO_2/Si(001): Size Effects. The Journal of Physical Chemistry C 2011, 115 (34), 16856-16866.

(117) Nolan, P. D.; Wheeler, M. C.; Davis, J. E.; Mullins, C. B. Mechanisms of Initial Dissociative Chemisorption of Oxygen on Transition-Metal Surfaces. Accounts of Chemical Research 1998, 31 (12), 798-804.

(118) Nie, Y.; Li, L.; Wei, Z. Recent advancements in Pt and Pt-free catalysts for oxygen reduction reaction. Chemical Society Reviews 2015, 44 (8), 2168-2201.

(119) Doebelin, N.; Kleeberg, R. Profex: a graphical user interface for the Rietveld refinement program BGMN. Journal of applied crystallography 2015, 48 (5), 1573-1580.

(120) Downs, R. T.; Hall-Wallace, M. The American Mineralogist crystal structure database. American Mineralogist 2003, 88 (1), 247-250.

(121) Zhang, G.; Yang, D.; Sacher, E. X-ray photoelectron spectroscopic analysis of Pt nanoparticles on highly oriented pyrolytic graphite, using symmetric component line shapes. The Journal of Physical Chemistry C 2007, 111 (2), 565-570.

(122) Parkinson, C. R.; Walker, M.; McConville, C. F. Reaction of atomic oxygen with a Pt(1 1 1) surface: chemical and structural determination using XPS, CAICISS and LEED. Surface Science 2003, 545 (1–2), 19-33.

(123) Peuckert, M.; Yoneda, T.; Betta, R. A. D.; Boudart, M. Oxygen Reduction on Small Supported Platinum Particles. Journal of The Electrochemical Society 1986, 133 (5), 944-947.

(124) Mitchell, D. R. G. Circular Hough transform diffraction analysis: A software tool for automated measurement of selected area electron diffraction patterns within Digital Micrograph™. Ultramicroscopy 2008, 108 (4), 367-374.

(125) Birkholz, M.; Fewster, P. F.; Genzel, C. Thin Film Analysis by X-Ray Scattering, Wiley: 2006.

(126) Mittemeijer, E. J.; Scardi, P. Diffraction Analysis of the Microstructure of Materials, Springer Berlin Heidelberg: 2003.

(127) Suryanarayana, C.; Norton, M. G. X-ray diffraction: a practical approach, Springer Science & Business Media: 2013.

(128) Young, R. A. The rietveld method, International union of crystallography: 1993; Vol. 5.

(129) Downs, R. T.; Hall-Wallace, M. The American Mineralogist crystal structure database. American Mineralogist 2003, 88 (1), 247-250.

(130) Davis, S. M.; Somorjai, G. A. The effect of surface oxygen on hydrocarbon reactions catalyzed by platinum crystal surfaces with variable kink concentrations. Surface Science 1980, 91 (1), 73-91.

(131) Smith, C. E.; Biberian, J. P.; Somorjai, G. A. The effect of strongly bound oxygen on the dehydrogenation and hydrogenation activity and selectivity of platinum single crystal surfaces. Journal of Catalysis 1979, 57 (3), 426-443.

(132) Barr, T. L.; Seal, S. Nature of the use of adventitious carbon as a binding energy standard. Journal of Vacuum Science & Technology A 1995, 13 (3), 1239-1246.

(133) Kohiki, S.; Oki, K. Problems of adventitious carbon as an energy reference. Journal of Electron Spectroscopy and Related Phenomena 1984, 33 (4), 375-380.

(134) Evans, S. Correction for the effects of adventitious carbon overlayers in quantitative XPS analysis. Surface and interface analysis 1997, 25 (12), 924-930.

(135) Piao, H.; McIntyre, N. Adventitious carbon growth on aluminium and gold–aluminium alloy surfaces. Surface and interface analysis 2002, 33 (7), 591-594.

(136) Heister, K. The measurement of the specific surface area of soils by gas and polar liquid adsorption methods—Limitations and potentials. Geoderma 2014, 216, 75-87.

(137) Swift, P. Adventitious carbon—the panacea for energy referencing? Surface and Interface Analysis 1982, 4 (2), 47-51.

(138) Blyth, R. I. R.; Buqa, H.; Netzer, F. P.; Ramsey, M. G.; Besenhard, J. O.; Golob, P.; Winter, M. XPS studies of graphite electrode materials for lithium ion batteries. Applied Surface Science 2000, 167 (1–2), 99-106.

(139) Li, X.; Liu, M.; Lai, S. Y.; Ding, D.; Gong, M.; Lee, J.-P.; Blinn, K. S.; Bu, Y.; Wang, Z.; Bottomley, L. A. In situ probing of the mechanisms of coking resistance on catalyst-modified anodes for solid oxide fuel cells. Chemistry of Materials 2015, 27 (3), 822-828.

(140) Yang, M.-L.; Zhu, Y.-A.; Fan, C.; Sui, Z.-J.; Chen, D.; Zhou, X.-G. DFT study of propane dehydrogenation on Pt catalyst: effects of step sites. Physical Chemistry Chemical Physics 2011, 13 (8), 3257-3267.

(141) Bai, L.; Zhou, Y.; Zhang, Y.; Liu, H.; Tang, M. Influence of Calcium Addition on Catalytic Properties of PtSn/ZSM-5 Catalyst for Propane Dehydrogenation. Catalysis Letters 2009, 129 (3), 449.

(142) Huang, L.; Xu, B.; Yang, L.; Fan, Y. Propane dehydrogenation over the PtSn catalyst supported on alumina-modified SBA-15. Catalysis Communications 2008, 9 (15), 2593-2597.

(143) Beuther, H.; Larson, O. A.; Perrotta, A. J. The Mechanism of Coke Formation on Catalysts. In Studies in Surface Science and Catalysis; Delmon, B.; Froment, G. F., Eds.; Elsevier: 1980; pp 271-282.

(144) Guisnet, M.; Magnoux, P. Organic chemistry of coke formation. Applied Catalysis A: General 2001, 212 (1–2), 83-96.

(145) Smith, C.; Biberian, J.; Somorjai, G. The effect of strongly bound oxygen on the dehydrogenation and hydrogenation activity and selectivity of platinum single crystal surfaces. Journal of Catalysis 1979, 57 (3), 426-443.

(146) Wintterlin, J.; Völkening, S.; Janssens, T. V. W.; Zambelli, T.; Ertl, G. Atomic and Macroscopic Reaction Rates of a Surface-Catalyzed Reaction. Science 1997, 278 (5345), 1931-1934.

(147) Nesselberger, M.; Ashton, S.; Meier, J. C.; Katsounaros, I.; Mayrhofer, K. J. J.; Arenz, M. The Particle Size Effect on the Oxygen Reduction Reaction Activity of Pt Catalysts: Influence of Electrolyte and Relation to Single Crystal Models. Journal of the American Chemical Society 2011, 133 (43), 17428-17433.

(148) Toyoda, E.; Jinnouchi, R.; Hatanaka, T.; Morimoto, Y.; Mitsuhara, K.; Visikovskiy, A.; Kido, Y. The d-Band Structure of Pt Nanoclusters Correlated with the Catalytic Activity for an Oxygen Reduction Reaction. The Journal of Physical Chemistry C 2011, 115 (43), 21236-21240.

(149) Mason, M. G. Electronic structure of supported small metal clusters. Physical Review B 1983, 27 (2), 748-762.

(150) Roduner, E. Size matters: why nanomaterials are different. Chemical Society Reviews 2006, 35 (7), 583-592.

(151) Zhou, L.; Zachariah, M. R. Size resolved particle work function measurement of free nanoparticles: Aggregates vs. spheres. Chemical Physics Letters 2012, 525, 77-81.

(152) Parker, D. H.; Bartram, M. E.; Koel, B. E. Study of high coverages of atomic oxygen on the Pt(111) surface. Surface Science 1989, 217 (3), 489-510

(153) Briot, P.; Auroux, A.; Jones, D.; Primet, M. Effect of particle size on the reactivity of oxygen-adsorbed platinum supported on alumina. Applied Catalysis 1990, 59 (1), 141-152.

(154) Hammer, B.; Nørskov, J. K. Theoretical surface science and catalysis—calculations and concepts. Advances in catalysis 2000, 45, 71-129.

(155) Ciraci, S.; Batra, I. P. Theory of the quantum size effect in simple metals. Physical Review B 1986, 33 (6), 4294-4297.

(156) Jalan, V.; Taylor, E. Importance of interatomic spacing in catalytic reduction of oxygen in phosphoric acid. Electrochemical Society, Journal 1983, 130, 2299-2302.

(157) Appleby, A. Oxygen reduction on bright osmium electrodes in 85% orthophosphoric acid. Journal of The Electrochemical Society 1970, 117 (9), 1157-1159.

(158) Shin, J.; Choi, J.-H.; Cha, P.-R.; Kim, S. K.; Kim, I.; Lee, S.-C.; Jeong, D. S. Catalytic activity for oxygen reduction reaction on platinum-based core-shell nanoparticles: all-electron density functional theory. Nanoscale 2015, 7 (38), 15830-15839.

(159) Mills, A. Final Analysis: Porous Platinum Morphologies: Platinised, Sponge and Black. 2007.

(160) Hall, S. B.; Khudaish, E. A.; Hart, A. L. Electrochemical oxidation of hydrogen peroxide at platinum electrodes. Part II: effect of potential. Electrochimica Acta 1998, 43 (14), 2015-2024.

(161) Choudhary, V. R.; Samanta, C.; Jana, P. Decomposition and/or hydrogenation of hydrogen peroxide over Pd/Al_2O_3 catalyst in aqueous medium: Factors affecting the rate of H_2O_2 destruction in presence of hydrogen. Applied Catalysis A: General 2007, 332 (1), 70-78.

(162) Lousada, C. M.; Yang, M.; Nilsson, K.; Jonsson, M. Catalytic decomposition of hydrogen peroxide on transition metal and lanthanide oxides. Journal of Molecular Catalysis A: Chemical 2013, 379, 178-184.

(163) Bianchi, G.; Mazza, F.; Mussini, T.; UNIV, M. Cathodic Reduction of Oxygen and Hydrogen Peroxide on Platinum, Palladium and Iridium Smooth Electrodes, Defense Technical Information Center: 1961.

(164) Hasnat, M. A.; Rahman, M. M.; Borhanuddin, S. M.; Siddiqua, A.; Bahadur, N. M.; Karim, M. R. Efficient hydrogen peroxide decomposition on bimetallic Pt–Pd surfaces. Catalysis Communications 2010, 12 (4), 286-291.

(165) MacInnes, D. A. The Mechanism of the Catalysis of the Decomposition of Hydrogen Peroxide by Colloidal Platinum. Journal of the American Chemical Society 1914, 36 (5), 878-881,.

(166) Hall, S. B.; Khudaish, E. A.; Hart, A. L. Electrochemical oxidation of hydrogen peroxide at platinum electrodes. Part 1. An adsorption-controlled mechanism. Electrochimica Acta 1998, 43 (5), 579-588.

(167) Ono, Y.; Matsumura, T.; Kitajima, N.; Fukuzumi, S. Formation of superoxide ion during the decomposition of hydrogen peroxide on supported metals. The Journal of Physical Chemistry 1977, 81 (13), 1307-1311.

(168) Kitajima, N.; Fukuzumi, S.; Ono, Y. Formation of superoxide ion during the decomposition of hydrogen peroxide on supported metal oxides. The Journal of Physical Chemistry 1978, 82 (13), 1505-1509.

(169) Gerischer, R. Über die katalytische Zersetzung von Wasserstoffsuperoxyd an metallischem Platin. Zeitschrift für physikalische Chemie (Neue Folge) 6 (3 - 4), 178-200.

(170) Schaeffer, J.; Fonseca, L.; Samavedam, S.; Liang, Y.; Tobin, P.; White, B. Contributions to the effective work function of platinum on hafnium dioxide. Applied physics letters 2004, 85 (10), 1826-1828.

(171) Međedović, S.; Locke, B. R. Platinum catalysed decomposition of hydrogen peroxide in aqueous-phase pulsed corona electrical discharge. Applied Catalysis B: Environmental 2006, 67 (3–4), 149-159.

(172) Kirkpatrick, M. J.; Locke, B. R. Effects of platinum electrode on hydrogen, oxygen, and hydrogen peroxide formation in aqueous phase pulsed corona electrical discharge. Industrial & engineering chemistry research 2006, 45 (6), 2138-2142.

(173) Katsounaros, I.; Schneider, W. B.; Meier, J. C.; Benedikt, U.; Biedermann, P. U.; Auer, A. A.; Mayrhofer, K. J. Hydrogen peroxide electrochemistry on platinum: towards understanding the oxygen reduction reaction mechanism. Physical Chemistry Chemical Physics 2012, 14 (20), 7384-7391.

(174) Chiang, Y. S.; Craddock, J.; Mickewich, D.; Turkevich, J. Study with Fast-Mixing Techniques of the Titanium (III) and Hydrogen Peroxide Reaction. The Journal of Physical Chemistry 1966, 70 (11), 3509-3515.

(175) Saito, E.; Bielski, B. H. J. The Electron Paramagnetic Resonance Spectrum of the HO_2 Radical in Aqueous Solution. Journal of the American Chemical Society 1961, 83 (21), 4467-4468,.

(176) Keating, K. B.; Rozner, A. G.; Youngblood, J. L. The effect of deformation on catalytic activity of platinum in the decomposition of hydrogen peroxide. Journal of Catalysis 1965, 4 (5), 608-619.

(177) Burch, R.; Bond, G.; Webb, G. Specialist periodical reports. Catalysis 1985, 7, 149.

(178) Trasatti, S. Electronegativity, work function, and heat of adsorption of hydrogen on metals. Journal of the Chemical Society, Faraday Transactions 1: Physical Chemistry in Condensed Phases 1972, 68 (0), 229-236.

(179) Nørskov, J. K.; Rossmeisl, J.; Logadottir, A.; Lindqvist, L.; Kitchin, J. R.; Bligaard, T.; Jonsson, H. Origin of the overpotential for oxygen reduction at a fuel-cell cathode. The Journal of Physical Chemistry B 2004, 108 (46), 17886-17892.

(180) Sabatier, P. La catalyse en chimie organique, Nouveau Monde éditions: 2014.

(181) Gay, C.; Collins, J.; Gebicki, J. M. Hydroperoxide assay with the ferric–xylenol orange complex. Analytical biochemistry 1999, 273 (2), 149-155.

(182) Rimstidt, J. D. Geochemical Rate Models: An Introduction to Geochemical Kinetics, Cambridge University Press: 2013.

(183) Pollyea, R. M.; Rimstidt, J. D. Rate equations for modeling carbon dioxide sequestration in basalt. Applied Geochemistry 2017, 81, 53-62.

(184) Steiner, M. G.; Babbs, C. F. Quantitation of the hydroxyl radical by reaction with dimethyl sulfoxide. Archives of Biochemistry and Biophysics 1990, 278 (2), 478-481.

(185) Babbs, C. F.; Gale, M. J. Colorimetric assay for methanesulfinic acid in biological samples. Analytical Biochemistry 1987, 163 (1), 67-73.

(186) Lasaga, A. C. Rate laws of chemical reactions. Rev. Mineral.;(United States) 1981, 8.

(187) Ou, L.; Yang, F.; Liu, Y.; Chen, S. First-principle study of the adsorption and dissociation of O_2 on Pt (111) in acidic media. The Journal of Physical Chemistry C 2009, 113 (48), 20657-20665.

(188) Arruda, T. M.; Shyam, B.; Ziegelbauer, J. M.; Mukerjee, S.; Ramaker, D. E. Investigation into the competitive and site-specific nature of anion adsorption on Pt using in situ X-ray absorption spectroscopy. The Journal of Physical Chemistry C 2008, 112 (46), 18087-18097.

(189) Keating, K.; Rozner, A.; Youngblood, J. The effect of deformation on catalytic activity of platinum in the decomposition of hydrogen peroxide. Journal of Catalysis 1965, 4 (5), 608-619.

(190) van Hardeveld, R.; Hartog, F. Influence of Metal Particle Size in Nickel-on-Aerosil Catalysts on Surface Site Distribution, Catalytic Activity, and Selectivity. Advances in Catalysis 1972, 22, 75-113.

(191) Balbuena, P. B.; Calvo, S. R.; Lamas, E. J.; Salazar, P. F.; Seminario, J. M. Adsorption and Dissociation of H_2O_2 on Pt and Pt− Alloy Clusters and Surfaces. The Journal of Physical Chemistry B 2006, 110 (35), 17452-17459.

(192) Sweeney, W.; Lee, J.; Abid, N.; DeMeo, S. Efficient Method for the Determination of the Activation Energy of the Iodide-Catalyzed Decomposition of Hydrogen Peroxide. Journal of Chemical Education 2014, 91 (8), 1216-1219.

(193) Wang, Y.; Balbuena, P. B. Potential Energy Surface Profile of the Oxygen Reduction Reaction on a Pt Cluster: Adsorption and Decomposition of OOH and H_2O_2. Journal of Chemical Theory and Computation 2005, 1 (5), 935-943.

(194) Panchenko, A.; Koper, M.; Shubina, T.; Mitchell, S.; Roduner, E. Ab initio calculations of intermediates of oxygen reduction on low-index platinum surfaces. Journal of the Electrochemical Society 2004, 151 (12), A2016-A2027.

(195) Gu, Z.; Balbuena, P. B. Absorption of Atomic Oxygen into Subsurfaces of Pt(100) and Pt(111): Density Functional Theory Study. The Journal of Physical Chemistry C 2007, 111 (27), 9877-9883.

(196) Stanca, S. E.; Hänschke, F.; Ihring, A.; Zieger, G.; Dellith, J.; Kessler, E.; Meyer, H. G. Chemical and Electrochemical Synthesis of Platinum Black. Scientific Reports 2017, 7, 1074.

(197) Velleman, P. F.; Welsch, R. E. Efficient Computing of Regression Diagnostics. The American Statistician 1981, 35 (4), 234-242.

(198) Moya-Laraño, J.; Corcobado, G. Plotting partial correlation and regression in ecological studies. Web Ecology 2008, 8 (1), 35-46.

(199) Tabib Zadeh Adibi, P.; Zhdanov, V. P.; Langhammer, C.; Grönbeck, H. Transient bimodal particle size distributions during Pt sintering on alumina and silica. The Journal of Physical Chemistry C 2015, 119 (2), 989-996.

(200) Houk, L. R.; Challa, S. R.; Grayson, B.; Fanson, P.; Datye, A. K. The Definition of "Critical Radius" for a Collection of Nanoparticles Undergoing Ostwald Ripening. Langmuir 2009, 25 (19), 11225-11227.

(201) Finsy, R. On the Critical Radius in Ostwald Ripening. Langmuir 2004, 20 (7), 2975-2976.

(202) Plessow, P. N.; Abild-Pedersen, F. Sintering of Pt Nanoparticles via Volatile PtO_2: Simulation and Comparison with Experiments. ACS Catalysis 2016, 6 (10), 7098-7108.

(203) Parkinson, C.; Walker, M.; McConville, C. F. Reaction of atomic oxygen with a Pt(111) surface: Chemical and structural determination using XPS, CAICISS and LEED, 2003; Vol. 545, p 19-33.

(204) Peuckert, M.; Yoneda, T.; Dalla Betta, R.; Boudart, M. Oxygen reduction on small supported platinum particles. Journal of the Electrochemical Society 1986, 133 (5), 944-947.

(205) Bockris, J. O. M.; Conway, B. E.; White, R. E. Modern aspects of electrochemistry, Springer Science & Business Media: 2012; Vol. 22.

(206) Balasubramanian, B.; Barbir, F.; Neutzler, J. Oi" Hmal operating temperature and pressure of PEM fuel cell systems in automotive applications. 1999.

(207) Rahim, A.; Hasbi, M.; Forde, M. M.; Jenkins, R. L.; Hammond, C.; He, Q.; Dimitratos, N.; Lopez-Sanchez, J. A.; Carley, A. F.; Taylor, S. H. Oxidation of methane to methanol with hydrogen peroxide using supported gold–palladium alloy nanoparticles. Angewandte Chemie 2013, 125 (4), 1318-1322.

(208) Narsimhan, K.; Iyoki, K.; Dinh, K.; Román-Leshkov, Y. Catalytic Oxidation of Methane into Methanol over Copper-Exchanged Zeolites with Oxygen at Low Temperature. ACS Central Science 2016, 2 (6), 424-429.

(209) Agarwal, N.; Freakley, S. J.; McVicker, R. U.; Althahban, S. M.; Dimitratos, N.; He, Q.; Morgan, D. J.; Jenkins, R. L.; Willock, D. J.; Taylor, S. H. Aqueous Au-Pd colloids catalyze selective CH_4 oxidation to CH_3OH with O_2 under mild conditions. Science 2017, 358 (6360), 223-227.

Appendix A Chapter 1

Abundance and Speciation of Surface Oxygen on Nanosized Platinum Catalysts and Effect on Catalytic Activity

Acknowledgements

F. M. M. and R. S. M. gratefully acknowledge financial support from the Virginia Tech Institute for Critical Technology and Applied Science (ICTAS) through a Junior Faculty Collaborative Grant (ICTAS-JFC 175884). R. S. M. gratefully acknowledges the Virginia Tech College of Science Roundtable Alumni Advisory Group for financial support provided through a "Make-a-Difference" Scholarship, as well as the Department of Geosciences for support provided by Sir Aubrey and Madam Eula Orange Scholarship funds. The authors also thank Dr. Robert Bodnar and Mr. Charles Farley for support with selected experiments.

Supporting Information

Table S1.1 provides a summary of synthesis methods, characterization results, and the motivation for previous studies that characterized Pt black synthesized by chemical reduction or electrochemical deposition.

Table S1.1. Summary of previous studies that characterized platinum black.

Reference	Synthesis method	Characterization Results	Purpose
80	Electrodeposited from H_2PtCl_6	SEM imaging AFM imaging Grains in the order of nanometers Fractal morphology aggregate thickness = 1 µm	Temperature annealing studies
68	Obtained by Fisher CO in the form of a powder *(chemically reduced)*	SSA = 16.7 m^2/g Roughly spherical particles Diameter of ~ 100 Å Surface covered with monolayer of oxygen	Catalytic cracking of propane Temperature dependence of activity
61	Electrodeposited from H_2PtCl_6	SEM imaging Roughness factor (RF) varied from 10-100	Peroxide sensor
84	Elecrodeposited from H_2PtCl_6	SEM imaging Porous structures Diameter 3-200 nm	Dielectrophoretic assembly of microparticles
71	Two preps: - Chemical reduction of PtO_2 *(Adams' method)* - Chemical reduction of H_2PtCl_6 by formaldehyde	SSA = 30.5 m^2/g Diameter ~92 Å SSA = 24.0 m^2/g Diameter ~116 Å	Crystallite size effects on the oxygen reduction reaction (ORR)
72	Chemical reduction	SSA = 30 m^2/g Diameter ~100 Å	Crystallite size effects on oxide formation
75	Chemical reduction	SSA = 24.5 m^2/g Diameter ~ 100 Å	Sintering and loss of surface area in fuel cells
85	Chemical reduction of H_2PtCl_6 by formaldehyde	TEM imaging SSA = 8 m^2/g Diameter (TEM) 80 Å Diameter (XRD) 115 Å	Sintering studies

76	Obtained from Englehard *(chemical reduction)*	SSA = 10 m^2/g	Crystallite size on electrochemical reduction of oxygen
65	Chemical reduction of PtO_2 to Pt during the hydrogenation reaction *(Adams' method)*	Oxyegen content between 10-20%	Catalytic reduction of organic compounds
73	Chemical reduction *(Adam's method)*	SEM imaging SSA = 24 – 29 m^2/g	Description of platinized platinum, platinum sponge and platinum black
70	Obtained from Johnson Matthey *(Chemical reduction)*	SSA = 30 m^2/g	Loss of surface area at 150 ºC
78	Chemical reduction of H_2PtCl_6 with HCHO	TEM imaging crystallite size = 5 - 12 nm	Sintering of Pt black in the presence of hydrogen

Table S1.2 provides a summary of synthesis methods, characterization results, and the motivation of previous studies that characterized Pt nanopowder synthesized by chemical vapor deposition methods.

Table S1.2. Summary of previous studies that report morphology and characterization of platinum nanoparticles obtained by chemical vapor deposition.

Reference	Synthesis method	Characterization Results	Purpose
62	Chemical vapor deposition	Irregularly shaped nanoparticles deposited on carbon nanotubes. Crystallite size 1-30 nm	For use as fuel cell electrode catalyst
92	Combustion chemical vapor deposition	(Pseudo) round shaped particles deposited on carbon black aggregates. Crystallite size 5-10 nm Pt and O are both present in EDX spectrum	Development of a economically viable chemical vapor deposition technique
94	Single step low temperature vaporization	(Pseudo) round shaped nanoparticles enveloped on porous graphene. TEM analysis. Crystallite size ranges between 5-few tens of nanometers No bond between Pt and C was observed on XPS	Development of a formulation with enhanced lifetime
95	Chemical vapor deposition	Round shaped particles forming predominantly flat clusters. STM analysis Crystallite size 3-6 nm Exposure to air increased XPS signal around signal reported from both water and PtO_2	Scanning Tunneling microscopy studies on platinum nanoparticles deposited on basal graphite
93	Vacuum deposition	Ultrafine platinum nanoparticles dispersed on carbon-film. STM analysis Crystallite size 2-4 nm Halves of Cubo-octahedra (111) and (100) faces exposed	Study the effects of the preparation procedures and the support materials on shape of supported ultrafine platinum nanoparticles

Figure S1.1 shows scanning electron microscopy analysis performed on dry powder samples, in the as received condition, loaded on double coated carbon conductive tape (Ted Pella, USA). Images were collected using a FEI Quanta 600 FEG at an accelerating voltage of 20 KeV.

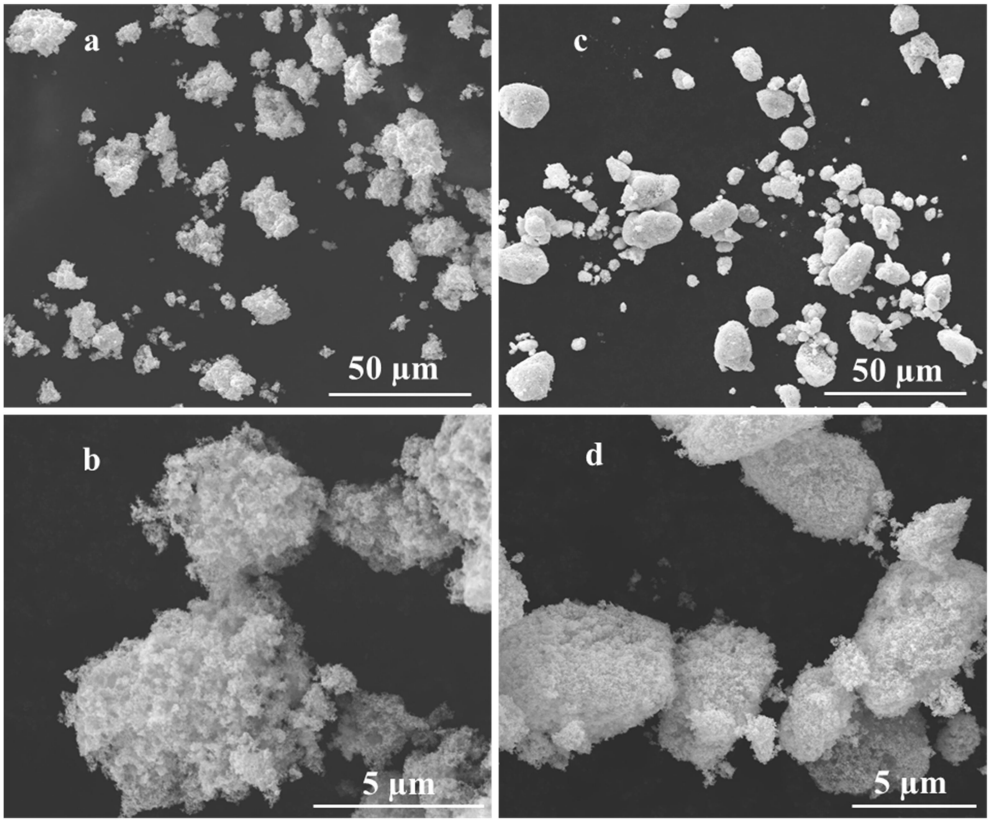

Figure S1.1. Scanning electron microscopy (SEM) images of dry, as received, Pt black (a–b) and Pt nanopowder (c–d).

Figure S1.2 shows TEM selected area electron diffraction (SAED) patterns for Pt black and Pt nanopowder and the particle aggregates from which those patterns were obtained. SAED patterns indicate that the featured aggregates of both Pt black and Pt nanopowder are polycrystalline.

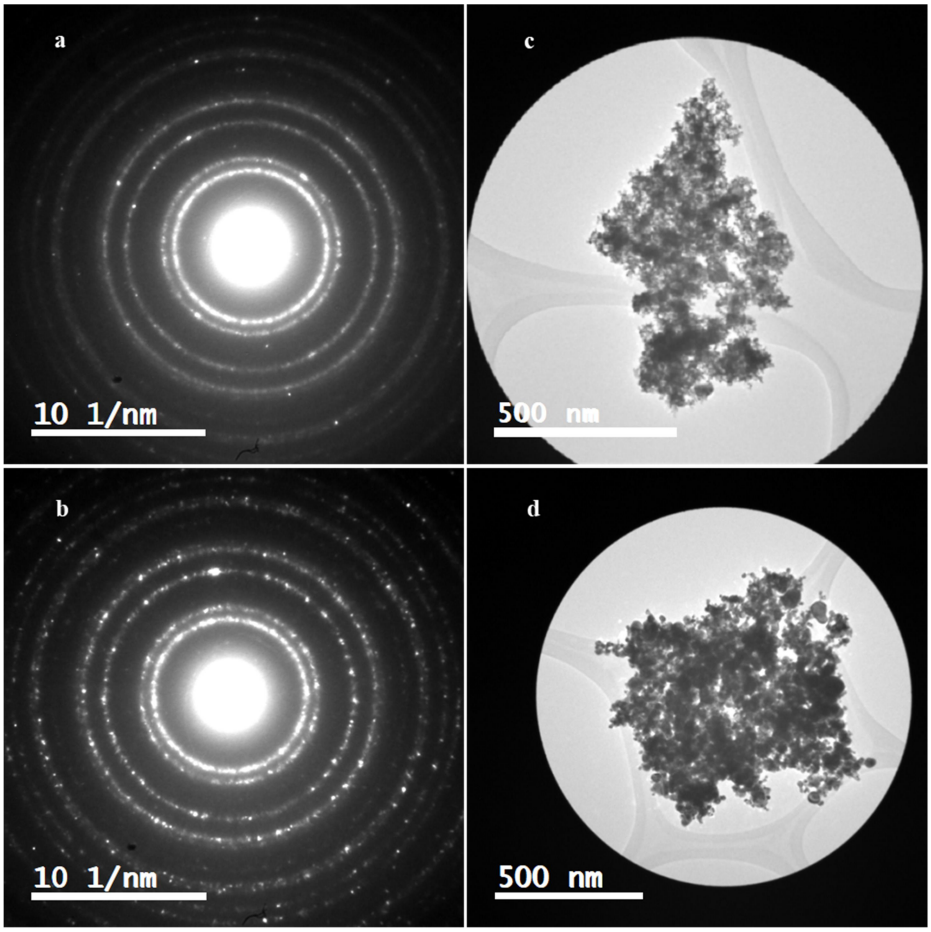

Figure S1.2. SAED (a) obtained with camera length of 120 mm and 20s of exposure time of an aggregate of Pt black-AsRec (c) and SAED (b) obtained with camera length of 120 mm and 20s of exposure time of an aggregate of Pt nanopowder-AsRec (d).

TEM selected area electron diffraction

The diffraction patterns for Pt black-AsRec and Pt nanopowder-AsRec are mostly continuous rings, which confirm both samples are polycrystalline at the nanoscale **(Figure S1.2)**. The measured d-spacings of Pt black are smaller than those of Pt nanopowder for all four characteristic FCC reflections **(Table S1.3)**. The differences were statistically significant for the (111) and (200) (p-value=0.034 and 0.007, respectively) but not for the (311) and (220) (p-value=0.075 and 0.410, respectively). This result indicates that the average unit cell dimension of Pt black is smaller than Pt nanopowder, which is consistent with the result obtained from XRD Rietveld analysis.

Table S1.3. Selected area electron diffraction d-spacing measurements of Pt nanopowder and Pt black.

	(111)	(200)	(220)	(311)
Pt nanopowder	2.28(1)	1.97(9)	1.39(4)	1.18(9)
Pt black	2.27(4)	1.97(0)	1.39(2)	1.18(6)

Figure S1.3 shows the full XRD spectra of both Pt black and Pt nanopowder in the as received conditions, subjected to BET outgassing conditions and subjected to TGA heating conditions (in air or nitrogen).

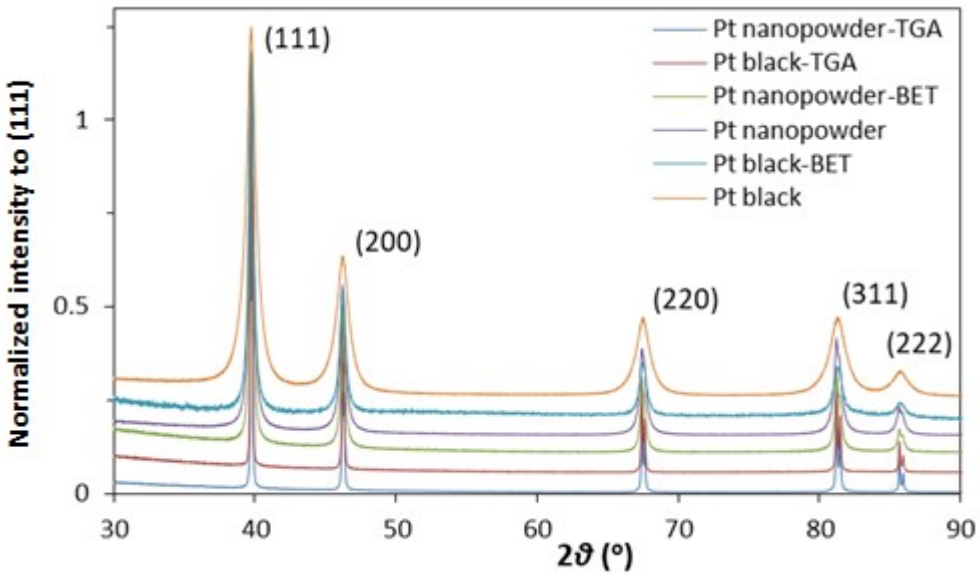

Figure S1.3. X-ray diffraction spectra of Pt nanopowder and Pt black. The y-axis of the plot is offset in increments of 0.05 between each curve.

Scherrer analysis based on the first four reflections (111, 200, 220, and 311) for as received Pt nanopowder and Pt black indicated average crystallite sizes of 28.6 ± 2.4 nm and 9.5 ± 0.7 nm, respectively. Heating the samples at 300 ºC for 22 h increased the average Scherrer for Pt nanopowder and Pt black to 49.4 ± 9.3 nm and 25.5 ± 6.2 nm, respectively. Scherrer analysis of the samples subjected to TGA procedure showed that the FWHM of all four samples were only affected by instrumental broadening, which indicates crystallite size dimensions of > 1µm.

Table S1.4 shows Rietveld refinement parameters for silicon standard and the Pt samples. The instrumental broadening was modeled using the fundamental parameters approach and a silicon standard. The factors for goodness-of-fit (GOF, R_{wp}=7.36% and χ^2=2.02) and visual inspection of the refined pattern for silicon indicate that the FPA configuration adequately describes the weight function of the instrument. Thus, it can be assumed that any additional broadening of the peaks for the Pt samples is due to effects of crystal size and/or microstrain.

Table S1.4. Selected results of Rietveld analysis. Uncertainties given in parentheses.

	Crystal size (nm)	Unit cell dimension (Å)	Microstrain	GOF
Silicon (standard)	>1000	5.431(8)	0	2.25
Pt nanopowder	22.70(4)	3.923(1)	0	2.26
Pt black	11.31(4)	3.920(6)	Anys. 2.7×10^{-5}	3.78
Pt nanopowder-BET	40.2(3)	3.923(2)	0	2.07
Pt black-BET	21.7(2)	3.922(0)	Anys. 0.8×10^{-5}	3.02
Pt nanopowder-TGA	>1000	3.923(8)	0	2.27
Pt-black-TGA	>1000	3.923(7)	0	1.66

Figure S1.4 shows the observed, calculated and difference patterns of Rietveld fitting for each sample.

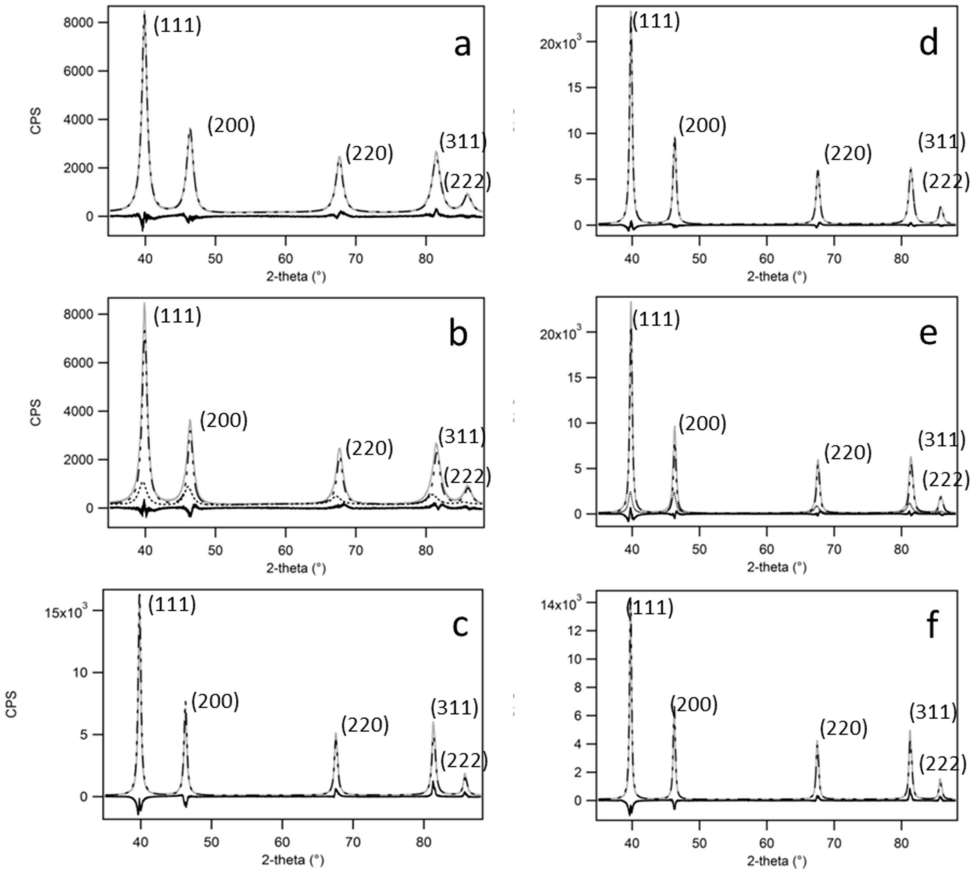

Figure S1.4. Full profile Rietveld analysis of a) Pt black-AsRec, b) Pt black-BET, c) Pt black-TGA, d) Pt nanopowder-AsRec, e) Pt nanopowder-BET and f) Pt nanopowder-TGA.

Figure S1.5 shows high-resolution XPS analysis for Pt black, Pt black-TGA, Pt nanopowder and Pt nanopowder-TGA, for the C1s, O1s and Pt4f peaks.

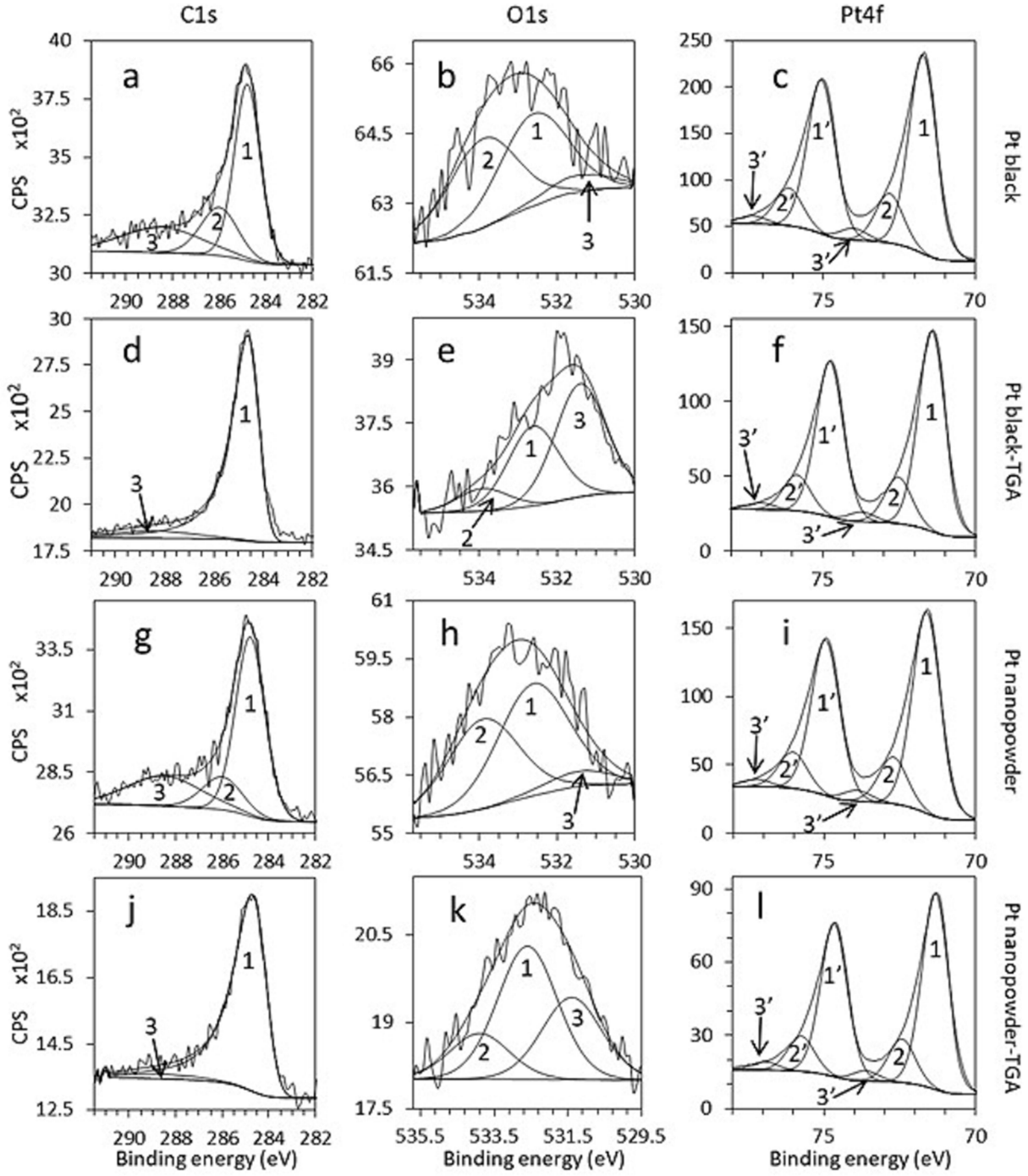

Figure S1.5. High resolution XPS analysis of Pt black (a - c), Pt black-TGA (d - f), Pt nanopowder (g - i) and Pt nanopowder-TGA (j - l).

Table S1.5 provides information of the Pt1 peak position (see S.I. Figure E), the area of each component from the $Pt4f_{7/2}$ XPS peak and area ratios between those three components.

Analysis of the Pt4f peak is very challenging due to the simultaneous effect of particle size and oxidation state as well as the overlap of some PtO_x components with the surface Pt-Pt components[121]. The Pt4f spectra were deconvoluted into symmetric doublets labeled 1, 2 and 3 ($4f_{7/2}$), and 1', 2' and 3' ($4f_{5/2}$), following the approach used by Zhang et al. (2007) **(Figure S1.5 c, f, i and l)**[121]. The position of Pt1 (bulk Pt-Pt) was allowed to vary at 71.5 ± 0.5 eV to account for particle size effects on the Pt binding energy. The other peaks were attributed as follows Pt2 (1.1 eV above Pt1, surface Pt-Pt + Pt-(O) structures) and Pt3 (2.3 eV above Pt1, PtO_x structures). The components of $Pt4f_{5/2}$ were all set at 3.3 eV above their counterpart $Pt4f_{7/2}$ components.

The position of the Pt1 peak correlates with particle size. The Pt1 peak shifted to lower energies in the order of Pt black-AsRec > Pt nanopowder-AsRec > Pt black-TGA_{air} > Pt nanopowder-TGA_{air}. This order is consistent with the particle size order determined by XRD Rietveld analysis. The ratio of Pt1/Pt2 is 1.08 times larger on Pt nanopowder than on Pt black in the as received condition, indicating a higher percentage of bulk Pt-Pt bonds relative to Pt-(O) and surface Pt-Pt bonds on Pt nanopowder ($p = 0.041$). In contrast, the difference of Pt1/Pt2 between the two catalysts after being exposed to TGA heating conditions was not statistically significant ($p = 0.753$).

Table S1.5. High res XPS Pt4f7/2 peak area analysis.

	Pt1 position	Pt1	Pt2	Pt3	Pt3/Pt2	Pt1/Pt2	Pt1/Pt3
Pt black	71.66±0.02	78.02±0.07	19.05±0.05	2.93±0.08	0.15±0.01	4.09±0.01	26.67±0.72
Pt black-TGA	71.43±0.01	79.11±0.25	18.39±0.16	2.51±0.16	0.14±0.01	4.30±0.05	31.65±2.10
Pt nanopowder	71.65±0.04	79.65±0.73	17.94±0.35	2.41±0.38	0.13±0.02	4.44±0.13	33.68±6.0
Pt nanopowder-TGA	71.27±0.11	78.15±2.46	18.69±1.52	3.15±0.96	0.17±0.04	4.21±0.45	26.28±7.45

Figure S1.6 shows TGA curves of Pt black and Pt nanopowder heated to 700 ^{o}C.

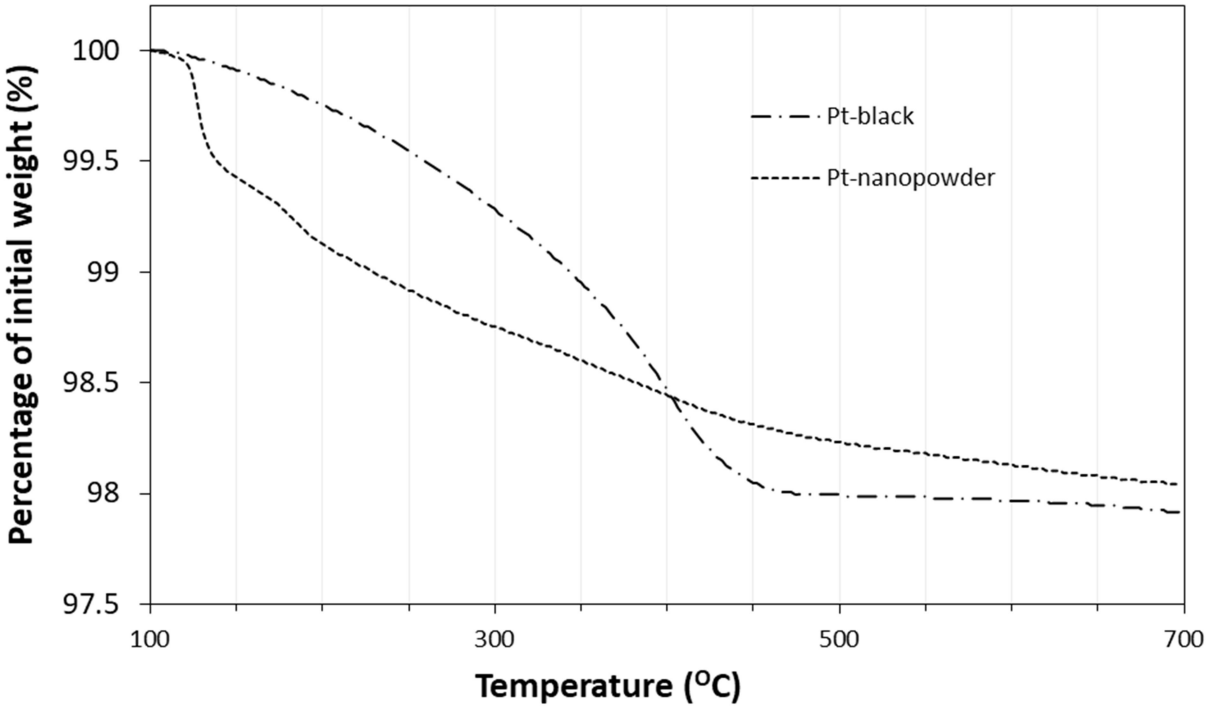

Figure S1.6. Thermogravimetric analysis of Pt black and Pt nanopowder in air.

Table S1.6. Rate measurements for Pt black-BET, Pt black-air, Pt nanopowder-BET and Pt nanopowder-air at different conditions of $C_{H_2O_2}$, pH and temperature.

Catalyst	Temp., K	$1/T$	pH	$C_{H_2O_2}$ $(mol \cdot L^{-1})$	log $C_{H_2O_2}$	R, $mol.m^{-2}.s^{-1}$	log R
Pt black-BET	295	0.00339	5.99	0.0001	-4	1.15×10^{-06}	-5.94
Pt black-BET	315	0.00317	5.88	0.0001	-4	2.09×10^{-06}	-5.68
Pt black-BET	295	0.00339	5.9	0.001	-3	1.05×10^{-05}	-4.98
Pt black-BET	316	0.00316	5.86	0.001	-3	1.55×10^{-05}	-4.81
Pt black-BET	275	0.00363	5.87	0.0001	-4	3.14×10^{-07}	-6.50
Pt black-BET	275	0.00363	5.89	0.001	-3	2.35×10^{-06}	-5.63
Pt black-air	295	0.00339	5.9	0.0001	-4	1.71×10^{-06}	-5.77
Pt black-air	296	0.00338	5.83	0.001	-3	1.54×10^{-05}	-4.81
Pt black-air	320	0.00312	5.8	0.001	-3	3.57×10^{-05}	-4.45
Pt black-air	322	0.00310	5.8	0.0001	-4	7.57×10^{-06}	-5.12
Pt black-air	296	0.00338	5.77	0.0003	-3.52	5.31×10^{-06}	-5.27
Pt black-air	324	0.00309	5.8	0.0003	-3.52	1.41×10^{-05}	-4.85
Pt black-air	296	0.00338	5.86	0.001	-3	1.94×10^{-05}	-4.71
Pt black-air	275	0.00363	5.9	0.0001	-4	6.5×10^{-07}	-6.19
Pt nanopowder-BET	295	0.00339	5.85	0.0001	-4	7.34×10^{-06}	-5.13
Pt nanopowder-BET	315	0.00318	5.8	0.0001	-4	9.69×10^{-06}	-5.01
Pt nanopowder-BET	296	0.00338	5.85	0.001	-3	6.59×10^{-05}	-4.18
Pt nanopowder-BET	314	0.00318	5.87	0.001	-3	1.4×10^{-04}	-3.85
Pt nanopowder-air	295	0.00339	6.02	0.0001	-4	7.71×10^{-06}	-5.11
Pt nanopowder-air	315	0.00317	5.83	0.0001	-4	1.33×10^{-05}	-4.88
Pt nanopowder-air	294	0.00340	5.91	0.001	-3	7.97×10^{-05}	-4.10
Pt nanopowder-air	316	0.00316	5.72	0.001	-3	1.14×10^{-04}	-3.94
Pt nanopowder-air	275	0.00363	5.69	0.0001	-4	3.55×10^{-06}	-5.45
Pt nanopowder-air	276	0.00362	5.75	0.001	-3	2.29×10^{-05}	-4.64

Appendix B Chapter 2

Mechanism and Kinetics of Hydrogen peroxide Decomposition on Platinum Nanocatalysts

Acknowledgements

F. M. M. and R. S. M. gratefully acknowledge financial support from the Virginia Tech Institute for Critical Technology and Applied Science (ICTAS) through a Junior Faculty Collaborative Grant (ICTAS-JFC 175884). R. S. M. gratefully acknowledges the Virginia Tech College of Science Roundtable Alumni Advisory Group for financial support provided through a "Make-a-Difference" Scholarship, as well as the Department of Geosciences for support provided by Sir Aubrey and Madam Eula Orange Scholarship funds. The authors also thank Dr. Robert Bodnar and Mr. Charles Farley for support with selected experiments.

Supporting Information

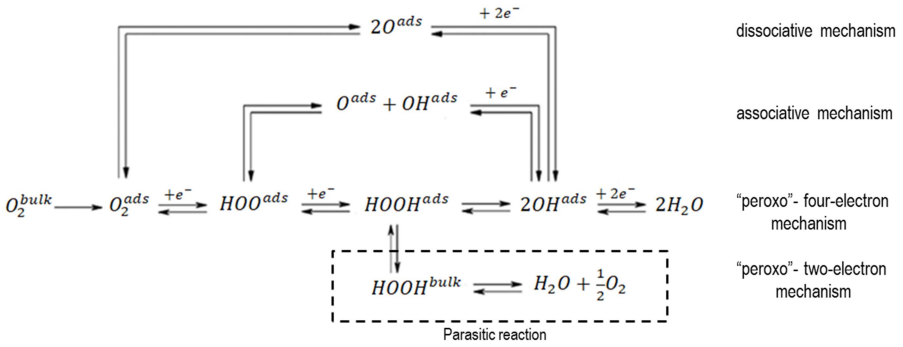

Figure S2.1. Oxygen reduction reaction mechanisms (reproduced with permission from ref[173]. (Copyright 2012 Royal Society of Chemistry)[173].

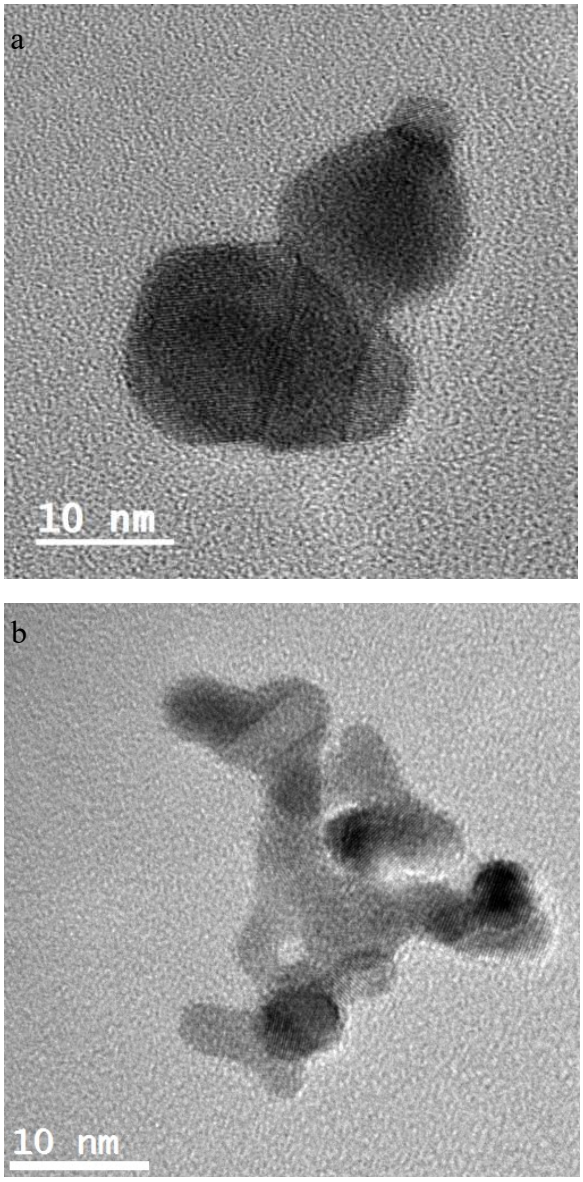

Figure S2.2. Transmission electron microscopy image of a small cluster of Pt nanopowder (a) and Pt black (b). Each cluster is formed by a few nanocrystals loosely attached.

Table S2.1. Rate measurements for Pt nanopowder and Pt black at different conditions of $C_{H_2O_2}$, pH and temperature.

Catalyst	Temp., K	$1/T$	pH	$C_{H_2O_2}$ $(mol \cdot L^{-1})$	log $C_{H_2O_2}$	R, $mol.m^{-2}.s^{-1}$	log R
Pt nanopowder	275	0.00363	9.17	0.0001	-4.00	1.8×10^{-06}	-5.74
Pt nanopowder	293	0.00341	9.25	0.0001	-4.00	4.52×10^{-06}	-5.35
Pt nanopowder	275	0.00363	7.87	0.0003	-3.52	5.99×10^{-06}	-5.22
Pt nanopowder	274	0.00365	4.82	0.001	-3.00	1.45×10^{-05}	-4.84
Pt nanopowder	275	0.00363	3.7	0.0001	-4.00	2.21×10^{-06}	-5.66
Pt nanopowder	293	0.00341	3.02	0.0001	-4.00	3.76×10^{-06}	-5.42
Pt nanopowder	293	0.00341	9.3	0.0001	-4.00	9.43×10^{-06}	-5.03
Pt nanopowder	293	0.00341	6.68	0.0001	-4.00	1.06×10^{-05}	-4.98
Pt nanopowder	293	0.00341	9.25	0.001	-3.00	1.02×10^{-04}	-3.99
Pt nanopowder	293	0.00341	3.06	0.001	-3.00	1.97×10^{-05}	-4.71
Pt nanopowder	275	0.00363	3.24	0.001	-3.00	1.39×10^{-05}	-4.86
Pt nanopowder	275	0.00363	9.65	0.0001	-4.00	5.28×10^{-06}	-5.28
Pt nanopowder	293	0.00341	4.44	0.0005	-3.30	1.74×10^{-05}	-4.76
Pt nanopowder	293	0.00341	6	0.0005	-3.30	3.61×10^{-05}	-4.44
Pt nanopowder	293	0.00341	3.8	0.0001	-4.00	4.88×10^{-06}	-5.31
Pt nanopowder	293	0.00341	8.5	0.0001	-4.00	8.41×10^{-06}	-5.08
Pt nanopowder	293	0.00341	8.36	0.001	-3.00	1.08×10^{-04}	-3.97
Pt nanopowder	293	0.00341	6.26	0.001	-3.00	5.00×10^{-05}	-4.3
Pt nanopowder	293	0.00341	5.14	0.001	-3.00	4.67×10^{-05}	-4.33
Pt nanopowder	293	0.00341	6.77	0.00025	-3.60	1.77×10^{-05}	-4.75
Pt nanopowder	293	0.00341	3.94	0.00025	-3.60	1.44×10^{-05}	-4.84
Pt nanopowder	274	0.00365	7.96	0.0001	-4.00	8.64×10^{-06}	-5.06
Pt nanopowder	276	0.00362	3.11	0.0001	-4.00	3.61×10^{-06}	-5.44
Pt nanopowder	275	0.00364	3.33	0.001	-3.00	2.58×10^{-05}	-4.59
Pt nanopowder	276	0.00363	8.49	0.001	-3.00	5.37×10^{-05}	-4.27
Pt nanopowder	275	0.00363	3.05	0.0001	-4.00	1.13×10^{-06}	-5.95
Pt nanopowder	278	0.0036	8.2	0.001	-3.00	3.01×10^{-05}	-4.52
Pt nanopowder	327	0.00306	3.48	0.0001	-4.00	1.13×10^{-05}	-4.95
Pt nanopowder	318	0.00314	5.91	0.0003	-3.52	3.71×10^{-05}	-4.43
Pt nanopowder	323	0.0031	3.5	0.001	-3.00	1.01×10^{-04}	-4
Pt nanopowder	316	0.00317	8.6	0.001	-3.00	1.42×10^{-04}	-3.85
Pt nanopowder	318	0.00315	5.94	0.001	-3.00	1.04×10^{-04}	-3.98
Pt nanopowder	323	0.0031	6	0.0003	-3.52	3.64×10^{-05}	-4.44
Pt nanopowder	317	0.00316	3.44	0.0003	-3.52	3.60×10^{-05}	-4.44
Pt nanopowder	316	0.00317	8.58	0.0003	-3.52	3.89×10^{-05}	-4.41
Pt black	293	0.00341	3.07	0.0001	-4.00	4.14×10^{-07}	-6.38
Pt black	293	0.00341	5.39	0.0001	-4.00	1.17×10^{-06}	-5.93

Pt black	293	0.00341	8.7	0.0001	-4.00	1.02×10^{-06}	-5.99
Pt black	293	0.00341	2.91	0.0005	-3.30	3.29×10^{-06}	-5.48
Pt black	293	0.00341	6.23	0.0005	-3.30	4.62×10^{-06}	-5.34
Pt black	293	0.00341	7.57	0.0005	-3.30	4.02×10^{-06}	-5.4
Pt black	293	0.00341	9.17	0.0005	-3.30	2.87×10^{-06}	-5.54
Pt black	293	0.00341	3.06	0.001	-3.00	4.86×10^{-06}	-5.31
Pt black	293	0.00341	5.39	0.001	-3.00	6.50×10^{-06}	-5.19
Pt black	293	0.00341	8.87	0.001	-3.00	7.05×10^{-06}	-5.15
Pt black	293	0.00341	6.84	0.001	-3.00	5.63×10^{-06}	-5.25
Pt black	293	0.00341	3.8	0.0001	-4.00	6.69×10^{-07}	-6.17
Pt black	293	0.00341	7.6	0.0001	-4.00	5.16×10^{-07}	-6.29
Pt black	293	0.00341	4.09	0.00025	-3.60	7.34×10^{-07}	-6.13
Pt black	293	0.00341	6.45	0.00025	-3.60	8.22×10^{-07}	-6.09
Pt black	274	0.00365	2.91	0.0001	-4.00	1.61×10^{-07}	-6.79
Pt black	274	0.00365	9.3	0.0001	-4.00	2.47×10^{-07}	-6.61
Pt black	277	0.00361	8.01	0.001	-3.00	2.97×10^{-06}	-5.53
Pt black	277	0.00361	3.34	0.001	-3.00	1.63×10^{-06}	-5.79
Pt black	275	0.00363	3.29	0.0003	-3.52	6.97×10^{-07}	-6.16
Pt black	280	0.00357	7.7	0.0003	-3.52	6.37×10^{-07}	-6.2
Pt black	311	0.00322	5.5	0.0001	-4.00	1.28×10^{-06}	-5.89
Pt black	324	0.00309	8.75	0.0001	-4.00	2.41×10^{-06}	-5.62
Pt black	319	0.00314	3.48	0.0001	-4.00	1.00×10^{-06}	-6.00
Pt black	320	0.00313	3.49	0.0003	-3.52	5.20×10^{-06}	-5.28
Pt black	315	0.00318	8.82	0.0003	-3.52	5.33×10^{-06}	-5.27
Pt black	319	0.00313	5.78	0.001	-3.00	1.47×10^{-05}	-4.83
Pt black	320	0.00313	3.48	0.001	-3.00	1.60×10^{-05}	-4.8
Pt black	317	0.00316	8.55	0.001	-3.00	1.31×10^{-05}	-4.88
Pt black	316	0.00317	5.85	0.0003	-3.52	4.25×10^{-06}	-5.37
Pt-Liu-3nm	293	0.00341	1.12	0.0025	-2.60	7.52×10^{-07}	-6.12
Pt-Liu-3nm	293	0.00341	1.12	0.005	-2.30	1.75×10^{-06}	-5.75
Pt-Liu-3nm	293	0.00341	7.27	0.0025	-2.60	1.77×10^{-06}	-5.75
Pt-Liu-3nm	293	0.00341	7.27	0.005	-2.30	3.40×10^{-06}	-4.47
Pt-Liu-3nm	293	0.00341	10.96	0.0025	-2.60	2.00×10^{-06}	-5.70
Pt-Liu-3nm	293	0.00341	10.96	0.005	-2.30	4.21×10^{-06}	-5.38

Table S2.2. Rate measurements for Pt nanopowder and Pt black heated at 240 ^{o}C for 24h at different condition of $C_{H_2O_2}$, pH and temperature.

Catalyst	Temp., K	$1/T$	pH	$C_{H_2O_2}$ $(mol \cdot L^{-1})$	log $C_{H_2O_2}$	R, $mol.m^{-2}.s^{-1}$	log R
Pt nanopowder	295	0.00339	5.85	0.0001	-4.00	7.34×10^{-06}	-5.13
Pt nanopowder	315	0.00318	5.8	0.0001	-4.00	9.69×10^{-06}	-5.01
Pt nanopowder	296	0.00338	5.85	0.001	-3.00	8.26×10^{-05}	-4.08
Pt nanopowder	314	0.00318	5.87	0.001	-3.00	1.40×10^{-04}	-3.85
Pt nanopowder	322	0.00310	5.88	0.0003	-3.52	3.02×10^{-05}	-4.52
Pt nanopowder	296	0.00338	5.91	0.0003	-3.52	1.86×10^{-05}	-4.73
Pt black	295	0.00339	5.9	0.0001	-4.00	1.71×10^{-06}	-5.77
Pt black	295	0.00338	5.83	0.001	-3.00	1.26×10^{-05}	-4.90
Pt black	320	0.00312	5.8	0.001	-3.00	3.02×10^{-05}	-4.52
Pt black	322	0.00310	5.8	0.0001	-4.00	4.23×10^{-06}	-5.37
Pt black	295	0.00338	5.77	0.0003	-3.52	3.64×10^{-06}	-5.44
Pt black	323	0.00309	5.8	0.0003	-3.52	1.07×10^{-05}	4.97

Evaluation of •HO in solution during the decomposition of H_2O_2 by Pt black

The presence of •OH in solution was evaluated for the catalyzed decomposition of H_2O_2 at $C_{H_2O_2} = 100\ \mu M$ and $C_{H_2O_2} = 1000\ \mu M$ on Pt black. Absorbance measurements at 420 nm following the protocol described in section 3.4 resulted in an absorbance of 0.004 and 0.002 for the decomposition of H_2O_2 at each of the studied concentrations. The concentrations of •OH calculated from the determined absorbance values were negative. This result indicates that the amount of •OH species formed and released into solution during the decomposition of H_2O_2 on Pt black was negligible and below the limit of detection of this method for both tested $C_{H_2O_2}$ conditions.

Cyclic voltammetry of Pt nanopowder and Pt black

Cyclic voltammetry analysis performed in 0.5 M H_2SO_4/H_2O electrolyte showed that Pt black and Pt nanopowder oxidize from Pt to Pt(O) at 0.54 V vs Ag/AgCl and reduce from Pt(O) to Pt at 0.19 V vs Ag/AgCl. These processes occur at similar potentials for both materials. A significant reduction peak is observed in the first cycle for both catalysts, indicating that the surface of both catalysts is partially oxidized in the original state. Comparison of the voltammograms obtained in neutral electrolyte (0.1 M Na_2SO_4/H_2O) shows that the reduction peak shifts to more negative potentials, -0.27 and –0.32 V vs Ag/AgCl for Pt black and Pt nanopowder, respectively. The potential of Pt oxidation, however, remained unchanged. This result indicates that while the mechanism of reduction of Pt(O) is pH-dependent the mechanism of Pt oxidation is not.

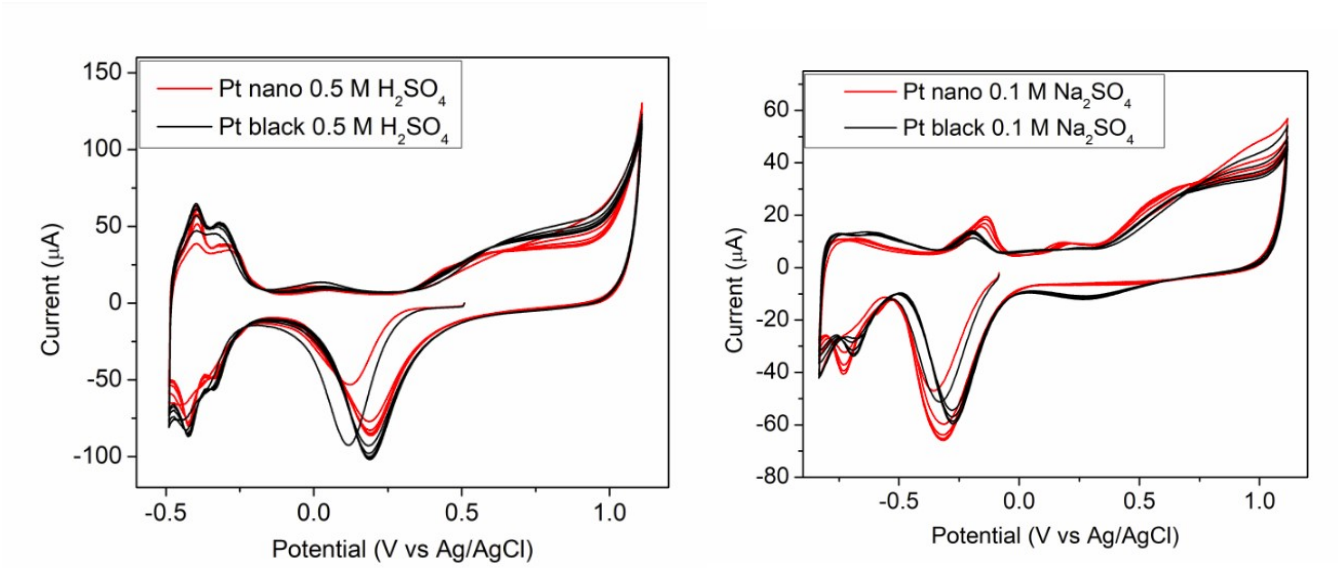

Figure S2.3. Cyclic voltammogram for Pt nanopowder (red) and Pt black (black).

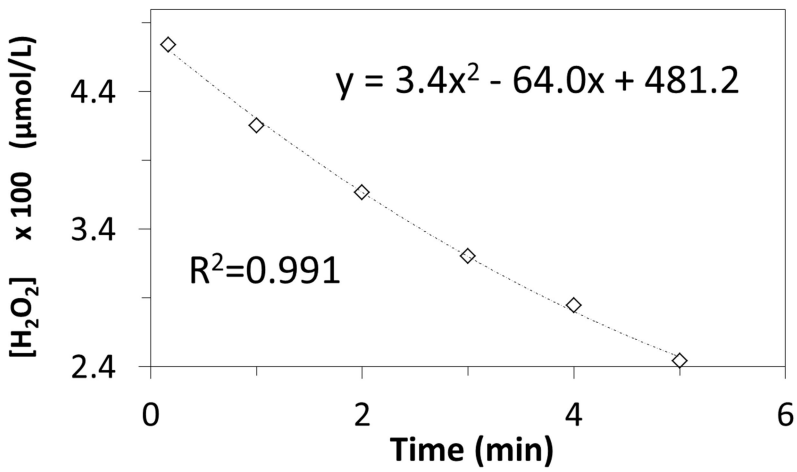

Figure S2.4. Example of the initial rate method. The initial rate of H_2O_2 decomposition was determined by the derivative of the quadratic regression extrapolated to t=0. For a quadratic regression, that value is the coefficient of the term with power of 1. In the example of the figure the initial rate of H_2O_2 decomposition is 64.0 $\frac{mol_{H_2O_2}}{L \cdot min}$.

Table S2.3. Rate measurements for Pt nanopowder and Pt black submitted to H_2O_2 pre-treatment exposure. The conditions of $\boldsymbol{C_{H_2O_2}}$, pH and temperature were maintained constant for all runs.

Catalyst	Temp., $\boldsymbol{K}$	$\boldsymbol{1/T}$	pH	$\boldsymbol{C_{H_2O_2}}$ $(\boldsymbol{mol \cdot L^{-1}})$	log $\boldsymbol{C_{H_2O_2}}$	$\boldsymbol{C^{pre}_{H_2O_2}}$	$\boldsymbol{\log C^{pre}_{H_2O_2}}$	R, $\boldsymbol{mol.m^{-2}.s}$	log r
Pt nanopowder	295	0.00338	5.84	0.0001	-4.00	0.98	-0.01	9.07×10^{-06}	-5.04
Pt nanopowder	295	0.00338	5.87	0.0001	-4.00	0.0098	-1.01	9.13×10^{-06}	-5.04
Pt nanopowder	295	0.00338	5.82	0.0001	-4.00	0.00098	-2.01	9.88×10^{-06}	-5.00
Pt nanopowder	295	0.00338	5.91	0.0001	-4.00	0.000098	-3.01	1.08×10^{-05}	-4.96
Pt black	295	0.00338	5.99	0.0001	-4.00	0.98	-0.01	3.05×10^{-06}	-5.51
Pt black	294	0.00340	6.02	0.0001	-4.00	0.0098	-1.01	3.17×10^{-06}	-5.49
Pt black	294	0.00340	6.07	0.0001	-4.00	0.00098	-2.01	2.50×10^{-06}	-5.60
Pt black	294	0.00340	6.1	0.0001	-4.00	0.000098	-3.01	2.36×10^{-06}	-5.62

Appendix C Chapter 3

Effect of platinum chemisorbed oxygen on catalytic activity of platinum nanocatalysts in the decomposition of hydrogen peroxide

Acknowledgements

F. M. M. and R. S. M. gratefully acknowledge financial support from the Virginia Tech Institute for Critical Technology and Applied Science (ICTAS) through a Junior Faculty Collaborative Grant (ICTAS-JFC 175884). R. S. M. gratefully acknowledges the Virginia Tech College of Science Roundtable Alumni Advisory Group for financial support provided through a "Make-a-Difference" Scholarship, as well as the Department of Geosciences for support provided by Sir Aubrey and Madam Eula Orange Scholarship funds. The authors also thank Dr. Robert Bodnar and Mr. Charles Farley for support with selected experiments.

Supporting Information

Table S3.1. Experimental particle size (d) of platinum black as function of heating time and heating temperature.

T (°C)	T (K)	time (s)	d (nm)
95	368	86400	8.7
95	368	75600	8.6
95	368	46800	7.6
95	368	60	11.4
240	513	86400	8.8
240	513	13500	7.7
300	573	79200	19.3
338	611	86400	8.7
432	705	5400	9.2
432	705	10800	8.3
438	711	5400	8.6
450	723	5400	11.5
450	723	5400	9.6
450	723	2400	10.9
453	725.6	5400	8.3
453	725.8	1920	8.2
453	726.1	600	8.0
453	726.3	180	9.2
454	727.1	60	10.2
454	727.2	120	9.7
455	728.4	620	10.3
457	730.1	75600	8.6
465	738.3	690	13.8
475	748.5	780	27.3
484	757.2	600	41.9
491	764	1200	51.2
498	771.4	2130	36.9
498	771.4	5400	38.1
500	773	3600	39.0
502	774.7	645	36.6
504	777	180	30.6
505	778.2	120	12.8
506	778.7	60	10.9
508	780.6	600	50.9
524	797.3	180	34.2
525	797.6	360	31.7
525	797.6	540	65.1
525	797.6	1560	70.7
533	806.4	900	70.7
552	825.2	60	18.8
553	825.8	180	60.3
554	826.8	1800	60.0
554	827.2	600	79.6
554	827.7	5400	76.1
556	829.2	120	82.0
567	839.6	55800	72.5
700*	973.2*		154.8*

* this sample was obtained at the end of thermogravimetric analysis in air. The sample was heated steadily at 10 °C/min from 95 °C to 700 °C.

Table S3.2. Fraction of platinum black surface covered with chemisorbed oxygen sites (θ) as function of heating time and heating temperature.

T	T (K)	time (s)	S_{Pt}	$S_{Pt(O)}$	θ
95	368	46800	0.53	0.019	0.29
95	368	75600	0.50	0.020	0.32
95	368	5400	0.45	0.015	0.26
95	368	600	0.36	0.007	0.16
95	368	86400	0.36	0.020	0.45
250	523	13500	0.56	0.021	0.30
250	523	60	0.35	0.016	0.38
250	523	600	0.44	0.016	0.29
250	523	64800	0.44	0.018	0.33
250	523	86400	0.45	0.020	0.36
250	523	86400	0.35	0.019	0.44
250	523	1800	0.35	0.016	0.36
453	726	5400	0.43	0.017	0.30
453	726	1920	0.45	0.018	0.32
453	726	180	0.46	0.014	0.23
454	727	60	0.37	0.013	0.29
454	727	120	0.36	0.017	0.37
455	728	620	0.63	0.018	0.23
461	734	86400	0.42	0.024	0.46
465	738	690	0.57	0.020	0.28
470	743	1380	0.36	0.019	0.41
470	743	720	0.35	0.016	0.38
470	743	60	0.36	0.015	0.34
470	743	300	0.37	0.014	0.30
471	744	180	0.37	0.023	0.49
471	744	120	0.30	0.021	0.56
475	748	48300	0.34	0.030	0.69
475	748	780	0.57	0.022	0.30
484	757	600	0.39	0.027	0.54
498	771	2100	0.46	0.026	0.46
498	771	5400	0.46	0.032	0.56
505	778	120	0.39	0.016	0.33
506	779	60	0.35	0.014	0.31
508	781	600	0.59	0.029	0.32
508	781	600	0.37	0.039	0.85
524	797	1560	0.49	0.049	0.79
524	797	1560	0.37	0.057	1.23
524	797	180	0.66	0.026	0.32
524	797	180	0.33	0.021	0.51
525	798	540	0.80	0.046	0.46
525	798	360	0.70	0.031	0.35
525	798	540	0.32	0.046	1.17
525	798	360	0.38	0.028	0.60
533	806	900	0.54	0.042	0.63
552	825	60	0.35	0.037	0.83
555	828	86400	0.46	0.069	1.21
555	828	5400	0.39	0.065	1.32
557	830	120	0.39	0.044	0.90
567	840	55800	0.40	0.072	1.44
700*	973*			0.074*	

* this sample was obtained at the end of thermogravimetric analysis in air. The sample was heated steadily at 10 ^{o}C/min from 95 ^{o}C to 700 ^{o}C.

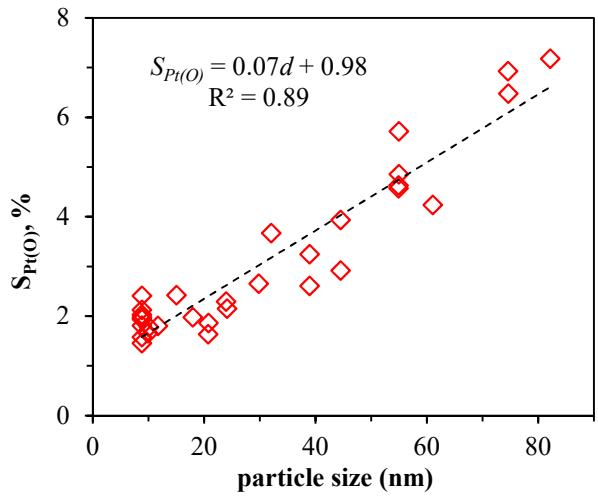

Figure S3.1. Correlation between surface chemisorbed oxygen abundance and particle size for platinum black samples heated in air.

The particle size of platinum black increases 2 times for samples heated in vacuum, but it is similar for platinum black samples that are heated in air and reached steady state d and θ as well as platinum black treated with concentrated H_2O_2. Similarly, the size of platinum nanopowder increases 1.5 times for samples heated in vacuum but remains the same for platinum nanopowder samples heated in air or treated with concentrated H_2O_2. The particle size of as received platinum nanopowder is twice that of as received platinum black.

The surface θ of platinum black maintains approximately constant when the sample is heated in vacuum (p-value = 0.12). In comparison θ increases 1.50 times for platinum black samples that are heated in air and reach steady state d and θ and 1.90 times for platinum black samples that are subjected to concentrated H_2O_2 (p-value = 0.01 and p-value < 0.01, respectively). Comparatively, the surface θ of platinum nanopowder maintains constant for samples heated in air (p-value = 0.93), heated in vacuum (p-value = 0.06) and samples that are subjected to concentrated H_2O_2 (p-value = 0.29). The surface θ of as received platinum nanopowder is 3.2 times higher than that of as received platinum black (p-value < 0.01).

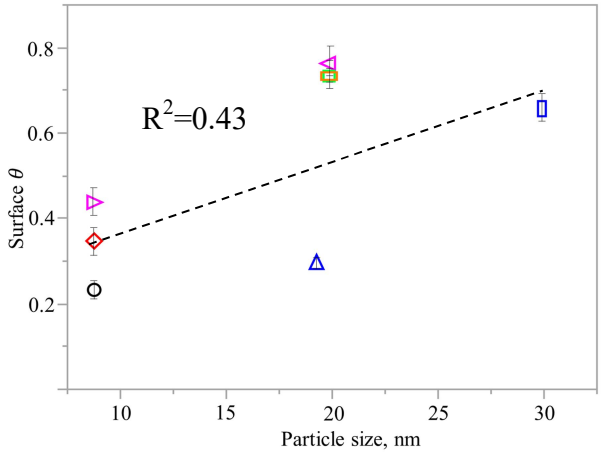

Figure S3.2. Surface θ and particle size of each set of samples used in the H_2O_2 decomposition rate study. As received platinum black (black ○) and as received platinum nanopowder (green □), platinum black heated in air (red ◊), platinum nanopowder heated in air (▭), platinum black heated in vacuum (blue △), platinum nanopowder heated in vacuum (blue ▯), platinum black pre-treated with concentrated H_2O_2 (pink ▷) and Pt nanopowder pre-treated with concentrated H_2O_2 (pink ◁).

The surface area normalized rate of H_2O_2 decomposition as function of $C_{H_2O_2}$, a_{H^+}, $\frac{1}{T}$, d and θ is given by

$$\boldsymbol{R} = 10^{1.2}\left(e^{\frac{(24\pm1.6)10^3}{R\cdot T}}\right)\left(C_{H_2O_2}^{0.92\pm0.03}\right)\left(a_{H^+}^{0.04\pm0.01}\right)\left(d^{-0.09\pm0.05}\right)\left(\theta^{0.89\pm0.05}\right) \quad \text{(S1)}$$

The rate model shown in equation S1 indicates that the catalytic activity of H_2O_2 decomposition by platinum nanocatalysts is strongly affected by surface θ (p-value<0.01). On the contrary, the effect of particle size is small and not statistically significant (p-value=0.06).

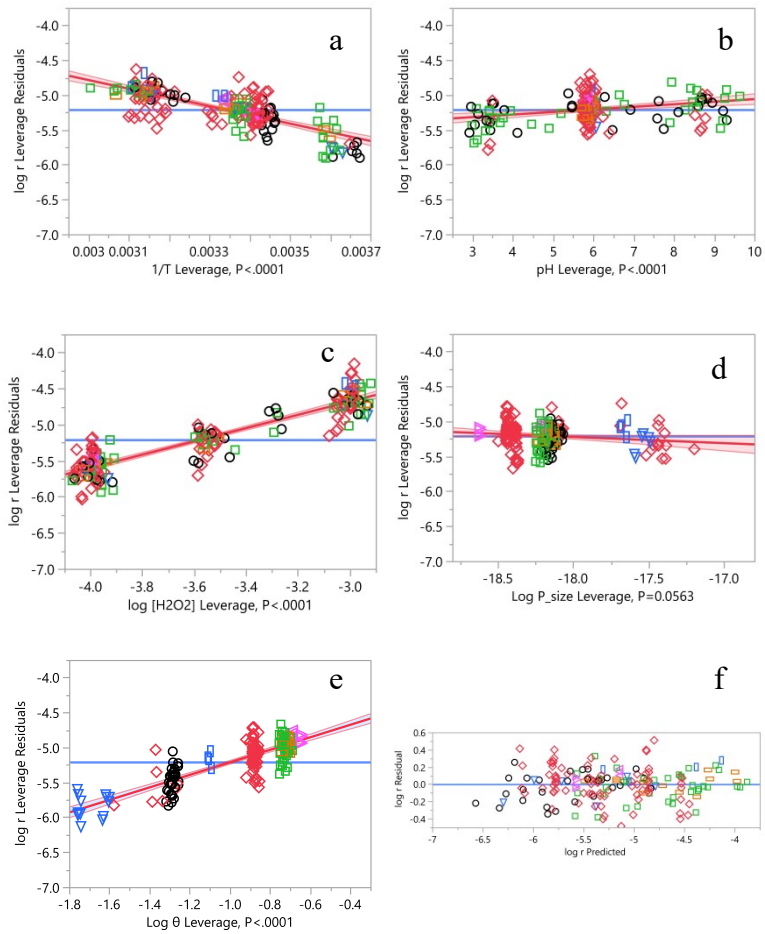

Figure S3.3. Partial regression graphs of the rate measurements of H_2O_2 decomposition as function of a) temperature, b) a_{H^+}, c) $C_{H_2O_2}$, d) particle size (d) and e) surface θ for samples of as received platinum black (black ○) and as received platinum nanopowder (green □), platinum black heated in air (red ◊), platinum nanopowder heated in air (▭), platinum black heated in vacuum (blue ▽), platinum nanopowder heated in vacuum (blue ▯), platinum black pre-treated with concentrated H_2O_2 (pink ▷) and Pt nanopowder pre-treated with concentrated H_2O_2 (pink ◁). f) shows the residuals plot for **Figure 3.1.**

The residuals plot of this regression **(Figure S3.3 f)** shows that the distribution of data points around the mean line is relatively symmetrical and homogeneous for all catalyst samples.

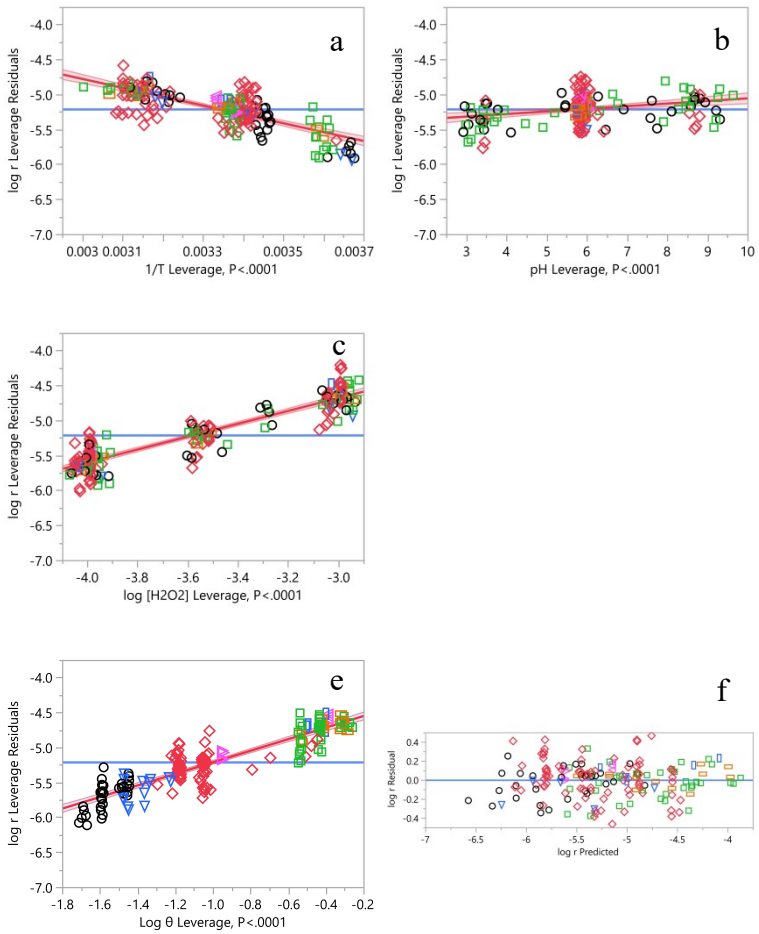

Figure S3.4. Partial regression graphs of the rate measurements of H_2O_2 decomposition as function of a) temperature, b) pH, c) $C_{H_2O_2}$ and e) surface θ for samples of as received platinum black (black ○) and as received platinum nanopowder (green □), platinum black heated in air (red ◊), platinum nanopowder heated in air (▭), platinum black heated in vacuum (blue ▽), platinum nanopowder heated in vacuum (blue ▯), platinum black pre-treated with concentrated H_2O_2 (pink ▷) and Pt nanopowder pre-treated with concentrated H_2O_2 (pink ◁). f) shows the residuals plot for **Figure 3.2**.

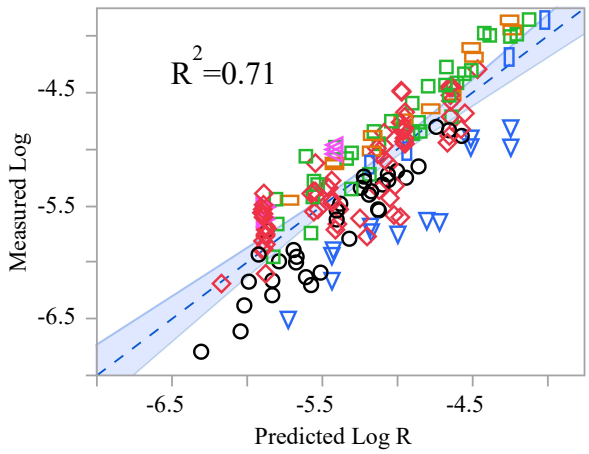

Figure S3.5. Rate measurements of H_2O_2 decomposition as function of $C_{H_2O_2}$, pH, temperature and particle size (d) for samples of as received platinum black (black ○) and as received platinum nanopowder (green □), platinum black heated in air (red ◊), platinum nanopowder heated in air (▭), platinum black heated in vacuum (blue ▽), platinum nanopowder heated in vacuum (blue ◘), platinum black pre-treated with concentrated H_2O_2 (pink ▷) and Pt nanopowder pre-treated with concentrated H_2O_2 (pink ◁).

As opposed to what was observed for the residuals plot of **Figures 3.1** and **3.2**, the residuals plot of **Figure S3.5** shows that the different nanocatalyst samples are not homogeneously and symmetrically distributed around the mean line **(Figure S3.6)**. The relative position of each catalyst in the residuals plot correlates with increasing surface θ. This result indicates that although particle size and surface θ are correlated for heated platinum black samples **(**see **Figure S3.1)**, the correlation is not obeyed by the overall catalyst sample set used in this study, which results in only limited capacity of particle size to account for the data variance generated by differences in surface θ.

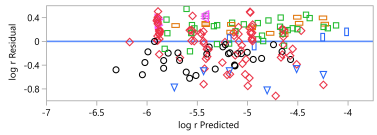

Figure S3.6. Residuals plot for **Figure S3.5** for samples of as received platinum black (black ○) and as received platinum nanopowder (green □), platinum black heated in air (red ◊), platinum nanopowder heated in air (▭), platinum black heated in vacuum (blue ▽), platinum nanopowder heated in vacuum (blue ▯), platinum black pre-treated with concentrated H_2O_2 (pink ▷) and Pt nanopowder pre-treated with concentrated H_2O_2 (pink ◁).

For comparison, if the rate measurements here studied were not regressed neither against particle size nor surface θ abundance, and only against $C_{H_2O_2}$, pH and temperature of reaction, the R^2 of this regression is only 0.54 **(Table 3.3, fourth entry) (Figure S3.7)**.

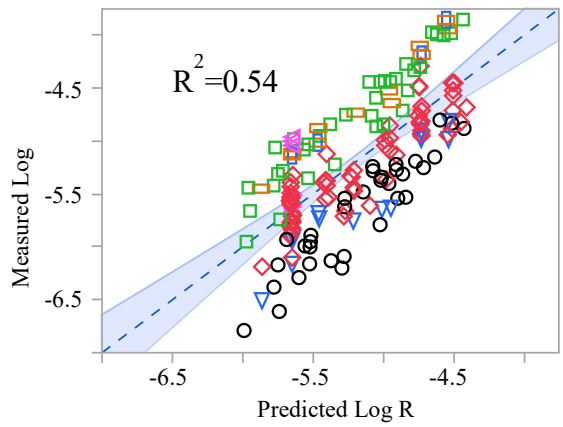

Figure S3.7. Rate measurements of H_2O_2 decomposition as function of $C_{H_2O_2}$, pH and temperature for samples of as received platinum black (black ○) and as received platinum nanopowder (green □), platinum black heated in air (red ◊), platinum nanopowder heated in air (▭), platinum black heated in vacuum (blue ▽), platinum nanopowder heated in vacuum (blue ▯), platinum black pre-treated with concentrated H_2O_2 (pink ▷) and Pt nanopowder pre-treated with concentrated H_2O_2 (pink ◁).

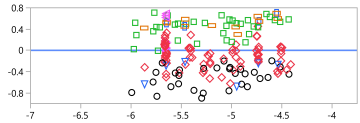

Figure S3.8. Residuals plot for **Figure S3.7** for for samples of as received platinum black (black ○) and as received platinum nanopowder (green □), platinum black heated in air (red ◊), platinum nanopowder heated in air (▭), platinum black heated in vacuum (blue ▽), platinum nanopowder heated in vacuum (blue ▯), platinum black pre-treated with concentrated H_2O_2 (pink ▷) and Pt nanopowder pre-treated with concentrated H_2O_2 (pink ◁).

The residuals plot when neither particle size nor surface θ are considered in the regression models shows that the difference between the catalytic activity of platinum black and platinum nanopowder is approximately 0.9 log scale, which matches what was determined in previous publications[18]. Heated platinum black samples, which have intermediate values of Pt(O) abundance between platinum black and platinum nanopowder exhibit intermediate catalytic activity between the two as received catalysts.

Table S3.3. Master Table with all rate measurements analyzed in this study, including rate measurements performed in the current study and rate measurements obtained in our previous studies[17-18]. For platinum black samples heated in air, particle size values *(d)* were determined using equation 2, and surface θ fraction was determined using equation 5 for heating T > 450 ^{o}C and equation 6 for heating T < 450 ^{o}C. For all other samples particle size and surface θ were determined for each sample set.

The sample key is platinum black as received **(A3)**, platinum nanopowder as received **(B3)**, platinum black heated in air **(A1)**, platinum nanopowder heated in air **(B1)**, platinum black heated in vacuum **(A2)**, platinum nanopowder heated in vacuum **(B2)**, platinum black pretreated with concentrated H_2O_2 **(A4)** and platinum nanopowder pretreated with concentrated H_2O_2 **(B4)**.

key	Ref.	$C_{H_2O_2}^{pre}, M$	Experimental Temp., K	1/T	a_{H^+}	pH	$C_{H_2O_2}, M$	$\log(C_{H_2O_2})$	Heating Temp., K	Heating time, s	Particle size *(d)*, m	$\log(d)$	$O_{Pt(O)}$	$S_{Pt(O)}$	θ	$\log(S_{Pt(O)})$	$\log(\theta)$	**R**, $mol/(m^2 s)$	log **R**
A1	*	N/A	318	0.0031	3.72×10^{-04}	3.43	3.0×10^{-04}	-3.5	368	604800	8.85×10^{-09}	-18.54	0.21	0.017	0.32	0.55	-1.15	2.46×10^{-06}	-5.61
A1	*	N/A	316	0.0032	2.69×10^{-09}	8.57	3.0×10^{-04}	-3.5	368	604800	8.85×10^{-09}	-18.54	0.21	0.017	0.32	0.55	-1.15	7.46×10^{-06}	-5.13
A2	*	N/A	295	0.0034	1.02×10^{-06}	5.99	1.0×10^{-04}	-4.0	573	79200	1.93×10^{-08}	-17.76	0.14	0.013	0.23	0.25	-1.45	6.91×10^{-07}	-6.16
A2	*	N/A	315	0.0032	1.05×10^{-06}	5.98	1.0×10^{-04}	-4.0	573	79200	1.93×10^{-08}	-17.76	0.14	0.013	0.23	0.25	-1.45	1.87×10^{-06}	-5.73
A2	*	N/A	295	0.0034	1.26×10^{-06}	5.9	1.0×10^{-03}	-3.0	573	79200	1.93×10^{-08}	-17.76	0.14	0.013	0.23	0.25	-1.45	1.26×10^{-05}	-4.9
A2	*	N/A	316	0.0032	1.38×10^{-06}	5.86	1.0×10^{-03}	-3.0	573	79200	1.93×10^{-08}	-17.76	0.14	0.013	0.23	0.25	-1.45	1.04×10^{-05}	-4.98
A2	*	N/A	295	0.0034	1.58×10^{-06}	5.8	3.0×10^{-04}	-3.5	573	79200	1.93×10^{-08}	-17.76	0.14	0.013	0.23	0.25	-1.45	1.79×10^{-06}	-5.75
A2	*	N/A	317	0.0032	1.48×10^{-06}	5.83	3.0×10^{-04}	-3.5	573	79200	1.93×10^{-08}	-17.76	0.14	0.013	0.23	0.25	-1.45	2.29×10^{-06}	-5.64
A1	*	N/A	295	0.0034	1.26×10^{-06}	5.9	1.0×10^{-04}	-4.0	523	86400	8.85×10^{-09}	-18.54	0.21	0.017	0.32	0.55	-1.15	1.44×10^{-06}	-5.84
A1	*	N/A	296	0.0034	1.48×10^{-06}	5.83	1.0×10^{-03}	-3.0	513	86400	8.85×10^{-09}	-18.54	0.21	0.017	0.32	0.55	-1.15	1.12×10^{-05}	-4.95
A1	*	N/A	320	0.0031	1.58×10^{-06}	5.8	1.0×10^{-03}	-3.0	513	86400	8.85×10^{-09}	-18.54	0.21	0.017	0.32	0.55	-1.15	2.69×10^{-05}	-4.57
A1	*	N/A	322	0.0031	1.58×10^{-06}	5.8	1.0×10^{-04}	-4.0	513	86400	8.85×10^{-09}	-18.54	0.21	0.017	0.32	0.55	-1.15	3.77×10^{-06}	-5.42
A1	*	N/A	296	0.0034	1.70×10^{-06}	5.77	3.0×10^{-04}	-3.5	513	86400	8.85×10^{-09}	-18.54	0.21	0.017	0.32	0.55	-1.15	3.42×10^{-06}	-5.47
A1	*	N/A	324	0.0031	1.58×10^{-06}	5.8	3.0×10^{-04}	-3.5	513	86400	8.85×10^{-09}	-18.54	0.21	0.017	0.32	0.55	-1.15	8.10×10^{-06}	-5.09
A1	*	N/A	296	0.0034	1.38×10^{-06}	5.86	1.0×10^{-03}	-3.0	611	86400	8.85×10^{-09}	-18.54	0.21	0.017	0.32	0.55	-1.15	2.16×10^{-05}	-4.67
A1	*	N/A	296	0.0034	1.26×10^{-06}	5.9	1.0×10^{-04}	-4.0	611	86400	8.85×10^{-09}	-18.54	0.21	0.017	0.32	0.55	-1.15	1.99×10^{-06}	-5.7
A1	*	N/A	295	0.0034	1.82×10^{-06}	5.74	1.0×10^{-04}	-4.0	723	5400	8.85×10^{-09}	-18.54	0.21	0.017	0.32	0.55	-1.15	4.03×10^{-06}	-5.39
A1	*	N/A	295	0.0034	1.02×10^{-06}	5.99	1.0×10^{-04}	-4.0	773	3600	4.01×10^{-08}	-17.03	0.31	0.036	0.66	1.28	-0.42	4.83×10^{-06}	-5.32
A3	*	N/A	295	0.0034	1.00×10^{-06}	6	1.0×10^{-04}	-4.0	N/A	N/A	8.85×10^{-09}	-18.54	0.14	0.012	0.21	0.14	-1.55	1.92×10^{-06}	-5.72
A2	*	N/A	296	0.0034	1.32×10^{-06}	5.88	1.0×10^{-04}	-4.0	573	86400	1.93×10^{-08}	-17.76	0.14	0.013	0.23	0.25	-1.45	1.30×10^{-06}	-5.89
A1	*	N/A	295	0.0034	1.41×10^{-06}	5.85	1.0×10^{-03}	-3.0	723	5400	8.85×10^{-09}	-18.54	0.21	0.017	0.32	0.55	-1.15	1.19×10^{-05}	-4.93
A1	*	N/A	319	0.0031	1.26×10^{-06}	5.9	1.0×10^{-03}	-3.0	723	5400	8.85×10^{-09}	-18.54	0.21	0.017	0.32	0.55	-1.15	1.33×10^{-05}	-4.88
A1	*	N/A	319	0.0031	1.17×10^{-06}	5.93	1.0×10^{-03}	-3.0	723	5400	8.85×10^{-09}	-18.54	0.21	0.017	0.32	0.55	-1.15	1.93×10^{-05}	-4.71
A1	*	N/A	295	0.0034	1.38×10^{-06}	5.86	1.0×10^{-04}	-4.0	723	600	8.85×10^{-09}	-18.54	0.21	0.017	0.30	0.51	-1.19	8.03×10^{-07}	-6.1
A1	*	N/A	295	0.0034	1.38×10^{-06}	5.86	1.0×10^{-04}	-4.0	723	1200	8.85×10^{-09}	-18.54	0.21	0.017	0.31	0.54	-1.16	2.03×10^{-06}	-5.69

A1	*	N/A	295	0.0034	1.38×10^{-06}	5.86	1.0×10^{-04}	-4.0	723	1800	8.85×10^{-09}	-18.54	0.21	0.017	0.32	0.55	-1.15	1.97×10^{-06}	-5.71
A1	*	N/A	295	0.0034	1.38×10^{-06}	5.86	1.0×10^{-04}	-4.0	723	2400	8.85×10^{-09}	-18.54	0.21	0.017	0.32	0.55	-1.15	1.79×10^{-06}	-5.75
A1	*	N/A	295	0.0034	1.38×10^{-06}	5.86	1.0×10^{-04}	-4.0	723	2400	8.85×10^{-09}	-18.54	0.21	0.017	0.32	0.55	-1.15	2.07×10^{-06}	-5.68
A1	*	N/A	295	0.0034	1.58×10^{-06}	5.8	1.0×10^{-04}	-4.0	743	5400	2.11×10^{-08}	-17.68	0.23	0.020	0.37	0.70	-1.00	2.97×10^{-06}	-5.53
A1	*	N/A	295	0.0034	1.62×10^{-06}	5.79	1.0×10^{-03}	-3.0	743	5400	2.11×10^{-08}	-17.68	0.23	0.020	0.37	0.70	-1.00	5.10×10^{-05}	-4.29
A1	*	N/A	294	0.0034	1.41×10^{-06}	5.85	1.0×10^{-04}	-4.0	703	5400	8.85×10^{-09}	-18.54	0.21	0.017	0.32	0.55	-1.15	1.28×10^{-06}	-5.89
A1	*	N/A	294	0.0034	1.58×10^{-06}	5.8	1.0×10^{-03}	-3.0	703	5400	8.85×10^{-09}	-18.54	0.21	0.017	0.32	0.55	-1.15	3.23×10^{-05}	-4.49
A1	*	N/A	294	0.0034	1.26×10^{-06}	5.9	3.0×10^{-04}	-3.5	703	5400	8.85×10^{-09}	-18.54	0.21	0.017	0.32	0.55	-1.15	4.57×10^{-06}	-5.34
A1	*	N/A	319	0.0031	1.20×10^{-06}	5.92	3.0×10^{-04}	-3.5	703	5400	8.85×10^{-09}	-18.54	0.21	0.017	0.32	0.55	-1.15	9.20×10^{-06}	-5.04
A1	*	N/A	321	0.0031	4.68×10^{-07}	6.33	1.0×10^{-04}	-4.0	703	5400	8.85×10^{-09}	-18.54	0.21	0.017	0.32	0.55	-1.15	2.97×10^{-06}	-5.53
A1	*	N/A	320	0.0031	9.12×10^{-07}	6.04	1.0×10^{-03}	-3.0	703	5400	8.85×10^{-09}	-18.54	0.21	0.017	0.32	0.55	-1.15	3.51×10^{-05}	-4.45
A1	*	N/A	293	0.0034	8.51×10^{-07}	6.07	1.0×10^{-04}	-4.0	703	10800	8.85×10^{-09}	-18.54	0.21	0.017	0.32	0.55	-1.15	2.93×10^{-06}	-5.53
A1	*	N/A	318	0.0031	1.00×10^{-06}	6	1.0×10^{-03}	-3.0	703	10800	8.85×10^{-09}	-18.54	0.21	0.017	0.32	0.55	-1.15	3.55×10^{-05}	-4.45
A1	*	N/A	293	0.0034	7.94×10^{-07}	6.1	1.0×10^{-04}	-4.0	711	5400	8.85×10^{-09}	-18.54	0.21	0.017	0.32	0.55	-1.15	2.77×10^{-06}	-5.56
A1	*	N/A	320	0.0031	8.51×10^{-07}	6.07	1.0×10^{-04}	-4.0	711	5400	8.85×10^{-09}	-18.54	0.21	0.017	0.32	0.55	-1.15	4.30×10^{-06}	-5.37
A1	*	N/A	319	0.0031	9.33×10^{-07}	6.03	1.0×10^{-04}	-4.0	703	10800	8.85×10^{-09}	-18.54	0.21	0.017	0.32	0.55	-1.15	4.07×10^{-06}	-5.39
A1	*	N/A	294	0.0034	1.58×10^{-06}	5.8	1.0×10^{-03}	-3.0	711	5400	8.85×10^{-09}	-18.54	0.21	0.017	0.32	0.55	-1.15	1.72×10^{-05}	-4.76
A1	*	N/A	294	0.0034	9.55×10^{-07}	6.02	1.0×10^{-03}	-3.0	703	16200	8.85×10^{-09}	-18.54	0.21	0.017	0.32	0.55	-1.15	1.52×10^{-05}	-4.82
A1	*	N/A	294	0.0034	9.77×10^{-07}	6.01	1.0×10^{-03}	-3.0	703	10800	8.85×10^{-09}	-18.54	0.21	0.017	0.32	0.55	-1.15	1.45×10^{-05}	-4.84
A1	*	N/A	293	0.0034	7.76×10^{-07}	6.11	1.0×10^{-04}	-4.0	703	16200	8.85×10^{-09}	-18.54	0.21	0.017	0.32	0.55	-1.15	1.54×10^{-06}	-5.81
A1	*	N/A	320	0.0031	9.33×10^{-07}	6.03	1.0×10^{-04}	-4.0	703	16200	8.85×10^{-09}	-18.54	0.21	0.017	0.32	0.55	-1.15	2.83×10^{-06}	-5.55
A1	*	N/A	293	0.0034	1.58×10^{-06}	5.8	3.0×10^{-04}	-3.5	703	16200	8.85×10^{-09}	-18.54	0.21	0.017	0.32	0.55	-1.15	4.70×10^{-06}	-5.33
A1	*	N/A	318	0.0031	9.33×10^{-07}	6.03	3.0×10^{-04}	-3.5	703	16200	8.85×10^{-09}	-18.54	0.21	0.017	0.32	0.55	-1.15	1.02×10^{-05}	-4.99
A1	*	N/A	294	0.0034	1.26×10^{-06}	5.9	1.0×10^{-03}	-3.0	703	16200	8.85×10^{-09}	-18.54	0.21	0.017	0.32	0.55	-1.15	3.30×10^{-05}	-4.48
A3	*	N/A	324	0.0031	1.78×10^{-09}	8.75	1.0×10^{-04}	-4.0	N/A	N/A	8.85×10^{-09}	-18.54	0.14	0.012	0.21	0.14	-1.55	2.89×10^{-06}	-5.54
A3	*	N/A	319	0.0031	3.31×10^{-04}	3.48	1.0×10^{-04}	-4.0	N/A	N/A	8.85×10^{-09}	-18.54	0.14	0.012	0.21	0.14	-1.55	1.12×10^{-06}	-5.95
A3	*	N/A	320	0.0031	3.24×10^{-04}	3.49	3.0×10^{-04}	-3.5	N/A	N/A	8.85×10^{-09}	-18.54	0.14	0.012	0.21	0.14	-1.55	5.78×10^{-06}	-5.24
A3	*	N/A	315	0.0032	1.51×10^{-09}	8.82	3.0×10^{-04}	-3.5	N/A	N/A	8.85×10^{-09}	-18.54	0.14	0.012	0.21	0.14	-1.55	5.96×10^{-06}	-5.22
A1	*	N/A	323	0.0031	1.78×10^{-09}	8.75	1.0×10^{-04}	-4.0	368	604800	8.85×10^{-09}	-18.54	0.21	0.017	0.32	0.55	-1.15	1.95×10^{-06}	-5.71
A1	*	N/A	324	0.0031	1.62×10^{-09}	8.79	1.0×10^{-04}	-4.0	368	604800	8.85×10^{-09}	-18.54	0.21	0.017	0.32	0.55	-1.15	2.18×10^{-06}	-5.66
A1	*	N/A	324	0.0031	3.98×10^{-07}	6.4	1.0×10^{-03}	-3.0	368	604800	8.85×10^{-09}	-18.54	0.21	0.017	0.32	0.55	-1.15	1.51×10^{-05}	-4.82
A1	*	N/A	327	0.0031	3.63×10^{-04}	3.44	1.0×10^{-03}	-3.0	368	604800	8.85×10^{-09}	-18.54	0.21	0.017	0.32	0.55	-1.15	1.15×10^{-05}	-4.94
A1	*	N/A	318	0.0031	1.66×10^{-09}	8.78	1.0×10^{-03}	-3.0	368	604800	8.85×10^{-09}	-18.54	0.21	0.017	0.32	0.55	-1.15	2.10×10^{-05}	-4.68
A1	*	N/A	320	0.0031	1.26×10^{-06}	5.9	3.0×10^{-04}	-3.5	368	604800	8.85×10^{-09}	-18.54	0.21	0.017	0.32	0.55	-1.15	4.35×10^{-06}	-5.36
A1	*	N/A	294	0.0034	1.41×10^{-06}	5.85	1.0×10^{-04}	-4.0	775	645	4.09×10^{-08}	-17.01	0.31	0.034	0.62	1.22	-0.48	2.63×10^{-06}	-5.58
A1	*	N/A	294	0.0034	1.41×10^{-06}	5.85	1.0×10^{-04}	-4.0	368	434700	8.85×10^{-09}	-18.54	0.21	0.017	0.32	0.55	-1.15	3.25×10^{-06}	-5.49
A1	*	N/A	294	0.0034	1.41×10^{-06}	5.85	1.0×10^{-04}	-4.0	757	600	2.98×10^{-08}	-17.33	0.21	0.026	0.47	0.94	-0.76	1.70×10^{-06}	-5.77
A1	*	N/A	294	0.0034	1.41×10^{-06}	5.85	1.0×10^{-04}	-4.0	728	609.6	8.85×10^{-09}	-18.54	0.21	0.017	0.30	0.51	-1.19	2.68×10^{-06}	-5.57
A1	*	N/A	294	0.0034	1.41×10^{-06}	5.85	1.0×10^{-04}	-4.0	523	600	8.85×10^{-09}	-18.54	0.21	0.017	0.31	0.53	-1.17	2.51×10^{-06}	-5.6
A1	*	N/A	294	0.0034	1.41×10^{-06}	5.85	1.0×10^{-04}	-4.0	726	5400	8.85×10^{-09}	-18.54	0.21	0.017	0.32	0.55	-1.15	3.20×10^{-06}	-5.49
A1	*	N/A	294	0.0034	1.41×10^{-06}	5.85	1.0×10^{-04}	-4.0	611	86400	8.85×10^{-09}	-18.54	0.21	0.017	0.32	0.55	-1.15	1.31×10^{-06}	-5.88

A1	*	N/A	294	0.0034	1.41×10^{-06}	5.85	1.0×10^{-04}	-4.0	771	2130	3.90×10^{-08}	-17.06	0.31	0.035	0.64	1.25	-0.45	3.75×10^{-06}	-5.43
A1	*	N/A	294	0.0034	1.41×10^{-06}	5.85	1.0×10^{-04}	-4.0	797	180	4.41×10^{-08}	-16.94	0.21	0.028	0.52	1.03	-0.66	2.49×10^{-06}	-5.6
B3	[18]	N/A	275	0.0036	6.76×10^{-10}	9.17	1.0×10^{-04}	-4.0	N/A	N/A	1.99×10^{-08}	-17.74	0.29	0.037	0.67	1.30	-0.40	1.80×10^{-06}	-5.74
B3	[18]	N/A	293	0.0034	5.62×10^{-10}	9.25	1.0×10^{-04}	-4.0	N/A	N/A	1.99×10^{-08}	-17.74	0.29	0.037	0.67	1.30	-0.40	4.52×10^{-06}	-5.35
B3	[18]	N/A	275	0.0036	1.35×10^{-08}	7.87	3.0×10^{-04}	-3.5	N/A	N/A	1.99×10^{-08}	-17.74	0.29	0.037	0.67	1.30	-0.40	5.99×10^{-06}	-5.22
B3	[18]	N/A	274	0.0036	1.51×10^{-05}	4.82	1.0×10^{-03}	-3.0	N/A	N/A	1.99×10^{-08}	-17.74	0.29	0.037	0.67	1.30	-0.40	1.45×10^{-05}	-4.84
B3	[18]	N/A	275	0.0036	2.00×10^{-04}	3.7	1.0×10^{-04}	-4.0	N/A	N/A	1.99×10^{-08}	-17.74	0.29	0.037	0.67	1.30	-0.40	2.21×10^{-06}	-5.66
B3	[18]	N/A	293	0.0034	9.55×10^{-04}	3.02	1.0×10^{-04}	-4.0	N/A	N/A	1.99×10^{-08}	-17.74	0.29	0.037	0.67	1.30	-0.40	3.76×10^{-06}	-5.42
B3	[18]	N/A	293	0.0034	5.01×10^{-10}	9.3	1.0×10^{-04}	-4.0	N/A	N/A	1.99×10^{-08}	-17.74	0.29	0.037	0.67	1.30	-0.40	9.43×10^{-06}	-5.03
B3	[18]	N/A	293	0.0034	2.09×10^{-07}	6.68	1.0×10^{-04}	-4.0	N/A	N/A	1.99×10^{-08}	-17.74	0.29	0.037	0.67	1.30	-0.40	1.06×10^{-05}	-4.98
B3	[18]	N/A	293	0.0034	5.62×10^{-10}	9.25	1.0×10^{-03}	-3.0	N/A	N/A	1.99×10^{-08}	-17.74	0.29	0.037	0.67	1.30	-0.40	1.02×10^{-04}	-3.99
B3	[18]	N/A	293	0.0034	8.71×10^{-04}	3.06	1.0×10^{-03}	-3.0	N/A	N/A	1.99×10^{-08}	-17.74	0.29	0.037	0.67	1.30	-0.40	1.97×10^{-05}	-4.71
B3	[18]	N/A	275	0.0036	5.75×10^{-04}	3.24	1.0×10^{-03}	-3.0	N/A	N/A	1.99×10^{-08}	-17.74	0.29	0.037	0.67	1.30	-0.40	1.39×10^{-05}	-4.86
B3	[18]	N/A	275	0.0036	2.24×10^{-10}	9.65	1.0×10^{-04}	-4.0	N/A	N/A	1.99×10^{-08}	-17.74	0.29	0.037	0.67	1.30	-0.40	5.28×10^{-06}	-5.28
B3	[18]	N/A	293	0.0034	3.63×10^{-05}	4.44	5.0×10^{-04}	-3.3	N/A	N/A	1.99×10^{-08}	-17.74	0.29	0.037	0.67	1.30	-0.40	1.74×10^{-05}	-4.76
B3	[18]	N/A	293	0.0034	1.00×10^{-06}	6	5.0×10^{-04}	-3.3	N/A	N/A	1.99×10^{-08}	-17.74	0.29	0.037	0.67	1.30	-0.40	3.61×10^{-05}	-4.44
B3	[18]	N/A	293	0.0034	1.58×10^{-04}	3.8	1.0×10^{-04}	-4.0	N/A	N/A	1.99×10^{-08}	-17.74	0.29	0.037	0.67	1.30	-0.40	4.88×10^{-06}	-5.31
B3	[18]	N/A	293	0.0034	3.16×10^{-09}	8.5	1.0×10^{-04}	-4.0	N/A	N/A	1.99×10^{-08}	-17.74	0.29	0.037	0.67	1.30	-0.40	8.41×10^{-06}	-5.08
B3	[18]	N/A	293	0.0034	4.37×10^{-09}	8.36	1.0×10^{-03}	-3.0	N/A	N/A	1.99×10^{-08}	-17.74	0.29	0.037	0.67	1.30	-0.40	1.08×10^{-04}	-3.97
B3	[18]	N/A	293	0.0034	5.50×10^{-07}	6.26	1.0×10^{-03}	-3.0	N/A	N/A	1.99×10^{-08}	-17.74	0.29	0.037	0.67	1.30	-0.40	5.00×10^{-05}	-4.3
B3	[18]	N/A	293	0.0034	7.24×10^{-06}	5.14	1.0×10^{-03}	-3.0	N/A	N/A	1.99×10^{-08}	-17.74	0.29	0.037	0.67	1.30	-0.40	4.67×10^{-05}	-4.33
B3	[18]	N/A	293	0.0034	1.70×10^{-07}	6.77	2.5×10^{-04}	-3.6	N/A	N/A	1.99×10^{-08}	-17.74	0.29	0.037	0.67	1.30	-0.40	1.77×10^{-05}	-4.75
B3	[18]	N/A	293	0.0034	1.15×10^{-04}	3.94	2.5×10^{-04}	-3.6	N/A	N/A	1.99×10^{-08}	-17.74	0.29	0.037	0.67	1.30	-0.40	1.44×10^{-05}	-4.84
B3	[18]	N/A	276	0.0036	1.10×10^{-08}	7.96	1.0×10^{-04}	-4.0	N/A	N/A	1.99×10^{-08}	-17.74	0.29	0.037	0.67	1.30	-0.40	8.64×10^{-06}	-5.06
B3	[18]	N/A	276	0.0036	7.76×10^{-04}	3.11	1.0×10^{-04}	-4.0	N/A	N/A	1.99×10^{-08}	-17.74	0.29	0.037	0.67	1.30	-0.40	3.61×10^{-06}	-5.44
B3	[18]	N/A	275	0.0036	4.68×10^{-04}	3.33	1.0×10^{-03}	-3.0	N/A	N/A	1.99×10^{-08}	-17.74	0.29	0.037	0.67	1.30	-0.40	2.58×10^{-05}	-4.59
B3	[18]	N/A	276	0.0036	3.24×10^{-09}	8.49	1.0×10^{-03}	-3.0	N/A	N/A	1.99×10^{-08}	-17.74	0.29	0.037	0.67	1.30	-0.40	5.37×10^{-05}	-4.27
B3	[18]	N/A	275	0.0036	8.91×10^{-04}	3.05	1.0×10^{-04}	-4.0	N/A	N/A	1.99×10^{-08}	-17.74	0.29	0.037	0.67	1.30	-0.40	1.13×10^{-06}	-5.95
B3	[18]	N/A	278	0.0036	6.31×10^{-09}	8.2	1.0×10^{-03}	-3.0	N/A	N/A	1.99×10^{-08}	-17.74	0.29	0.037	0.67	1.30	-0.40	3.01×10^{-05}	-4.52
B3	[18]	N/A	327	0.0031	3.31×10^{-04}	3.48	1.0×10^{-04}	-4.0	N/A	N/A	1.99×10^{-08}	-17.74	0.29	0.037	0.67	1.30	-0.40	1.13×10^{-05}	-4.95
B3	[18]	N/A	318	0.0031	1.23×10^{-06}	5.91	3.0×10^{-04}	-3.5	N/A	N/A	1.99×10^{-08}	-17.74	0.29	0.037	0.67	1.30	-0.40	3.71×10^{-05}	-4.43
B3	[18]	N/A	323	0.0031	3.16×10^{-04}	3.5	1.0×10^{-03}	-3.0	N/A	N/A	1.99×10^{-08}	-17.74	0.29	0.037	0.67	1.30	-0.40	1.01×10^{-04}	-4
B3	[18]	N/A	316	0.0032	2.51×10^{-09}	8.6	1.0×10^{-03}	-3.0	N/A	N/A	1.99×10^{-08}	-17.74	0.29	0.037	0.67	1.30	-0.40	1.42×10^{-04}	-3.85
B3	[18]	N/A	318	0.0031	1.15×10^{-06}	5.94	1.0×10^{-03}	-3.0	N/A	N/A	1.99×10^{-08}	-17.74	0.29	0.037	0.67	1.30	-0.40	1.04×10^{-04}	-3.98
B3	[18]	N/A	323	0.0031	1.00×10^{-06}	6	3.0×10^{-04}	-3.5	N/A	N/A	1.99×10^{-08}	-17.74	0.29	0.037	0.67	1.30	-0.40	3.64×10^{-04}	-4.44
B3	[18]	N/A	317	0.0032	3.63×10^{-04}	3.44	3.0×10^{-04}	-3.5	N/A	N/A	1.99×10^{-08}	-17.74	0.29	0.037	0.67	1.30	-0.40	3.60×10^{-04}	-4.44
B3	[18]	N/A	316	0.0032	2.63×10^{-09}	8.58	3.0×10^{-04}	-3.5	N/A	N/A	1.99×10^{-08}	-17.74	0.29	0.037	0.67	1.30	-0.40	3.89×10^{-04}	-4.41
A3	[18]	N/A	293	0.0034	8.51×10^{-04}	3.07	1.0×10^{-04}	-4.0	N/A	N/A	8.85×10^{-09}	-18.54	0.14	0.012	0.21	0.14	-1.55	4.14×10^{-07}	-6.38
A3	[18]	N/A	293	0.0034	4.07×10^{-06}	5.39	1.0×10^{-04}	-4.0	N/A	N/A	8.85×10^{-09}	-18.54	0.14	0.012	0.21	0.14	-1.55	1.17×10^{-06}	-5.93

A3	[18]	N/A	293	0.0034	2.00×10^{-09}	8.7	1.0×10^{-04}	-4.0	N/A	N/A	8.85×10^{-09}	-18.54	0.14	0.012	0.21	0.14	-1.55	1.02×10^{-06}	-5.99
A3	[18]	N/A	293	0.0034	1.23×10^{-03}	2.91	5.0×10^{-04}	-3.3	N/A	N/A	8.85×10^{-09}	-18.54	0.14	0.012	0.21	0.14	-1.55	3.29×10^{-06}	-5.48
A3	[18]	N/A	293	0.0034	5.89×10^{-07}	6.23	5.0×10^{-04}	-3.3	N/A	N/A	8.85×10^{-09}	-18.54	0.14	0.012	0.21	0.14	-1.55	4.62×10^{-06}	-5.34
A3	[18]	N/A	293	0.0034	2.69×10^{-08}	7.57	5.0×10^{-04}	-3.3	N/A	N/A	8.85×10^{-09}	-18.54	0.14	0.012	0.21	0.14	-1.55	4.02×10^{-06}	-5.4
A3	[18]	N/A	293	0.0034	6.76×10^{-10}	9.17	5.0×10^{-04}	-3.3	N/A	N/A	8.85×10^{-09}	-18.54	0.14	0.012	0.21	0.14	-1.55	2.87×10^{-06}	-5.54
A3	[18]	N/A	293	0.0034	8.71×10^{-04}	3.06	1.0×10^{-03}	-3.0	N/A	N/A	8.85×10^{-09}	-18.54	0.14	0.012	0.21	0.14	-1.55	4.86×10^{-06}	-5.31
A3	[18]	N/A	293	0.0034	4.07×10^{-06}	5.39	1.0×10^{-03}	-3.0	N/A	N/A	8.85×10^{-09}	-18.54	0.14	0.012	0.21	0.14	-1.55	6.50×10^{-06}	-5.19
A3	[18]	N/A	293	0.0034	1.35×10^{-09}	8.87	1.0×10^{-03}	-3.0	N/A	N/A	8.85×10^{-09}	-18.54	0.14	0.012	0.21	0.14	-1.55	7.05×10^{-06}	-5.15
A3	[18]	N/A	293	0.0034	1.45×10^{-07}	6.84	1.0×10^{-03}	-3.0	N/A	N/A	8.85×10^{-09}	-18.54	0.14	0.012	0.21	0.14	-1.55	5.63×10^{-06}	-5.25
A3	[18]	N/A	293	0.0034	1.58×10^{-04}	3.8	1.0×10^{-04}	-4.0	N/A	N/A	8.85×10^{-09}	-18.54	0.14	0.012	0.21	0.14	-1.55	6.69×10^{-07}	-6.17
A3	[18]	N/A	293	0.0034	2.51×10^{-08}	7.6	1.0×10^{-04}	-4.0	N/A	N/A	8.85×10^{-09}	-18.54	0.14	0.012	0.21	0.14	-1.55	5.16×10^{-07}	-6.29
A3	[18]	N/A	293	0.0034	8.13×10^{-05}	4.09	2.5×10^{-04}	-3.6	N/A	N/A	8.85×10^{-09}	-18.54	0.14	0.012	0.21	0.14	-1.55	7.34×10^{-07}	-6.13
A3	[18]	N/A	293	0.0034	3.55×10^{-07}	6.45	2.5×10^{-04}	-3.6	N/A	N/A	8.85×10^{-09}	-18.54	0.14	0.012	0.21	0.14	-1.55	8.22×10^{-07}	-6.09
A3	[18]	N/A	274	0.0036	1.23×10^{-03}	2.91	1.0×10^{-04}	-4.0	N/A	N/A	8.85×10^{-09}	-18.54	0.14	0.012	0.21	0.14	-1.55	1.61×10^{-07}	-6.79
A3	[18]	N/A	274	0.0036	5.01×10^{-10}	9.3	1.0×10^{-04}	-4.0	N/A	N/A	8.85×10^{-09}	-18.54	0.14	0.012	0.21	0.14	-1.55	2.47×10^{-07}	-6.61
A3	[18]	N/A	277	0.0036	9.77×10^{-09}	8.01	1.0×10^{-03}	-3.0	N/A	N/A	8.85×10^{-09}	-18.54	0.14	0.012	0.21	0.14	-1.55	2.97×10^{-06}	-5.53
A3	[18]	N/A	277	0.0036	4.57×10^{-04}	3.34	1.0×10^{-03}	-3.0	N/A	N/A	8.85×10^{-09}	-18.54	0.14	0.012	0.21	0.14	-1.55	1.63×10^{-06}	-5.79
A3	[18]	N/A	275	0.0036	5.13×10^{-04}	3.29	3.0×10^{-04}	-3.5	N/A	N/A	8.85×10^{-09}	-18.54	0.14	0.012	0.21	0.14	-1.55	6.97×10^{-07}	-6.16
A3	[18]	N/A	280	0.0036	2.00×10^{-08}	7.7	3.0×10^{-04}	-3.5	N/A	N/A	8.85×10^{-09}	-18.54	0.14	0.012	0.21	0.14	-1.55	6.37×10^{-07}	-6.2
A3	[18]	N/A	311	0.0032	3.16×10^{-06}	5.5	1.0×10^{-04}	-4.0	N/A	N/A	8.85×10^{-09}	-18.54	0.14	0.012	0.21	0.14	-1.55	1.28×10^{-06}	-5.89
A3	[18]	N/A	324	0.0031	1.78×10^{-09}	8.75	1.0×10^{-04}	-4.0	N/A	N/A	8.85×10^{-09}	-18.54	0.14	0.012	0.21	0.14	-1.55	2.41×10^{-06}	-5.62
A3	[18]	N/A	319	0.0031	3.31×10^{-04}	3.48	1.0×10^{-04}	-4.0	N/A	N/A	8.85×10^{-09}	-18.54	0.14	0.012	0.21	0.14	-1.55	1.00×10^{-06}	-6
A3	[18]	N/A	320	0.0031	3.24×10^{-04}	3.49	3.0×10^{-04}	-3.5	N/A	N/A	8.85×10^{-09}	-18.54	0.14	0.012	0.21	0.14	-1.55	5.20×10^{-06}	-5.28
A3	[18]	N/A	315	0.0032	1.51×10^{-09}	8.82	3.0×10^{-04}	-3.5	N/A	N/A	8.85×10^{-09}	-18.54	0.14	0.012	0.21	0.14	-1.55	5.33×10^{-06}	-5.27
A3	[18]	N/A	319	0.0031	1.66×10^{-06}	5.78	1.0×10^{-03}	-3.0	N/A	N/A	8.85×10^{-09}	-18.54	0.14	0.012	0.21	0.14	-1.55	1.47×10^{-05}	-4.83
A3	[18]	N/A	320	0.0031	3.31×10^{-04}	3.48	1.0×10^{-03}	-3.0	N/A	N/A	8.85×10^{-09}	-18.54	0.14	0.012	0.21	0.14	-1.55	1.60×10^{-05}	-4.8
A3	[18]	N/A	317	0.0032	2.82×10^{-09}	8.55	1.0×10^{-03}	-3.0	N/A	N/A	8.85×10^{-09}	-18.54	0.14	0.012	0.21	0.14	-1.55	1.31×10^{-05}	-4.88
A3	[18]	N/A	316	0.0032	1.41×10^{-06}	5.85	3.0×10^{-04}	-3.5	N/A	N/A	8.85×10^{-09}	-18.54	0.14	0.012	0.21	0.14	-1.55	4.25×10^{-06}	-5.37
A2	[17]	N/A	295	0.0034	1.02×10^{-06}	5.99	1.0×10^{-04}	-4.0	573	79200	1.93×10^{-08}	-17.76	0.14	0.015	0.27	0.39	-1.31	1.15×10^{-06}	-5.94
A2	[17]	N/A	315	0.0032	1.32×10^{-06}	5.88	1.0×10^{-04}	-4.0	573	79200	1.93×10^{-08}	-17.76	0.14	0.015	0.27	0.39	-1.31	2.09×10^{-06}	-5.68
A2	[17]	N/A	295	0.0034	1.26×10^{-06}	5.9	1.0E-03	-3.0	573	79200	1.93×10^{-08}	-17.76	0.14	0.015	0.27	0.39	-1.31	1.05×10^{-05}	-4.98
A2	[17]	N/A	316	0.0032	1.38×10^{-06}	5.86	1.0E-03	-3.0	573	79200	1.93×10^{-08}	-17.76	0.14	0.015	0.27	0.39	-1.31	1.55×10^{-05}	-4.81
A2	[17]	N/A	275	0.0036	1.35×10^{-06}	5.87	1.0×10^{-04}	-4.0	573	79200	1.93×10^{-08}	-17.76	0.14	0.015	0.27	0.39	-1.31	3.14×10^{-05}	-6.50
A2	[17]	N/A	275	0.0036	1.29×10^{-06}	5.89	1.0×10^{-03}	-3.0	573	79200	1.93×10^{-08}	-17.76	0.14	0.015	0.27	0.39	-1.31	2.35×10^{-06}	-5.63
A1	[17]	N/A	295	0.0034	1.26×10^{-06}	5.9	1.0×10^{-04}	-4.0	573	93600	8.80×10^{-09}	-18.55	0.21	0.017	0.32	0.55	-1.15	1.71×10^{-06}	-5.77
A1	[17]	N/A	296	0.0034	1.48×10^{-06}	5.83	1.0×10^{-03}	-3.0	573	93600	8.80×10^{-09}	-18.55	0.21	0.017	0.32	0.55	-1.15	1.54×10^{-05}	-4.81
A1	[17]	N/A	320	0.0031	1.58×10^{-06}	5.8	1.0×10^{-03}	-3.0	573	93600	8.80×10^{-09}	-18.55	0.21	0.017	0.32	0.55	-1.15	3.57×10^{-05}	-4.45
A1	[17]	N/A	322	0.0031	1.58×10^{-06}	5.8	1.0×10^{-04}	-4.0	573	93600	8.80×10^{-09}	-18.55	0.21	0.017	0.32	0.55	-1.15	7.57×10^{-06}	-5.12
A1	[17]	N/A	296	0.0034	1.70×10^{-06}	5.77	3.0×10^{-04}	-3.5	573	93600	8.80×10^{-09}	-18.55	0.21	0.017	0.32	0.55	-1.15	5.31×10^{-06}	-5.27

A1	17	N/A	324	0.0031	1.58×10^{-06}	5.8	3.0×10^{-04}	-3.5	573	93600	8.80×10^{-09}	-18.55	0.21	0.017	0.32	0.55	-1.15	1.41×10^{-05}	-4.85
A1	17	N/A	296	0.0034	1.38×10^{-06}	5.86	1.0×10^{-03}	-3.0	573	93600	8.80×10^{-09}	-18.55	0.21	0.017	0.32	0.55	-1.15	1.94×10^{-05}	-4.71
A1	17	N/A	275	0.0036	1.26×10^{-06}	5.9	1.0×10^{-04}	-4.0	573	93600	8.80×10^{-09}	-18.55	0.21	0.017	0.32	0.55	-1.15	6.50×10^{-07}	-6.19
B2	17	N/A	295	0.0034	1.41×10^{-06}	5.85	1.0×10^{-04}	-4.0	573	79200	3.00×10^{-08}	-17.32	0.29	0.034	0.62	1.22	-0.48	7.34×10^{-06}	-5.13
B2	17	N/A	315	0.0032	1.58×10^{-06}	5.8	1.0×10^{-04}	-4.0	573	79200	3.00×10^{-08}	-17.32	0.29	0.034	0.62	1.22	-0.48	9.69×10^{-06}	-5.01
B2	17	N/A	296	0.0034	1.41×10^{-06}	5.85	1.0×10^{-03}	-3.0	573	79200	3.00×10^{-08}	-17.32	0.29	0.034	0.62	1.22	-0.48	6.59×10^{-05}	-4.18
B2	17	N/A	314	0.0032	1.35×10^{-06}	5.87	1.0×10^{-03}	-3.0	573	79200	3.00×10^{-08}	-17.32	0.29	0.034	0.62	1.22	-0.48	1.40×10^{-04}	-3.85
B1	17	N/A	295	0.0034	9.55×10^{-07}	6.02	1.0×10^{-04}	-4.0	573	93600	1.99×10^{-08}	-17.74	0.29	0.037	0.67	1.30	-0.40	7.71×10^{-06}	-5.11
B1	17	N/A	315	0.0032	1.48×10^{-06}	5.83	1.0×10^{-04}	-4.0	573	93600	1.99×10^{-08}	-17.74	0.29	0.037	0.67	1.30	-0.40	1.33×10^{-05}	-4.88
B1	17	N/A	294	0.0034	1.23×10^{-06}	5.91	1.0×10^{-03}	-3.0	573	93600	1.99×10^{-08}	-17.74	0.29	0.037	0.67	1.30	-0.40	7.97×10^{-05}	-4.10
B1	17	N/A	316	0.0032	1.91×10^{-06}	5.72	1.0×10^{-03}	-3.0	573	93600	1.99×10^{-08}	-17.74	0.29	0.037	0.67	1.30	-0.40	1.14×10^{-04}	-3.94
B1	17	N/A	275	0.0036	2.04×10^{-06}	5.69	1.0×10^{-04}	-4.0	573	93600	1.99×10^{-08}	-17.74	0.29	0.037	0.67	1.30	-0.40	3.55×10^{-06}	-5.45
B1	17	N/A	276	0.0036	1.78×10^{-06}	5.75	1.0×10^{-03}	-3.0	573	93600	1.99×10^{-08}	-17.74	0.29	0.037	0.67	1.30	-0.40	2.29×10^{-05}	-4.64
A1	18	N/A	295	0.0034	1.26×10^{-06}	5.9	1.0×10^{-04}	-4.0	513	93600	8.80×10^{-09}	-18.55	0.21	0.017	0.32	0.55	-1.15	1.71×10^{-06}	-5.77
A1	18	N/A	296	0.0034	1.48×10^{-06}	5.83	1.0×10^{-03}	-3.0	513	93600	8.80×10^{-09}	-18.55	0.21	0.017	0.32	0.55	-1.15	1.26×10^{-05}	-4.90
A1	18	N/A	320	0.0031	1.58×10^{-06}	5.8	1.0×10^{-03}	-3.0	513	93600	8.80×10^{-09}	-18.55	0.21	0.017	0.32	0.55	-1.15	3.02×10^{-05}	-4.52
A1	18	N/A	322	0.0031	1.58×10^{-06}	5.8	1.0×10^{-04}	-4.0	513	93600	8.80×10^{-09}	-18.55	0.21	0.017	0.32	0.55	-1.15	4.23×10^{-06}	-5.37
A1	18	N/A	296	0.0034	1.70×10^{-06}	5.77	3.0×10^{-04}	-3.5	513	93600	8.80×10^{-09}	-18.55	0.21	0.017	0.32	0.55	-1.15	3.65×10^{-06}	-5.44
A1	18	N/A	324	0.0031	1.58×10^{-06}	5.8	3.0×10^{-04}	-3.5	513	93600	8.80×10^{-09}	-18.55	0.21	0.017	0.32	0.55	-1.15	1.07×10^{-05}	-4.97
B1	18	N/A	295	0.0034	1.41×10^{-06}	5.85	1.0×10^{-04}	-4.0	513	86400	1.99×10^{-08}	-17.74	0.29	0.037	0.67	1.30	-0.40	7.34×10^{-06}	-5.13
B1	18	N/A	315	0.0032	1.58×10^{-06}	5.8	1.0×10^{-04}	-4.0	513	86400	1.99×10^{-08}	-17.74	0.29	0.037	0.67	1.30	-0.40	9.69×10^{-06}	-5.01
B1	18	N/A	296	0.0034	1.41×10^{-06}	5.85	1.0×10^{-03}	-3.0	513	86400	1.99×10^{-08}	-17.74	0.29	0.037	0.67	1.30	-0.40	6.56×10^{-05}	-4.18
B1	18	N/A	314	0.0032	1.35×10^{-06}	5.87	1.0×10^{-03}	-3.0	513	86400	1.99×10^{-08}	-17.74	0.29	0.037	0.67	1.30	-0.40	1.40×10^{-04}	-3.85
B1	18	N/A	322	0.0031	1.32×10^{-06}	5.88	3.0×10^{-04}	-3.5	513	86400	1.99×10^{-08}	-17.74	0.29	0.037	0.67	1.30	-0.40	3.02×10^{-05}	-4.52
B1	18	N/A	296	0.0034	1.26E-06	5.9	3.0×10^{-04}	-3.5	513	86400	1.99×10^{-08}	-17.74	0.29	0.037	0.67	1.30	-0.40	1.86×10^{-05}	-4.73
B4	18	0.98	295	0.0034	1.45×10^{-06}	5.84	1.0×10^{-04}	-4.0	N/A	N/A	1.99×10^{-08}	-17.74	0.31	0.038	0.70	1.34	-0.36	9.07×10^{-06}	-5.04
B4	18	0.0098	295	0.0034	1.35×10^{-06}	5.87	1.0×10^{-04}	-4.0	N/A	N/A	1.99×10^{-08}	-17.74	0.31	0.038	0.70	1.34	-0.36	9.13×10^{-06}	-5.04
B4	18	0.00098	295	0.0034	1.51×10^{-06}	5.82	1.0×10^{-04}	-4.0	N/A	N/A	1.99×10^{-08}	-17.74	0.31	0.038	0.70	1.34	-0.36	9.88×10^{-06}	-5
B4	18	0.000098	295	0.0034	1.23×10^{-06}	5.91	1.0×10^{-04}	-4.0	N/A	N/A	1.99×10^{-08}	-17.74	0.31	0.038	0.70	1.34	-0.36	1.08×10^{-05}	-4.96
A4	18	0.98	295	0.0034	1.02×10^{-06}	5.99	1.0×10^{-04}	-4.0	N/A	N/A	8.80×10^{-09}	-18.55	0.22	0.022	0.40	0.78	-0.92	3.05×10^{-06}	-5.51
A4	18	0.0098	294	0.0034	9.55×10^{-07}	6.02	1.0×10^{-04}	-4.0	N/A	N/A	8.80×10^{-09}	-18.55	0.22	0.022	0.40	0.78	-0.92	3.17×10^{-06}	-5.49
A4	18	0.00098	294	0.0034	8.51×10^{-07}	6.07	1.0×10^{-04}	-4.0	N/A	N/A	8.80×10^{-09}	-18.55	0.22	0.022	0.40	0.78	-0.92	2.50×10^{-06}	-5.6
A4	18	0.000098	294	0.0034	7.94×10^{-07}	6.1	1.0×10^{-04}	-4.0	N/A	N/A	8.80×10^{-09}	-18.55	0.22	0.022	0.40	0.78	-0.92	2.36×10^{-06}	-5.62

* These measurements were obtained in the present study.